PRACA DOKTORSKA

**Yuriy Stepanenko**



# Laser spectroscopy of molecular complexes

Praca doktorska wykonana pod kierunkiem Doc. dr hab. Andrzeja Mordzińskiego w Zakładzie Fotochemii i Spektroskopii Instytutu Chemii Fizycznej Polskiej Akademii Nauk.



Warszawa 2002

*In memory of my beloved wife Tania this work would make great pleasure to her.*

Przede wszystkim chcę gorąco podziękować mojemu promotorowi doc. dr hab. Andrzejowi Mordzińskiemu za stworzenie warunków do samodzielnej pracy i możliwości do samorealizacji, za cenne uwagi i wskazówki. Andrzeju dziękuję również za czas, który mi poświęciłeś wnikliwie analizując wyniki moich badań.

Pani Prof. Grabowskiej wyrażam wielką wdzięczność za wsparcie naukowe oraz stałą gotowość do dyskusji.

Chcę również podziękować dr A. Kyryczenko za wielką pomoc przy obliczeniach teoretycznych oraz doc. dr hab. A. L. Sobolewskiemu za cenne wskazówki. Moim kolegom z Centrum Laserowego za pomoc techniczną i mile spędzony czas. Dziękuję wszystkim kolegom z Zakładu Fotochemii i Spektroskopii Instytutu Chemii Fizycznej, w szczególności kierownikowi Prof. J. Walukowi.

Также хочу сказать огромное спасибо моим дорогим маме, папе и сестричке Ире, которые оказали мне неоценимую духовную поддержку в написании этой работы.

## Streszczenie.

W pracy są przedstawione wyniki badań spektroskopowych molekularnych mikroklasterów pochodnych antracenu z cząsteczkami rozpuszczalników, takich jak woda, metanol, chloroform, czterochlorek węgla oraz benzen, w warunkach strumienia naddźwiękowego. Wszystkie badania były przeprowadzone z detekcją optyczna oraz masowo rozdzielczymi metodami spektroskopii laserowej. Dane powstałe w wyniku tych badań są porównywane do danych z literatury dla klasterów innych układów aromatycznych z cząsteczkami rozpuszczalników, obliczeń struktury takich kompleksów metodami dynamiki molekularnej oraz obliczeń metodami *ab initio*. Dla większości badanych kompleksów zostały zaproponowane struktury.



## Abstract.

The results of the spectroscopical investigations of the molecular microclusters of the anthracene derivatives with solvents (water, methanol, chloroform, carbon tetrachloride and benzene) under supersonic jet conditions are presented in this work. All studies were carried out by means of optical detection and mass selective laser spectroscopy methods. The data obtained are compared with other complexes of aromatic molecules with solvent molecules known from the literature as well as obtained from molecular dynamic and *ab initio* calculations. The structures for the majority of the studied microclusters are proposed.

Contents.

## CHAPTER 1. Spectroscopy of molecular clusters in supersonic molecular beam - a historical review.

During the two last decades interest in molecular spectroscopy has effectively developed from "isolated molecule" to the more complex systems e.g. "molecule-molecule" connected by van der Waals forces. Understanding of such weak intermolecular interactions on microscopic scale gives us some deep insight into many chemical and biological processes. Van der Waals interactions together with hydrogen bonding are the most important factors controlling the structure in many biological systems. They lead to stabilization and determine the structure of large biomolecules, for example - DNA.

A quantitative estimation of weak intermolecular forces demands an investigation of well-defined isolated complexes of atoms or molecules held together by van der Waals weak interaction or by hydrogen bond. It became possible after developing the technique of supersonic molecular beams. Supersonic jets allow to "cool" translational and internal degrees of freedom by expansion of molecular gas into vacuum. As a result, weakly bonded complexes are formed, whose lifetimes are of the order of several microseconds (time of expansion). During this time one can assume that the complexes are isolated each from other and they can be investigated without mutual perturbations.

Due to small concentrations of van der Waals complexes in the supersonic beam the most suitable method of exploration is the UV spectroscopy. The excitation of a molecule or complex after absorption of UV radiation can be detected with a very high sensitivity. The simplest method is to monitor the spontaneous emission of fluorescence. It can be done with high temporal resolution and low signal to noise ratio. The IR or microwave spectroscopies are not so favorable, because in corresponding spectral region the probability of the spontaneous emission is very low due to $\nu^3$ rule. In such experiments absorption has to be detected instead of

emission of radiation. This leads to complicated schemes of experimental apparatus and to the necessity of developing new techniques such as slit nozzles, multipass absorption cells or pulsed microwave radiation sources. Another very powerful method in UV spectroscopy, especially useful for high sensitivity and mass-selective detection of molecular complexes is the absorption of the second photon by excited molecule or complex, providing the energy sufficient to ionize the complex. The next advantage of the UV spectroscopy is the ability of obtaining the information of the dynamic behavior of molecules and complexes after absorbtion of small amount of energy. Due to suitable Franck-Condon factors, a part of photon energy is deposited as vibrational energy in the electronically excited state. For van der Waals clusters this means that vibrational energy can reach the energy of dissociation of weakly bonded complex. An important point is the study of dynamic of processes that occur inside the complex after absorbing the energy of radiation. In particular, it is interesting in which way the absorbed energy is distributed among vibrational modes of molecules within the complex van der Waals modes including. A review of early works on UV spectroscopy of complexes is given by Castelman and Keesee [1].

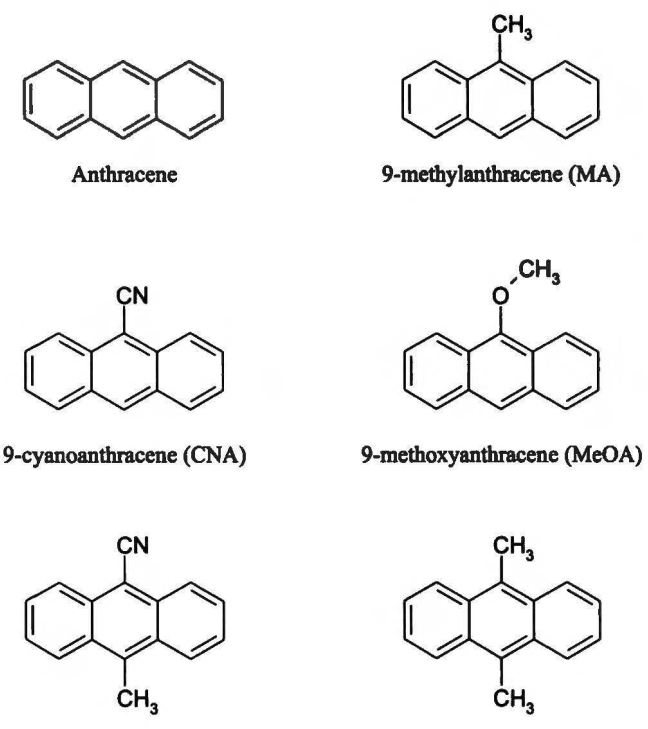


**Figure 1.1.** Anthracene and its derivatives studied in this work.

In the last decade studies of the weak intermolecular interactions between aromatic molecules and selected solvent molecules ($H_2O$, $CH_3OH$, $CCl_4$, $CHCl_3$, $C_6H6$, $NH_3$) have found an increasing interest. Molecular spectroscopy of systems seeded in the supersonic beams is the convenient way to study the isolated molecular complexes in the gas phase.

Before going further into the details of spectroscopic studies of the microsolvated substituted anthracenes and understanding their cluster structure, the "bare" molecule itself has to be investigated. The detailed information about the rôle of the substituents has to be obtained. A review of papers on microsolvatation in substituted benzenes was made by B. Brutschy in [2]. Naphtalene derivatives were intensively studied by D. H. Levy [3] and J. A. Warren [4] groups.

Also the spectroscopy of anthracenes is relatively well known. They have been intensively studied both in the supersonic beams and low temperature matrices [5,6]. More recently also theoretical works concerning the structure of anthracene and its derivatives have been published [13-21].

Pioneering investigations of anthracene under supersonic jet conditions were carried out by A. Zewail's [7, 8, 11, 12] and J. Jortner's [9, 10] groups. In the work [7] the fluorescence excitation and single vibronic level fluorescence (SVL) spectra of jet-cooled anthracene are presented and analyzed.

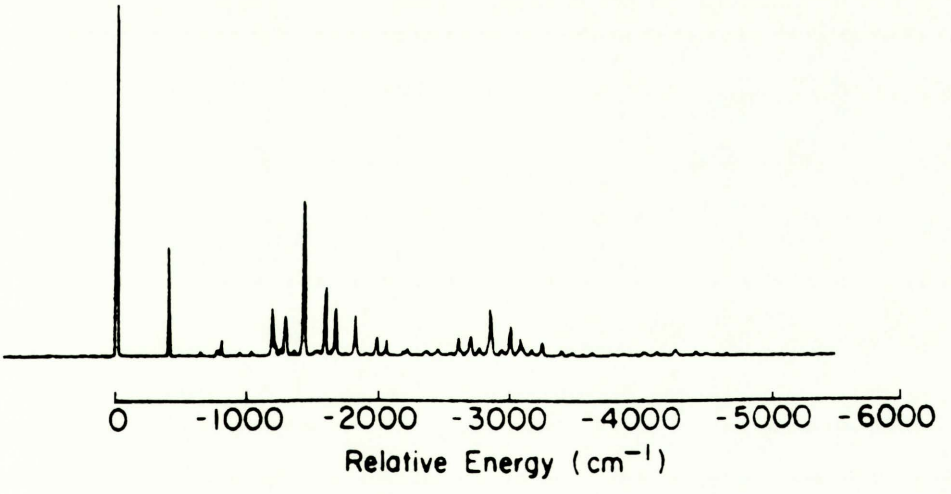


**Figure 1.2.** $0^0$ –level dispersed fluorescence spectrum of the anthracene molecule [7].

Figure 1.2 shows the dispersed fluorescence ($S_1 \rightarrow S_0$) spectrum of anthracene seeded in helium by excitation to the origin. The spectrum is very simple within a low frequency spectral region. The main molecular progression is built on 378 $cm^{-1}$ mode assigned to $12_1^0$ "breathing"

ring vibration. Authors analyzed the vibrational structure in terms of $a_g$ and $b_{1g}$ fundamentals. Comparing their results to earlier works (Raman and IR studies in low temperature matrices) they were able to identify nine $a_g$ modes and six $b_{1g}$ fundamental vibrational modes.

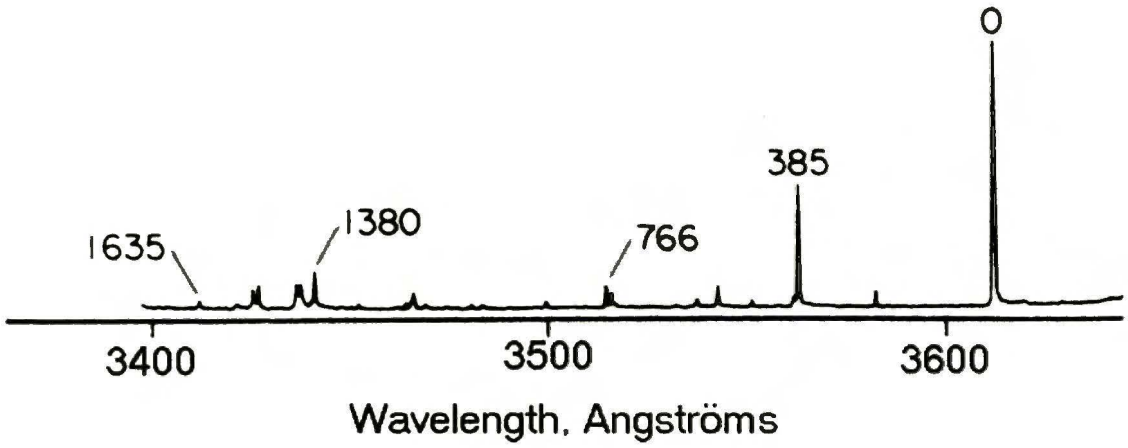


**Figure 1.3.** Normalized fluorescence excitation spectrum of the anthracene measured in the pulsed supersonic jet system [7]. Bands are labeled (in $cm^{-1}$) to give an idea of the energy scale.

Figure 1.3 shows fluorescence excitation ($S_1 \leftarrow S_0$) spectrum of "bare" anthracene. In order to assign the excited state vibrations, correlation with the ground state vibrational modes was performed. Dispersed fluorescence spectra have been taken by the excitation of the specific bands in the fluorescence excitation spectrum. By selective excitation of some vibrational modes, the corresponding bands between $S_1$ and $S_0$ electronic states will be enhanced.

At lower energies (0-1200 $cm^{-1}$) the authors of ref. [7] observe the fluorescence excitation spectrum mostly consisting of well-separated lines, assigned to fundamentals. Single vibronic level fluorescence spectra in this region are also composed from the discrete lines. Time-resolved experiments have shown the singly exponential fluorescence decay [11, 12].

In the spectral range 1300-1600 $cm^{-1}$ (distance from the 0-0 transition) of the fluorescence excitation spectrum, one can observe many overlapping vibronic lines. Fluorescence of most vibronic levels exhibits the exponential decay, except two transitions (1380 and 1420 $cm^{-1}$).

Quantum beats are observed on the fluorescence decay curves for these lines. This region could be characterized by restricted intramolecular vibrational energy redistribution (IVR).

At high energies (1600-2000 $cm^{-1}$) intensity of the fluorescence rapidly decrease. In addition, many bands in this energy region are inhomogeneously broadened. Due to the high density of states, fast dissipation of excitation energy via the nonradiative decay process takes place.

A number of theoretical works on the electronic and vibronic structure of anthracene derivatives, studied by *ab initio* [13, 14] and semi-empirical methods [15, 16, 17], both in the ground and first electronically excited states have been carried out. The geometry and vibrational structure of anthracene in the ground and excited states, calculated with *ab initio* methods, has been reported in [18, 19]. Authors of ref. [13] state that anthracene remains planar in $S_1$ and $T_1$ states and its geometry is not very different from the ground state. This conclusion is in agreement with experimental observation that the 0-0 band is the most intense transition in the fluorescence excitation spectrum. The main goal in this article was to assign the excited state vibronic structure. Most of vibrations in the excited state do not change significantly in comparison to the ground state, but one can notice some important differences. The strongest overtone is the $12a_g$ band, which is dominant in the spectrum. The standard deviation of the difference between the calculated with 3-21G basis set [20] frequencies and the experimental values for all modes was about 2.5%. The publication [14] presented normal mode calculations for the lowest excited state ($S_1$) of benzene, naphthalene and anthracene. The results are compared with the corresponding properties in the ground state ($S_0$) and with the existing experimental data for these molecules. It was found that the overall changes between anthracene geometries in the ground and first excited state are small what is in a good agreement with [13]. Additionally, these authors have assigned some of the remaining unassigned bands i.e. at 232, 473, 678, 775, 895 and 966 $cm^{-1}$ to the $b_{2g}$ vibrational modes. In the paper [17] the direct calculations by semiempirical QCFF/PI method [21] of vibrational anharmonicities were reported. Also these authors considered various possible sources of

spectral broadening of vibronic transitions and discuss their relationship to dynamic processes such as intramolecular vibrational redistribution (IVR). Theoretical study of calculated single vibronic level fluorescence spectra has also been reported [21].

The presence of one or two substituents modifies the vibronic spectra of anthracene, in particular the low frequency vibrational region. The most frequently studied anthracene derivatives, discussed in the literature, are these substituted in 9- and 10- positions of anthracene ring.

The work [22] reports on fluorescence excitation and single vibronic level fluorescence spectra of jet-cooled 9-cyanoanthracene. This system preserves many of the excited state dynamic and spectroscopic properties of the parent anthracene molecule. At the same time it exhibits the effects of lowering of the molecular symmetry from $D_{2h}$ to $C_{2v}$ and introducing the permanent dipole moment. On other hand, as a model for microscopic solvation, molecules with cyano group have unique characteristics, because they have three sites where solvent molecule could be attached, the triple bond of CN group, the nitrogen atom with unpaired electrons and π-electrons of anthracene moiety. Incorporation of the cyano group in the anthracene framework results in a red shift of the lowest $S_1 \leftarrow S_0$ electronic transition. Vibronic structure of this molecule in the first electronically excited state resembles main features of anthracene spectrum. The dominant in anthracene moiety, the breathing vibrational mode ($12a_g$) is modified (shifted) to 377 $cm^{-1}$. Substitution in 9 position of anthracene by a cyano group leads to appearing of new spectral features in low frequency region, at 128 $cm^{-1}$ and 214 $cm^{-1}$. The author in [23] assigns 128 $cm^{-1}$ vibronic mode to the in-plane bending mode of the cyano group coupled with ring vibration. The intense 214 $cm^{-1}$ mode, corresponds rather to another coupled cyano group vibration., than restricted 237 $cm^{-1}$ mode of anthracene [24]. Substitution of the 9- and 10- positions by the carbonitrile groups [25] significantly modifies the frequencies as well as the number of vibronic bands active in the fluorescence excitation spectrum. Authors

were unable to assign all low frequency vibronic bands to fundamental modes or their combinations, except the 95 $cm^{-1}$ band, which is due to the presence of the cyano groups.

In the case of 9-methoxyanthracene the lone pair electrons of the oxygen atom make this molecule an interesting candidate to study the microscopic solvation. In [26] authors reported the laser induced fluorescence spectrum recorded in a range 26700-28400 $cm^{-1}$ and a low-resolution dispersed fluorescence spectrum obtained by exciting the 0-0 transition of 9-methoxyanthracene. The structure of the vibronic spectra of this molecule is not so rich as for other anthracene derivatives studied by S. Hirayama's group. Due to poor vibronic structure authors in [26] easily assign some of the transitions to the $12a_g$ mode progression, which is dominating in all anthracene derivatives spectra. Low frequency modes 73 $cm^{-1}$, 105 $cm^{-1}$ were assigned to methyl group torsion, and 211 $cm^{-1}$, 236 $cm^{-1}$ were assigned to the combined bending–torsion mode of the methoxy group. Also it was found that the fluorescence decays for all vibronic transitions are singly exponential with the average lifetime about 20 ns. By excitation of bands with energy higher than 682 $cm^{-1}$ the fluorescence lifetime dramatically decreases.

In [27] the fluorescence excitation and dispersed fluorescence spectra of 9-methylanthracene were presented. Here the spectra in the low frequency range are dominated by the progression of methyl group torsion. The role of the methyl group torsion in the vibronic spectra of benzene derivatives was intensively studied in M. Ito group [28]. The authors of [27] examine the molecule in terms of possible models for the methyl torsional barrier in the case of 9-methylanthracene. Two low frequency modes 56 $cm^{-1}$ and 69 $cm^{-1}$ appear in fluorescence excitation spectrum. The single vibronic level dispersed fluorescence spectra clearly indicate that these vibronic modes of the excited state correspond to electronic ground state vibrations at 79 $cm^{-1}$ and 104 $cm^{-1}$. The low frequency modes of 9-methylanthracene can be described as the hindered rotation of the methyl group. The authors of ref. [27] assume that the potential barrier to methyl rotation must be about 100 $cm^{-1}$ in order to distribute this vibration to one of the

observed bands at 56 $cm^{-1}$ or 69 $cm^{-1}$. The single vibronic fluorescence recorded for higher energy transitions clearly shows the similarity of the vibronic energy redistribution processes in 9-methylanthracene to the processes that took place in the "bare" anthracene. These include increasing line broadening and lack of sharp structure, decreasing resonance fluorescence and the red-shifted bands. The single vibronic level fluorescence spectra allowed authors of ref. [27] to estimate quantitatively the relative rates of intramolecular vibronic energy redistribution in the 9-methylanthracene.

The influence of methyl group substitution on the intra- and intermolecular dynamics in the anthracene molecule is discussed also in [29]. In this article authors extend their studies to 2-methylanthracene. Fluorescence excitation spectrum of the jet-cooled 2-methylanthracene is presented and analyzed. The authors of [29] made the preliminary assignment of vibrational modes in the first electronically excited state. The spectrum is dominated by the progression the low-frequency torsion of the methyl group. The barrier estimated by authors [29] for the methyl group rotation in the excited $S_1$ state, is $V_3$ =70 $cm^{-1}$. This is to be compared with the ground state barrier, $V_3 \approx 300$ $cm^{-1}$. The change by 60° in the dihedral conformation of the methyl group with respect to the anthracene framework in $S_1$ electronically excited state was observed.

Theoretical studies with application of the electron density functional theory to the ground state of methylanthracenes substituted in 1-, 2- and 9- positions were carried out in [30] in order to understand how the position of substitution influences the ground state properties of the molecules.

The fluorescence excitation and dispersed fluorescence spectra of 9,10-cyanomethylanthrecene were measured in [24]. The fluorescence excitation spectrum for this molecule is more complex than for those of the parent anthracenes. There are many low frequency modes in the blue side from 0-0 transition in fluorescence excitation spectrum of 9,10-cyanomethylantracene. Authors suggest that these modes are due to the internal rotation of the methyl group and assign them to the $S_1 \leftarrow S_0$ transitions between rotational levels. The long

progression of these modes (39 $cm^{-1}$, 44 $cm^{-1}$) may suggest the geometry changes along this torsional coordinate during $S_1 \leftarrow S_0$ excitation. Also it was found that almost all vibrational transitions in the fluorescence excitation spectrum exhibit a doublet structure. Single vibronic level fluorescence spectra obtained for the excitation to the different vibronic transitions allow authors to make assignments of some ground state vibrational modes and their conformity to the excited state vibrational bands. Theoretical *ab initio* calculations carried out in [24] have shown a $\frac{\pi}{6}$ phase shift of the methyl group in the $S_1$ state in comparison to the ground state. The energy barriers for the rotation of the methyl group were calculated as 17 $cm^{-1}$ and 39 $cm^{-1}$ in the ground $S_0$ state and first electronically excited state, $S_1$, respectively.

And the last, but not least member of anthracene family under consideration is 9,10-dimethylanthracene. First experiments under supersonic jet conditions with this interesting molecule were reported by F. Tanaka *et al* [31]. One has to expect the similar behavior of this molecule to the rest of anthracenes. But the structure of the fluorescence excitation spectra is completely different from those reported for other anthracene derivatives. The fluorescence excitation spectrum shows a very rich vibrational structure in the low frequency region due to the coupled torsional motion of the two methyl groups. Fluorescence lifetimes of the main bands decrease rapidly with the excitation energy, which is in the contrast with other substituted anthracenes in the 9-, 10- positions. One of the transitions exhibits the different fluorescence lifetime which is dependent on the excitation wavelength within the band. Authors don't discuss such a behavior of the molecule. Further discussion of the 9,10-dimethylanthracene structure in the ground and first electronically excited state and *ab initio* theoretical calculations will be presented later in this work.

Pioneering works in the study of the complexes with rare gases molecules in supersonic jet were done by J. Jortner and co-workers [32, 33]. They have investigated the complexes formed between the large aromatic hydrocarbons, like anthracene, tetracene and pentacene, and the rare

gases neon: argon, krypton and xenone in order to model the microscopic solvent effects. For all these molecules, complexes with the stechiometry up to 1:7 were observed. For all these species the bands due to complexes were found to be red shifted relative to the "bare" molecule transitions and band intensities of complexes were proportional to $P_0^{2n}$, where $P_0$ - denotes the pressure of the rare gas, $n$ - coordination number of the complex. By close examination of the peak positions of the complexes it was found that the additivity relation was not fulfilled. This fact allows the authors to conclude that addition of a rare gas atom did not occur at the same geometry. In [34] authors were able to synthesize the anthracene, tetracene and pentacene molecules embedded in large clusters and have measured the fluorescence excitation and dispersed fluorescence spectra of these systems. The spectral shifts and line broadening of the 0-0 transition of anthracene increased with the stagnation pressure in range $P = 1000 - 2500$ torr and were independent in the range of pressure $P = 6000 - 14000$ torr. It was shown that energy-resolved and time-resolved emission spectroscopy of aromatic molecules in large argon clusters had provided the completed evidence for the occurrence of slow vibrational relaxation process on the nanosecond time scale. It is in contrast with vibrational relaxation occurring on the picosecond time scale for aromatic molecules in the rare-gas matrices [35, 36]. The paper [37] reports on the structure of van der Waals anthracene-argon$_n$ ($n$=1-6) clusters. Using the information about spectral shift ($\delta\nu$) and linewidths of the $S_1 \leftarrow S_0$ transition, the ionization energy shifts ($\delta$I.E.), the threshold widths and their comparison with the theoretical calculations, authors were able to determine the structure of the anthracene-argon clusters. It was shown that there are only two stable types of the geometry of anthracene-argon complexes, which represented different spectral features. One of them exhibits spectral features of cold, rigid like clusters, while the second was assigned to more or less "hot" clusters with most likely the same geometry as the "cold" ones, but excited to higher van der Waals vibrational levels via intracluster vibrational relaxation of anthracene molecule.

The absorption and fluorescence spectra of the complexes of 9,10-dichloroanthracene with argon$_n$ ($n$=1-4) were studied in [38]. From the absence of complex structure of the $S_1 \leftarrow S_0$ transition of the 9,10-dichloroanthracene-$Ar_1$ and 9,10-dichloroanthracene-$Ar_2$, authors conclude that only one chemical isomer exists for such complexes. The $S_1 \leftarrow S_0$ transition of the complexes with higher coordination number ($n$=3-6) exhibited some additional structure, which may be due to chemical isomers. Spectral shifts of $S_1 \leftarrow S_0$ transitions in 9,10-dichloroanthracene-$Ar_1$ and 9,10-dichloroanthracene-$Ar_2$ are additive. This fact, according to authors of ref. [38], may be the evidence for the two-sided configuration of the 9,10-dichloroanthracene-$Ar_2$ complex.

Helium clusters with aromatic molecules were studied in [39, 40]. Authors were able to probe the excitation of anthracene complexes up to 20 helium atoms by mass-selective methods without evidence of the fragmentation. All observed spectral shifts of the complexes were red with saturation of the shift at -38 $cm^{-1}$ for 12 helium atoms. It was observed that the spectra of anthracene-helium complexes with stechiometry up to 6 have a vibronic structure and this structure disappears in the spectra for larger complexes. The vibrational structure of the medium size anthracene-helium clusters ($n = 1-4$), according to authors of ref. [40], corresponds to nuclear excitations in the $S_1$ electronically excited state. The simplification of vibrational structure for larger clusters ($n$=5-20) can occur if the clusters become hot as more atoms are added.

The quantum mechanical calculations for the energetics, nuclear dynamics, spectral shifts and vibrational structure of anthracene-He$_n$ ($n$=1, 2) in the ground state and in the first excited $S_1$ electronic state were presented in [41]. The potential for anthracene-He cluster for both $S_0$ and $S_1$ states was described in terms of a sum of Lennard-Jones atom-atom potentials. For $S_1$ state, changes in dispersive energy and in repulsion interaction were also included in the calculations.

Large number of articles is devoted to the external heavy atom effect on the mechanisms and rates of intersystem crossing in the excited states of anthracene and other aromatic molecules. In [32] A. Amirav *et al.* have shown that tetracene exhibits a 1.5 times longer fluorescence lifetimes when complexed with Ar, but only one fourth of the lifetime of "bare" tetracene molecule is observed when complexed with Kr and even shorter lifetimes in the case of Xe clusters. Thus, the heavy atom effect is clearly present in tetracene clusters. In these clusters the triplet states, $T_n$ ($n \geq 2$) are situated lower than the $S_1$ state, and the strong spin-orbit coupling opens the channel for fast nonradiative process. Hirayama et al. [42] reported on lifetime measurements for the 9-cyanoanthracene embedded in the rare gases clusters for vibrationless $S_1 \leftarrow S_0$ transition and for the vibronic transitions. Experiment has shown the absence of the heavy atom effect on the intersystem crossing while exciting to the vibrationless transition. This may occur when $S_1$ state of the clusters remains lower than triplet $T_n$ ($n \geq 2$) states. However, when its energy is increased by only 214 $cm^{-1}$, a sudden drop of fluorescence lifetime (3 or even more times) is observed. Authors suggest that it is due to the energy flow from local vibrational modes to the intermolecular excited van der Waals modes. Exciting of these modes may lead to the dissociation of the cluster. In contrast to the 9-cyanoanthracene where the presence of the heavy atom does not invert the $S_1$-$T_2$ mutual position, the lifetime measurements for 9-methylanthracene clusters with rare gases (for this molecule $S_1 > T_2$ [43]) have shown the enhancement of the intersystem crossing rate.

There are also numerous interesting publications [25, 26, 31, 44, 45, 46, 47, 48] dedicated mostly to the influence of the clustering of various anthracene derivatives with rare gases on the intersystem crossing process, which could not be considered in this work.

Recently, attention increasingly turned to the interaction of polyatomics with solvent molecules ($H_2O$, $CH_3OH$, $C_6H_6$, $CHCl_3$, $CCl_4$). But the increasing complexity of these solvents adds a new level of challenge to the detailed structural characterization of the clusters. For small aromatic molecules, like benzene such investigations were carried out during last fifteen

years in groups of T. S. Zwier, B. Brutschy (complexes of substituted benzenes with water and methanol) and M. Ito (complexes of substituted benzenes with chloroform and carbon tetrachloride) by supersonic jet techniques [49-53,58, 62, 63].

Zwier with co-workers studied complexes of benzene molecule with water, methanol, chloroform and carbon tetrachloride. In [49], the resonant two-photon ionization (R2PI) spectra of benzene-$(H_2O)_n$ ($n$=1-5) complexes have been recorded. Authors conclude, using a combination of rotational band contour analysis and vibronic level analysis, that $C_6H_6$-$H_2O$ complex retains the sixfold symmetry of benzene with the oxygen atom on the sixfold axis. The complex involves a π hydrogen-bonding interaction. The structure of the $C_6H_6$-$(H_2O)_2$ complex incorporates two $H_2O$ molecules on one side of the benzene ring at a distance close to that in water dimer. The R2PI spectra of larger water clusters [50] are also consistent with an -O-H→π H-bond to benzene π-electron cloud. The clusters with $n$=3-5 were interpreted in terms of sequentially higher $H_2O$ rings and π hydrogen bonded with benzene ring via two or three $H_2O$ molecules. Addition of more $H_2O$ molecules does not seem to affect the benzene chromophore extensively. In [51] spectroscopical studies along with electron density theoretical calculations were extended to $(C_6H_6)_2$-$(H_2O)_8$ and $(C_6H_6)_2$-$(H_2O)_8$ gas-phase clusters. These investigations compared to DFT calculated minimum energy structures, vibrational frequencies, and IR intensities allow authors of [51] to assign the geometry as a cubic water octamers with $S_4$ and $D_{2d}$ symmetry attached to benzene via a π H-bond. In [52] Gruenloh *et al.* successfully characterized the topology of three isomers of the benzene-water$_9$ cluster with combination of the spectroscopic techniques and density functional theory calculations.

The R2PI studies were extended to the benzene-$(CH_3OH)_n$ ($n$=1-6) clusters [53]. The spectra of the 1:1 and 1:2 benzene-$CH_3OH$ clusters possess the vibronic level features, which are very similar to their aqueous counterparts. In the complexes with coordination numbers 1:1 the methanol molecule lies on or nearly to the sixfold axis of benzene. The spectral characteristics of the 1:2 cluster are consistent with both methanol molecules placed on the same side of

benzene. Higher $C_6H_6$-$(CH_3OH)_n$ clusters have shown some differences from the corresponding $C_6H_6$-$(H_2O)_n$ complexes. In [54] the studies of $C_6H_6$-$(CH_3OH)_n$ clusters with $n$=1-6 were continued using the resonant ion-dip infrared spectroscopy technique and theoretical *ab initio* calculations. The investigations of OH stretch vibrations of size-specific benzene-methanol$_n$ ($n$=1-6) clusters have confirmed the results of previous studies [53] for benzene-methanol complexes. The resonant two-photon ionization (R2PI), resonant ion-dip infrared (RIDIR) and infrared-ultraviolet (IR-UV) hole-burning spectroscopic techniques were applied to investigate the $(C_6H_6)_2$-$(CH_3OH)_3$ cluster [55].

Results of studies of the structure of water-methanol-benzene clusters have been reported by Hagemeister *et al.* [56]. The clusters benzene-water$_n$-methanol$_m$ ($m$+$n$=4, 5) exhibited in R2PI spectra the presence of H-bonded solvent cycles bounded to the $\pi$ system of benzene ring. Some of isomers of such complexes were theoretically predicted at the DFT B3LYP/6-31+G(d) level, but not all of isomers were observed experimentally.

The $S_0$-$S_1$ spectroscopy of the $C_6H_6$-$CCl_4$ complex formed in the supersonic jet has been reported by A. J. Gotch and coworkers in [57]. The structure of the van der Waals complexes was analyzed in terms of progressions involving the bend and stretch vibration of the van der Waals complex. Also by measuring the dispersed fluorescence spectra authors of ref. [57] were able to determine the ground and excited state binding energies of the complex. Vibronic bands analysis allowed to determine $C_s$ symmetry of the benzene-$CCl_4$ complex.

The spectroscopic studies of van der Waals complexes of fluorobenzene with $H_2O$, $CHCl_3$, $CCl_4$ conducted by Ito and co-workers [58] have shown that the ionization potential of the fluorobenzene molecule is reduced by the complexation. The authors suggest that the reduction in the ionization energy is due to the polarizability of surrounding solvent molecules and the Coulombic interaction between the ion and the photoejected electron trapped by the solvent molecules.

The spectroscopic studies of the substituted benzene derivatives were also carried out by many research groups. In particular, Mikami and collaborators studied microsolvatation of hydroxybenzenes [59, 60, 61]. Tarakeshwar and Kim [62, 63] studied microsolvated substituted benzenes by *ab initio* methods. Ito and co-workers intensively studied benzene derivatives microsolvated in many organic solvents [58].

Topp and co-workers extended their studies to the larger aromatic system i.e. anthracene clusters with water and methanol molecules [64, 65, 66, 67, 68]. The R2PI spectra of anthracene-water$_n$ ($n$=1-16) were reported in [64]. The results of this study are compared to previous data measured for the benzene- water$_n$, ($n$=1-8) clusters by T. S. Zwier's group [49, 51]. The spectral shifts of benzene- water$_n$, ($n$=1-3) clusters are observed at the blue side from the benzene electronic origin. In contrast to benzene-water clusters, anthracene-water clusters tend to reduce the $S_1 \leftarrow S_0$ transition energy of anthracene chromophore. Authors of ref. [64] conclude that for anthracene-$H_2O_1$ intermolecular hydrogen bond is destabilized by ionization. The water dimer cluster exhibits the strongest signal in the R2PI spectra of all clusters studied in [64]. Authors suggested that it is due to presence of multiple conformers of this clusters with similar binding energies and kinetic formation processes. Identification of multiple conformers can be done with IR-UV and UV-UV double resonance techniques. It was also suggested that the species with coordination number $n$=3 has a nonplanar geometry. The planar cyclic structures were assigned to tetramer and pentamer species. The authors [64] did not discuss the $n$=6 species due to the low signal to noise ratio in these spectra. The lowered dissociation energy for the heptamer water cluster with anthracene suggests that at least one water molecule is weakly bonded. It was found in earlier works of T. S. Zwier [49, 51] that tetramers are the basic building blocs for clusters. P. M. Palmer in [64], basing on this postulate, assigned the tetramer geometry for species $n$=8 and $n$=12.

In the following work authors focused their attention on the anthracene-methanol$_n$ ($n$=1-5) clusters [66]. The obtained results are compared with the benzene-methanol clusters [53]. The

clusters with coordination number $n$=1, 2 seem to be of the same geometry as those reported in ref. [53]. The anthracene-methanol$_1$ cluster exhibits an unusually large red shift on the $S_1 \leftarrow S_0$ transition, as compared to other clusters. This behavior, according to authors of ref. [53], suggests the presence of nearly-planar cyclic trimer, like the known isolated methanol cluster. It was observed, that n=6 cluster has two conformers. This was in good agreement to the known behavior of the isolated methanol clusters, in which the $n$=6 species is present in at least two comparable forms [69].

Much less attention was dedicated to the investigations of the structure of the clusters of anthracene derivatives with several solvents. The spectroscopic studies of the 1:1 complex of 9-cyanoanthracene with water, the structure analysis and theoretical calculations were presented in [70]. It was determined, that such a complex has side-type geometry, where water molecule is hydrogen-bonded to the π-electrons of the CN group of the 9-cyanoanthracene.

The complexes of 9-methoxyanthracene with alcohols were studied in [71]. The origin of the $S_1 \leftarrow S_0$ transitions of the complexes in most cases were blue shifted with respect to the $S_1 \leftarrow S_0$ transition of the bare molecule. The spectroscopic studies have revealed two kinds of complexation with protic solvents [72]. One of them was the "normal" van der Waals complex similar to those observed for other anthracenes, and the second, a complex for which hydrogen bond between solvent and oxygen atom of the methoxy group is formed.

In the chapter I have tried to present the state of the spectroscopic studies of the anthracenes, in particular anthracene clusters. As one may conclude from above overview, the studies of the complexes of anthracene are incomplete. At present time, with the appearance of new infrared double resonance techniques that helps to probe O-H stretching spectral region, it is easier to obtain spectroscopic information about the structure of complexes.

In this work I focused my attention on the anthracene derivatives. The six molecules (anthracene, 9-methylanthracene, 9-cyanoanthracene, 9-methoxyanthracene, 9,10-cyanomethyl-anthracene, 9,10-dimethylanthracene) have been chosen as the "base" aromatic molecules. The

main objective of this work was to deepen and extend the knowledge to the behavior of the anthracene derivatives clusters with organic solvents such as water, methanol, chloroform, carbon tetrachloride and benzene, and to try to determine their (clusters) structure, using the techniques available in the Institute of Physical Chemistry. Also I will try to show the role of different functional groups in very first steps of microsolvation process and how do they affect the clusters structure. I will also attempt to systematize the data known till now on the structure of the clusters of aromatic hydrocarbons with solvent molecules and to add to them the results of my research. Some of the results of this work have been already published [73] or are going to be published [24, 74] and presented on many conferences.

**References and notes**


1. A.W. Castelman, R.G. Keesee, *Ann. Rev. Phys. Chem.* **37** (1986) 525.
2. B. Brutschy, Chem. Rev. **100** (2000) 3891.
3. R. E. Smalley, L. Wharton, D. H. Levy, *J. Chem. Phys.* **63** (1975) 4977;
   R. E. Smalley, D. H. Levy, L. Wharton, *J. Chem. Phys.* **64** (1976) 3266;
   R. E. Smalley, L. Wharton, D. H. Levy, *J. Chem. Phys.* **66** (1977) 2750;
   J. E. Kenny, K. E. Johnson, W. Sharfin, D. H. Levy, *J. Chem. Phys.* **72** (1980) 1109;
   R. E. Smalley, L. Wharton, D. H. Levy, D. W. Chandler *J. Mol. Spectrosc.* **66** (1977) 365.
4. J. A. Warren, J. M. Hyes, G. J. Small, *Anal. Chem.* **54** (1982) 138.
5. R. Fraenkel, U Samuni, Y. Haas and B. Dick, *Chem. Phys. Lett.* **203** (1993) 523.
6. J. Wolf and G. Hohlneicher, *Chem. Phys.* **181** (1994) 185.
7. W.R. Lambert, P. M. Felker, J. A. Syage and A. H. Zewail, *J. Chem. Phys.* **81** (1984) 2195.
8. W. R. Lambert, P.M. Felker and A. H. Zewail, *J. Chem. Phys.* **75** (1981) 5958.
9. A. Amirav, U. Even and J. Jortner, *Chem. Phys.* **51** (1980) 31.
10. A. Amirav, U. Even and J. Jortner, *J. Anal. Chem.* **54** (1982) 1666.
11. W.R. Lambert, P. M. Felker and A. H. Zewail, *J. Chem. Phys.* **81** (1984) 2209.
12. W.R. Lambert, P. M. Felker and A. H. Zewail, *J. Chem. Phys.* **81** (1984) 2217.
13. S. Zilberg, U. Samuni, R. Fraenkel, Y.Haas, *Chem. Phys.* **186** (1994) 303.
14. G. S. Jas, K. Kuczera, *Chem. Phys.* **214** (1997) 229.
15. F. Zerbetto and M. Zgierski, *Chem. Phys.* **127** (1988) 17
16. S. Ramasesha, D. S. Galvao and Z. G. Soos, J. Phys. Chem. **97** (1993) 2823.
17. D. Gruner, An Nguyen, and P. Brumer, *J. Chem. Phys.* **101** (1994) 10366.
18. J. Szczepanski, M. Vala, D. Talbi, O. Parisel and Y. Ellinger, *J. Chem. Phys.* **98** (1993) 4494.
19. D. J. DeFrees, M. D. Miller, D. Talbi, F. Pauzat and Y. Ellinger, *Astrophys. J.* **408** (1993) 530.
20. W. H. Hehre, L. Radom, P. von R. Schleyer and J. A. Pople, *Ab initio* molecular orbital theory (Waley, New York, 1986).

21. A. Warshel, in *Modern theoretical Chemistry*, edited by G. A. Segal (Plenum, New York, 1977), Vol. 7, Part A.
22. A. Amirav, *Chem Phys* **124** (1988) 163.
23. S. Hirayama, *J. Chem. Phys.* **85** (1986) 6867.
24. A. Mordziński, A. Leś, D. H. Levy, Y. Stepanenko, L. Adamowicz, J. Rycombel, to be published.
25. S. Hirayama, F. Tanaka, K. Shobatake, *Chem. Phys. Lett.* **140** (1987) 447.
26. S. Hirayama, F. Tanaka, K. Shobatake, *Chem. Phys. Lett.* **153** (1988) 112.
27. J. A. Syage, P. M. Felker, D. H. Semmens, F. Al Adel and A. H. Zewail, *J. Chem. Phys.* **82** (1985) 2896.
28. J. Murakami, M. Ito and K. Kaya, *Chem. Phys. Lett.* **80** (1981) 203.
29. H. Lin, J. A. Hunter and J. Pfab, *Chem. Phys. Lett.* **210** (1993) 38.
30. C. W. Bauschlicher, Jr, S. R. Langhoff, *Chem. Phys.* **234** (1998) 79.
31. F. Tanaka, S. Hirayama, K. Shobatake, *Chem. Phys. Lett.* **195** (1992) 243.
32. A. Amirav, U. Even, J. Jortner, *J. Chem. Phys.* **75** (1981) 2489.
33. A. Amirav, U. Even, J. Jortner, *J. Phys. Chem.* **85** (1981) 309.
34. A. Amirav, U. Even, J. Jortner, *J. Phys. Chem.* **86** (1982) 3345.
35. K. Rebane and P. Saari, *J. Lumin.* **12/13** (1976) 23.
36. T. Tann, P. Saari, *Opt. Spectrosk.* **36** (1974) 328.
37. D.Uridat, V. Brenner, I. Dimicoli, J. Le Calvé, P. Millié, M. Mons, F. Piuzzi, *Chem. Phys.* **239** (1998) 151.
38. A. Amirav, M. Sonnenschein and J. Jortner, *Chem. Phys.* **88** (1984) 199.
39. U. Even, J. Jortner, D. Noy, N. Lavie and C. Cossart-Magos, *J. Chem. Phys.* 112 (2000) 8068.
40. U. Even, I. Al-Hroub and J. Jortner, *J. Chem. Phys.* **115** (2001) 2069.
41. A. Heidenreich, U. Even, and J. Jortner, *J. Chem. Phys.* **115** (2001) 10176.
42. S. Hirayama, K. Shobatake and K. Tobayashi, *Chem. Phys. Lett.* **121** (1985) 228.
43. F. Tanaka, M. Okamoto, S. Yamashita and H. Teranishi, *Chem. Phys. Lett.* **123** (1985)228.
44. A. Amirav and J. Jortner, *Chem. Phys. Lett.* **132** (1986) 335.
45. F. Tanaka, S. Hirayama, K. Shobatake, *Chem. Phys. Lett.* **164** (1989) 335.
46. F. Tanaka, Y. Tanaka, S. Hirayama, M. Kono, K. Shobatake, *Chem. Phys. Lett.* **252** (1996) 258.
47. F. Tanaka, K. Morimoto, H. Kubo, Y. Yada, S. Hirayama, M. Kono and K. Shobatake, *J. Chem. Soc., Faraday Trans.* **93** (1997) 3013.
48. L. C. T. Shoute, S. Hirayama, R. P. Steer, *Chem. Phys. Lett.* **338** (2001) 123.
49. A. J. Gotch, A. W. Garrett, D. L. Severance and T. S. Zwier, *Chem. Phys. Lett.* **178** (1991) 121.
50. A. J. Garrett and T. S. Zwier, *J. Chem. Phys.* **96** (1992) 3402.
51. C. J. Gruenloh, J. R. Carney, F. C. Hagemeister, C. A. Arrington and T.S. Zwier, S. Y. Fredericks, J. T. Wood III and K. D. Jordan, *J. Chem. Phys.* **109** (1998) 6601.
52. C. J. Gruenloh, J. R. Carney, F. C. Hagemeister, C. A. Arrington and T.S. Zwier, J. T. Wood III and K. D. Jordan, *J. Chem. Phys.* **113** (2000) 2290.
53. A. J. Garrett, D. L. Severance and T. S. Zwier, *J. Chem. Phys.* **96** (1992) 7245.
54. R. N. Pribble, F. C. Hagemeister and T. S. Zwier, *J. Chem. Phys.* **106** (1997) 2145.
55. R. N. Pribble, C. Gruenloh, T. S. Zwier, *Chem. Phys. Lett.* **262** (1996) 627.
56. F. C. Hagemeister, C. J. Gruenloh, T. S. Zwier, *Chem. Phys.* **239** (1998) 83.
57. A. J. Gotch, A. W. Garrett and T. S. Zwier. *J. Chem. Phys.* **95** (1991) 9699.
58. N. Gonohe, H. Abe, N. Mikami and M. Ito, *J. Chem. Phys.* **89** (1985) 3642.
59. S. Tanabe, T. Ebata, M. Fujii, N. Mikami, *Chem. Phys. Lett.* **215** (1993) 347.
60. N. Mikami, S. Sato, M. Ishigaki, *Chem. Phys. Lett.* **202** (1993) 431.
61. A. Fujii, A. Iwasaki, N. Mikami, *Chem . Lett.* (1997) 1099.

62. P. Tarakeshwar, K. S. Kim, B. Brutschy, *J. Chem. Phys.* **110** (1999) 8501.
63. P. Tarakeshwar, K. S. Kim, B. Brutschy, *J. Chem. Phys.* **112** (2000) 1769.
64. P. M. Palmer, M. R. Topp, *Chem. Phys.* **239** (1998) 65.
65. P. M. Palmer, M. R. Topp, *Chem. Phys. Lett.* **286** (1998) 113.
66. P. M. Palmer, M. R. Topp, *Chem. Phys. Lett.* **292** (1998) 307.
67. P. M. Andrews, B. A. Pryor, P. M. Palmer, M. R. Topp, *Chem. Phys. Lett.* **265** (1997) 224.
68. P. M. Andrews, B. A. Pryor, M. B. Berger, P. M. Palmer, M. R. Topp, *J. Phys. Chem. A.* **101** (1997) 6222.
69. U. Buck, I. Ettischer, *J. Chem. Phys.* **100** (1994) 6974.
70. K. Egashira, Y. Ohshima, O. Kajimoto, *Chem. Phys. Lett.* **334** (2001) 285.
71. F. Lahmani, E. Bréhéret and J. Sepioł, *J. Photochem. Photobiol. A: Chem* **62** (1991) 33.
72. F. Lahmani and J. Sepioł, *Chem. Phys. Lett.* **189** (1992) 479.
73. Y. Stepanenko, A. Vdovin, J. Jasny, J. Sepioł, A. Mordziński, *J. Mol. Struct.* **480-481** (1999) 595.
74. Y. Stepanenko, A. Sobolewski and A. Mordziński, *Chem. Phys. Lett.*, to be published.

## CHAPTER 2. Experimental and theoretical methods, instruments and objects

### *2.1. Experimental methods.*

Spectroscopy is one of the most powerful tools for probing the microscopic details of the structure of molecules and the dynamics of chemical processes.

Molecular gas-phase spectra are rich and very structured, and the information content is high if these spectra can be understood. Even in small molecules a very large number of quantum states are populated at ordinary laboratory temperatures. Each populated state may contribute in several lines to the spectrum. In effect, the spectrum consists of an enormous number of individual lines. In principle the more complex molecular spectrum is, the more information it contains. In order to resolve this information, it is important to reduce the number of spectral lines.

Supersonic jet spectroscopy is a simple and effective method used for obtaining the highly resolved spectra. It completely differs from corresponding methods applied to solid state. In supersonic jet spectroscopy all experiments are carried out in a gas flow. Mechanisms of band broadening in the gas phase and solid state differ essentially at low temperatures. In the gas phase all molecules are virtually isolated. Inhomogeneous broadening due to interactions with solvent molecules or other molecules, the main factor responsible for band broadening in a solid state, can be neglected. Electron phonon interactions are also absent in a gas phase. The main reasons of band broadening in the gas phase are population of higher rotational and vibrational states and the Doppler effect (nonuniform velocity distribution). Many rotational and even some vibrational states of electronic ground state will be populated at high temperatures. For a large molecule with large moment of inertia, rotational states can be found extremely dense (~0.1 $cm^{-1}$). In addition, all rotational sublevels are broad due to Doppler effect. The broadening due to this effect is comparable to the separation of rotational levels. For

this reason, each vibrational level will exhibit the rotational contour by several wavenumbers wide and increasing with temperature. As one can notice all these mechanisms are strongly temperature dependent.

In the gas phase spectral bandwidth is limited only by lifetime of the states involved in the transition. In contrast to the solid-state, where the electron-phonon interaction does influence the shape of vibrational band. Moreover, molecules in the gas phase have less opportunity to loose their energy nonradiatively, than in the solid state due to absence of interactions with the solvent molecules. Therefore, it is expected that the lifetime of fluorescence will be longer and the bands corresponding to vibronic transitions are narrower in the gas phase than in the condensed phase.

Nevertheless, for transitions from higher vibrational states, it is possible to observe the line broadening. It can be explained by intramolecular energy redistribution, a process that involves a scrambling of the vibrational energy level of the excited vibronic state over many vibrations to which it may be coupled [1]. One can observe line broadening in the emission spectra, while exciting relatively high vibronic states ($E_{vib}$>1800 $cm^{-1}$ for tetracene and $E_{vib}$>1300 $cm^{-1}$ for anthracene in a supersonic jet [2]), even upon the selective laser excitation.

It is then clear that for obtaining narrow bands in the gas phase low temperatures have to be used. This objective is effectively achieved in supersonic jet spectroscopy. The mechanism of cooling process in supersonic jet will be described below in this chapter. Supersonic jet was first proposed in 1951 as a molecular beam source by A. Kantovitz and J. Grey [3] and experimentally realized by G. Kistiakowski and W. Slitcher in the same year [4]. But only in 1974, with development of the narrow band dye lasers, first spectroscopic results were published [5].

### *2.1.1. Supersonic free jets and molecular beams. How it works?*

- Supersonic expansion of molecular species results in the depopulation of excited internal energy levels. Hence, the relative population of the lowest rotational, and also pure vibrational, energy levels is increased, both with expansion in vacuum of molecules under study, and with expansion with the use of inert gas as a carrying medium. This effect reduces spectral congestion and significantly simplifies recorded spectra due to the changes in Boltzmann distribution of molecules. Depopulation efficiency of excited rotational and vibrational energy levels will depend on nature of collision processes in the supersonic beam as well as on the particular structure of molecules used for experiment.

- The use of collimated beams can significantly lower the Doppler broadening effect for investigated molecules. Such a collimation can be realized by introducing one or even more skimmers, lowering of the Doppler effect by 10-50 times, depending on experimental conditions.

- Low translational temperatures, achievable in supersonic beams, can lead to formation of relatively large number of weakly bonded molecular complexes. It is difficult to obtain them under conditions of large number of collisions, for example under condition of static gas.

A supersonic free jet is formed when gas expands from high-pressure region to low-pressure region through the small orifice.

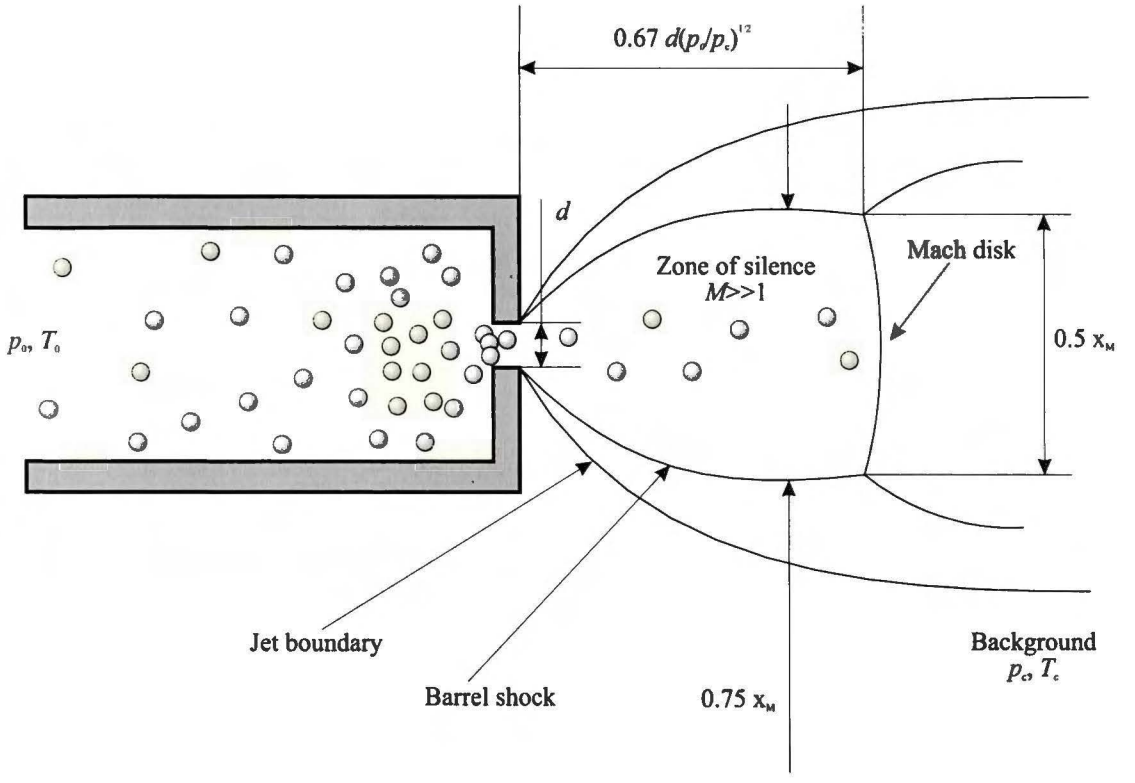


**Figure 2.1.** Schematic visualization of a continuous free jet expansion from a nozzle.

Figure 2.1 shows some of the basic features of a free jet expansion. As the area of the nozzle decreases toward to the exit, the pressure difference ($p_0$-$p_c$) will accelerate the carrier gas. If $p_0/p_c$ will be less than the critical value $\left(\frac{(\gamma+1)}{2}\right)^{\gamma(\gamma-1)}$, where $\gamma$ is the ratio of the heat capacities $C_p/C_v$, the flow will escape from the nozzle with the sonic speed ($M$=1, Mach number for local speed of sound is given by $v/a$, $v$ and $a$ being the flow speed of the jet and sound velocity, respectively). On the other hand, if the ratio of pressures is less than the critical value (< 2.1 for all gases) a stream will exit from the nozzle with the speed lower than the speed of sound. In the last case such an expansion to the low-pressure region proceeds with relatively low number of collisions (mean free path $\lambda_0 < d$, where $d$ - denotes nozzle diameter) and not accompanied by the changes in population distribution in the internal degree of freedom in the seeded molecules. Such an expansion with subsonic speeds does not have the previously described advantages of the supersonic expansion, which is very useful for spectroscopy. In supersonic

beams, the expansion proceeds with the speeds near to $M$=1. "Cold" molecules of the supersonic beam collide with relatively "warm" molecules in the vacuum chamber and form a shock wave around the beam. Shock wave dimensions were characterized in [6]. The distance from the nozzle to the Mach disk [see Figure 2.1] is approximated by the equation $x_M = 0.67d\left(\frac{p_0}{p_c}\right)^{1/2}$. The Mach disk and barrel shock diameters are approximately $0.5x_M$ ±25% and $0.75x_M$ ±25% respectively. The characteristics of the flow contained in the "barrel" allow spectroscopists to take full advantage of the cooling effects of the expansion, i.e. interesting complexes are formed and the spectra are less complicated due to the decrease of rotational temperature. If one considers the ideal gas expansion, neglecting the effect of heat conduction and viscosity, then the first law of thermodynamics can be used to estimate the changes in molecular density with distance from the nozzle, R. For expansion with constant $\gamma$:

$$\rho = \rho_0\left(1+\frac{(\gamma-1)}{2}M^2(R)\right)^{\frac{1}{\gamma-1}}.$$

With such an approach molecular density depends only on initial density $\rho_0$ and Mach number $M(R)$, which itself depends on the distance from the nozzle. On sufficient distances ($R/d$ > 10) the jet can be approximated as a spherical expansion from a point source and the Mach number can be evaluated as:

$$M(R) = A\left(\frac{R}{d}\right)^{\gamma-1} - \frac{(\gamma+1)/(\gamma-1)}{2A(R/d)^{\gamma-1}} \approx A\left(\frac{R}{d}\right)^{\gamma-1},$$

where for monoatomic gas $\gamma$ = 1.67, $A$ = 3.3.

Closer to the orifice ($R/d$ < 3), this approximation does not work and the following equation should be used:

$M(R) = 1.0 + A\left(\frac{R}{d}\right)^2 + B\left(\frac{R}{d}\right)^3$, where for ideal gases $A$ remains the same as in the previous equation, $B$ = -1.541.

The large number of collisions occurring during the first stages of a supersonic expansion do not only cool the expanding mixture, but can also produce the relatively large concentrations of molecular clusters. Seeded molecular species are cooled though the binary collisions, while the three-body collisions are responsible for the formation of clusters. It is significantly difficult to quantify the amount of clustering in a supersonic jet expansion. It was proposed by E. L. Knuth [7] the approximate analytical form that uses two dimensionless parameters $D^*$ and $C^*$ to determine the extent of clustering:

$$D^* = \frac{p_0}{(\varepsilon/\sigma^3)}\left(\frac{d}{\sigma}\right)^{0.4}\left(\frac{kT_0}{\varepsilon}\right)^{-2.4} >\sim 0.1$$

and

$$C^* = \frac{p_0}{(\varepsilon/\sigma^3)}\left(\frac{d}{\sigma}\right)^{0.88}\left(\frac{kT_0}{\varepsilon}\right)^{-2.3} >\sim 15$$

where $d$ is the nozzle diameter in cm, $p_0$ (in Torr) and $T_0$ (in K) are the reservoir stagnation pressure and temperature, $k$ is the Boltzmann constant, $\varepsilon$ is the Lennard-Jones parameter and $\sigma$ is the collisional cross-section.

Dimer formation exceeding 1% occurs if the parameter $D^*$ exceeds 0.1. For contributions larger than 10% of dimer formation $D^*$ must be larger than 0.4. Trimers and larger complexes of monoatomic gases will be formed if the parameter $C^*$ is greater than ~15.

Pulsed supersonic nozzles allow us to achieve higher molecular concentrations in jet, better vibrational "cooling", lower condensation in comparison to continuous expansions. In addition, a pulsed nozzle reduces stress for the vacuum system, used for jet expansion. For the nozzle with a diameter 1 mm and pressure 0.5 - 2.5. atm (frequently used parameters) it was shown that it is possible to reach the translational temperatures ($T_t$) about 0.6-10 K, rotational temperatures ($T_r$) ~2-50 K and vibrational temperatures ($T_v$) ~10-100 K. The effective rotational and vibrational "cooling" functions of seeded molecules in such pulsed jets are thus expected to be lower than in continuous supersonic free jets under corresponding conditions. These

characteristics allow obtaining better signal to noise ratio for transitions from the lowest rotational levels. The main disadvantage of the pulsed jet apparatus is the presence of movable mechanical parts that limit the working frequency of such a nozzle.

Also, one has to notice that the use of pinholes or skimmers allows to limit the velocity distribution of the molecules and to collimate the expanded gas mixture. Such systems are referred to as supersonic molecular beams. This technique gives the chance to reduce the Doppler broadening effect.

Apparatus for obtaining supersonic jet, usually consists of three main parts, namely: high vacuum chamber or chambers with an ejection system, the laser system for excitation the molecules studied and the detection part. The number of vacuum chambers and kind of detection system depends on the type of experiment, which one is going to carry out.

### *2.1.2.Spectroscopic techniques of detection of molecules in the supersonic beam.*

*a) laser induced fluorescence (LIF).*

This is the most popular method for the measurement of the electronic absorption spectrum of a molecule in a jet. The principle of this method is shown in Figure 2.2a.

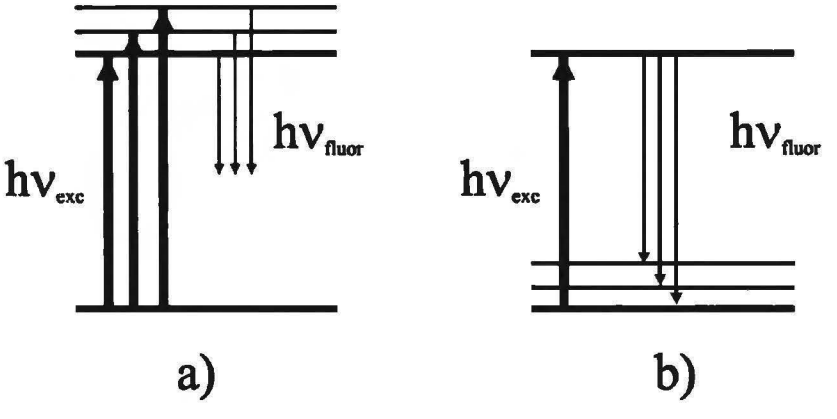


**Figure 2.2.** a) fluorescence excitation spectroscopy, b) dispersed fluorescence spectroscopy.

Tuneable laser light crosses the supersonic jet and the total fluorescence originated from the excited molecules in the jet is detected. By scanning the laser we detect the change of fluorescence intensity as a function of excitation wavelength. Generally, LIF spectrum corresponds to the absorption spectrum. However, the fluorescence excitation spectrum could not completely be identical with the absorption spectrum if the fluorescence quantum yields are not identical for different vibronic transitions. The spectral resolution is determined by the laser linewidth. The vibrational structure appearing in the fluorescence excitation spectra represents the vibrational levels in the electronic excited state.

*b) single vibronic level fluorescence (SVLF).*

The fluorescence originating from a particular excited transition is dispersed by a monochromator. As shown in Figure 2.2b the molecule is excited by the laser light of fixed frequency $\nu$ to a particular vibronic transition and the fluorescence dispersed by monochromator is observed. In this case, the resolution is limited by the resolution of the monochromator. The dispersed fluorescence spectra obtained in a supersonic jet are useful in obtaining the ground state vibrational levels of the molecule in the gas phase.

*c) resonance enhanced multiphoton ionisation (REMPI) TOF.*

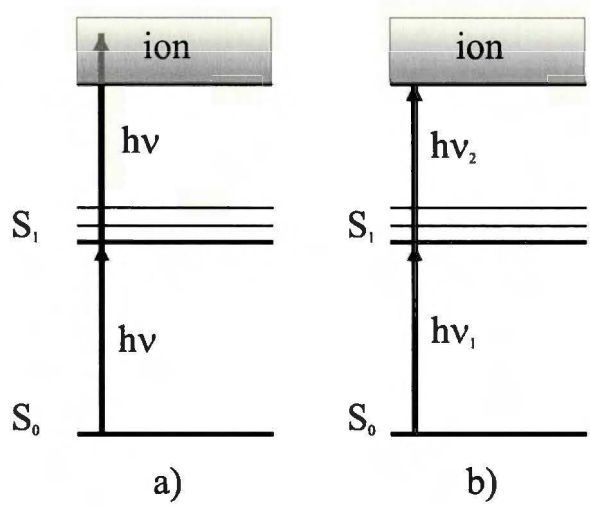


**Figure 2.3.** Multiphoton ionization spectroscopy a) one color two-photon ionization scheme, b) two-color two-photon ionization spectroscopy.

The principle of the resonance enhanced two-photon ionization spectroscopy is shown in Figure 2.3. In the case shown in Figure 2.3a, where ionization occurs with two photons and the first photon is resonant with the $S_1 \leftarrow S_0$ transition, the spectrum obtained is called a one-color resonant two-photon ionization spectrum. It is also possible to obtain multiphoton ionization spectrum by using two different photons. As shown on Figure 2.3b, the first laser of $\nu_1$ is used to excite a molecule to the $S_1$ state and then another photon $\nu_2$ is used to promote further the excited molecule to the ionization threshold. By scanning $\nu_2$ it is possible to ionize the molecule as shown on Figure 2.3b. Ions produced are then accelerated by the applied electric field. The delay time between ionization and reaching the detector by the ion (time-of-flight (TOF)) depends on the mass of the ion.

*d) spectral "hole burning" (two resonance vibration depletion)*

The fluorescence excitation spectrum of a mixture Fl(A+B) consists of bands belonging to the species A and B. In order to resolve and select the vibrational structure, a second (probe) laser is used. The probe laser is fixed on the selected transition. When the pump laser scans through transitions belonging to the species in a beam, the ground state population of these species is decreased. Since the time for total recovery of the initial ground state population in jets is usually long (>1 $\mu$s), the decrease of fluorescence signal emitted by the probe can monitor the reduced population. The decrease of the signal will be seen only when the probe laser is in resonance with the transition belonging to the selected species.

### *2.1.3. Vacuum system and nozzle construction.*

It is very important to make collision free conditions in a vacuum chamber. In order to maintain a constant low pressure conditions in the vacuum chambers, high rate diffusion pumps (6000 l/s, 2000 l/s) backed by fast rotary oil pumps (60 $m^3$/h, 90 $m^3$/h) are used. A part of the measurements was carried out on the rebuilt system. Here, the turbomolecular pump (650 l/s)

supported by Roots pump was applied. For differentially pumped two-chamber scheme, the turbomolecular pump (250 l/s) in combination with rotary oil pump (30 $m^3$/h) were used to evacuate the second chamber. The chambers were separated by 2 mm skimmer (*Beam Dynamics Inc.*) in order to collimate the molecular beam.

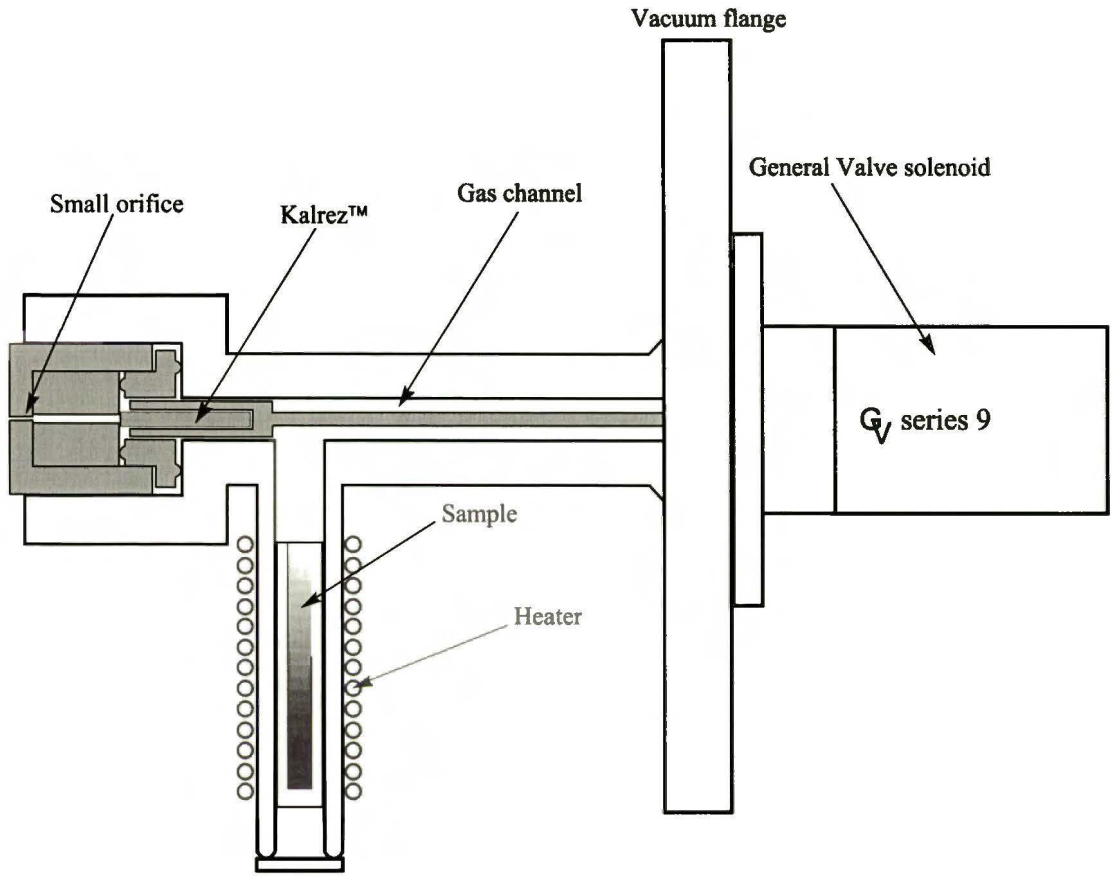


**Figure 2.4.** Schematic drawing of the modified "General Valve series 9" pulsed valve.

Figure 2.4 shows the schematic design of the pulsed valve used in our experiments. It is based on commercially available *General Valve Series 9*. Some modifications made possible to heat samples to the temperatures as high as 300 °C. Solenoid body was mounted on the massive metal flange to provide sufficient heat conductivity. Standard piston was replaced by the long metal needle. On the end of the needle a piece of high temperature Kalrez™ was mounted. The Kalrez™ provided precise and seal closing of the orifice. This modified nozzle was used both in TOF and LIF spectrometers. In order to obtain molecular clusters with solvents, the carrier

gas (helium 99.999% in my case) was passed through temperature regulated bubbling reservoir, containing solvent vapors. Concentration of the solvent in the carrier gas was controlled by the temperature of the reservoir. The temperature was regulated within -190 °C ÷ +80 °C range. The nozzle was operated with the repetition rate up to 10 Hz with typical pulse duration 150 ÷ 700 μs. The pulse duration was optimized during measurement to obtain the best experimental conditions.

### *2.1.4.Coherent light sources.*

Tunable dye lasers and optical parametric oscillators were used as coherent narrow-band light sources. Dye lasers were pumped by XeCl excimer laser (LPX 105i, Lambda Physik) or by frequency doubled or tripled Nd:YAG lasers (Surelite I-10, Powerlite 800 Continuum). Two different designs of dye laser resonator were used.

The first one used prism beam expander and a diffraction grating as an end mirror. Spectral width of the laser beam in such arrangement was <0.2 $cm^{-1}$ and the average energy, obtained from the oscillator, was typically 100-200μJ. The laser could be tuned over the whole spectral range of the dye laser applied by changing the incident angle of the diffraction grating.

Incident grating scheme was used in the resonator of the second dye laser. This design allows obtaining ~1.2 $cm^{-1}$ wide laser line. It was possible to achieve <0.1 $cm^{-1}$ spectral width of laser line by using Fabry-Perot etalon inside the optical cavity. The average energy was 100-150μJ and 50-100μJ with and without etalon, respectively. Changing the angle between end mirror and diffraction grating enabled tuning of this laser. Three different gratings 1200, 1800 and 2400 lines/mm were used to achieve optimal parameters of laser in different spectral regions. Both dye laser systems were constructed by Dr. Jan Jasny.

Typical tuning curve for dye lasers starts from ~330nm for a laser pumped by excimer laser and from ~368nm for a laser pumped by frequency tripled Nd:YAG laser. The dyes from

Lambda Physik and Exciton were used, as an active media in dye lasers. Concentration of dyes and a kind of solvent were taken from the information bulletins of the corresponding manufacturer [8, 9]. The dye solutions were optimized to achieve higher energy and/or a wider tuning range.

As an alternative source of tunable laser radiation, optical parametric oscillator was used. The operation principle of optical parametric oscillator (OPO) slightly differs from operation principle of lasers. The OPO is based on the parametric interaction of the strong pumping wave $\omega_p$ with molecules in a media (crystal in our case), which has a large nonlinear susceptibility. This phenomenon can be illustrated as an inelastic scattering of the pumping photon $\omega_p$ by a molecule where pumping photon is absorbed and two new photons $\omega_s$ and $\omega_i$ are generated. Two main conditions have to be fulfilled to start parametric oscillations. First, phase matching condition $k_p = k_s + k_i$, which may be regarded as the conservation of momentum for the three photons elaborated in the parametric process. Second, conservation of energy at all points of active media $\omega_p = \omega_s + \omega_i$. The phase matching condition selects infinite number of waves $\omega_s + \omega_i$ and only single pair $\omega_s$, $k_s$ and $\omega_i$, $k_i$ is determined by the orientation of the nonlinear crystal with respect to $k_p$. If nonlinear crystal is placed inside an optical resonator, oscillations on signal and idler waves can start when the gain exceeds the total losses. The optical cavity can be constructed in a way to be resonant for both signal and idler waves (doubly resonant oscillator) or only for one signal or idler wave (single resonant oscillator). Doubly resonant oscillators can be collinear or non-collinear. In non-collinear one each wave has its own resonator, in collinear arrangement the same resonator is used for signal and idler waves and both waves are emitted in the same direction.

There are two types of wave phase matching in nonlinear crystals. The first type is when ordinary pump wave "splits" into two extraordinary waves. Parametric oscillators built according this scheme have low threshold and high conversation coefficient. The main lack of such design is the relatively large spectral width of emitted signal and idler waves (~3-6 $cm^{-1}$

with 1 $cm^{-1}$ pumping) without using additional line narrowing elements in the optical cavity. The second type is when the extraordinary wave "splits" into ordinary and extraordinary waves. The basic advantages of this scheme are relatively narrow spectral width of generated radiation and ease of spatial separation of signal and idler beams by using beamsplitters. In this work the commercially available OPO (Continuum Sunlite) was used. The spectral range 440÷1800 nm was covered. Typical spectral linewidth was <0.2 $cm^{-1}$.

Recently, with availability of crystals with high optical nonlinearity ($\beta$-barium borate BBO), the popularity of parametrical generators has increased. One of the main advantages of the parametrical generator over dye lasers is their tunability in a wide spectral range (410 nm - 2.3 μm, pumped by 355 nm) without replacement of an active element. To achieve the UV spectral range the technique of nonlinear frequency doubling was used. As the nonlinear media for frequency doubling, BBO and KDP crystals were used. It allows obtaining the tunable laser radiation within the range 225-330 nm.

The wavelength calibration of all lasers was done by the spectrograph constructed by Dr. J. Jasny.

*2.1.5. Optical and mass selective detection.*

*a) optical detection.*

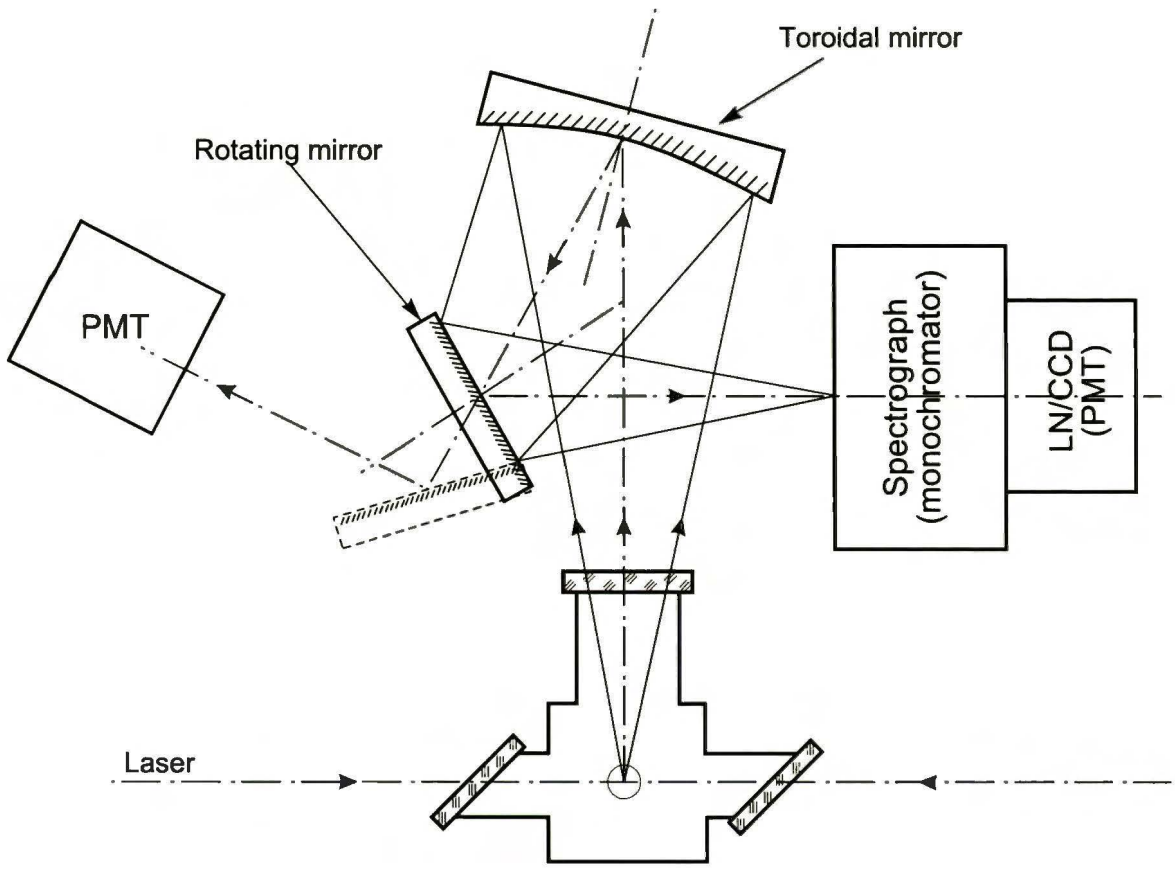


**Figure 2.5.** General scheme of the optical layout of the detection system.

Optical system was constructed by Dr. Jan Jasny. Schematic design is illustrated in the Figure 2.5. The detection system consists of the toroidal mirror, which serves as *f/1* optics and images the fluorescence onto the photomultiplier or monochromator slit. The rotating mirror allows a quick switching between the photomultiplier or the spectrograph/monochromator. Acton Research 0.275m spectrograph with 600 l/mm and 1800 l/mm diffraction gratings in combination with Princeton Instruments LN cooled CCD was used to obtain dispersed

fluorescence spectra. The system designed in this way allows to minimize the background signal from the scattered light and to improve the signal to noise ratio.

*b) mass resolved detection.*

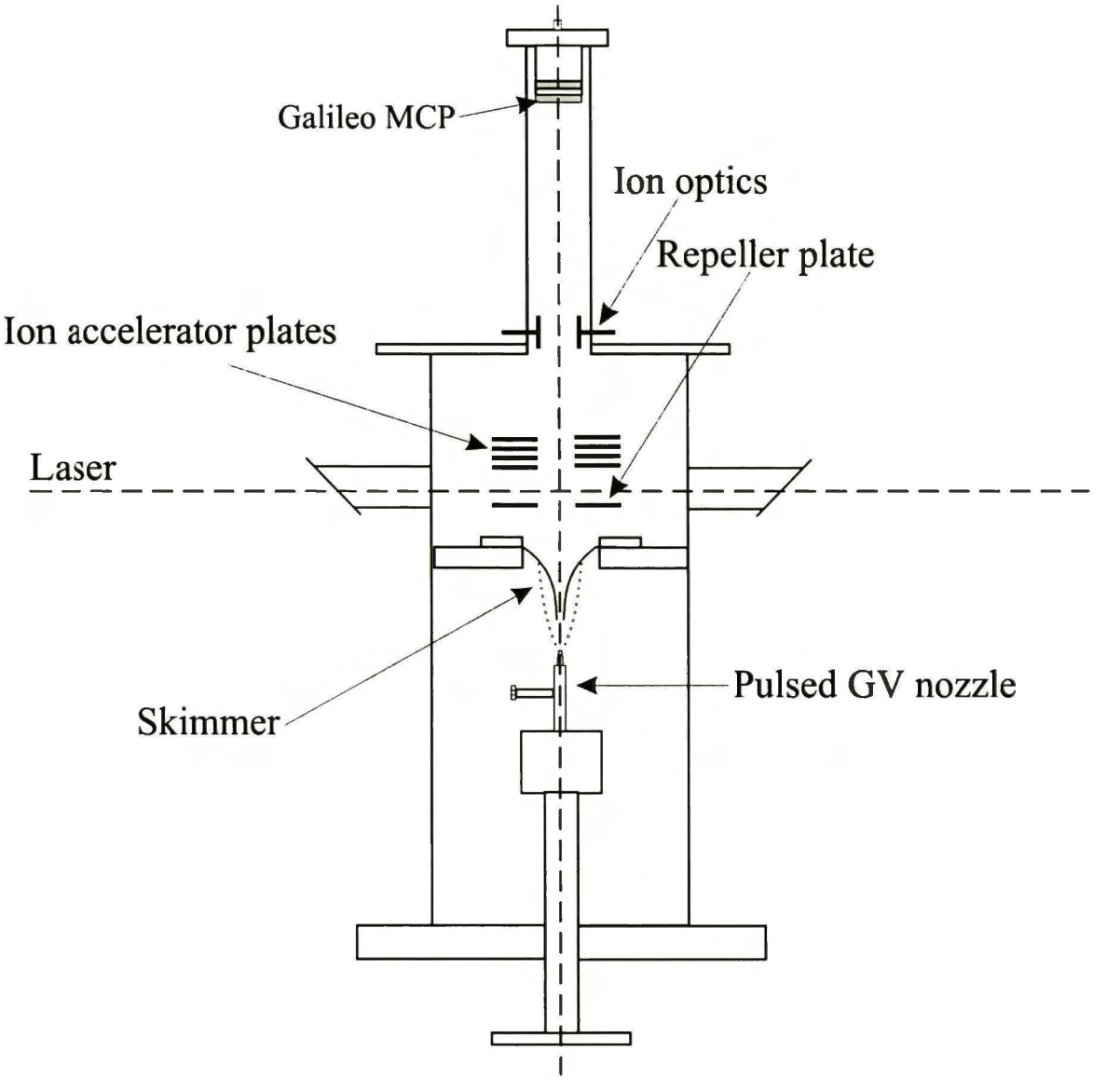


**Figure 2.6.** Linear time of flight mass spectrometer scheme.

Figure 2.6 presents the scheme of linear time of flight mass spectrometer. Ion extractor consists of a repeller plate, accelerator plates, ion optics and the drift tube. A 100 V/cm and 200 V/cm potentials were applied to the repeller plate and accelerator plates, respectively. A set of

microchannel plates (MCP) was used in order to detect the accelerated ions in mass resolved experiments. MCP were placed in Chevron geometry to obtain a maximum gain (typical gain for this geometry is $10^7$). Divider circuit recommended by the manufacturer was used in order to power up MCP detector.

Gated signal from the photomultiplier tube or from the micro channel plates was amplified by 300 MHz fast amplifier (Stanford Research SR445) and then digitized by digital oscilloscope (LeCroy 9310 or Tektronix 7104) and transferred to the computer via GPIB interface. The data acquired were analyzed in the home-made program and stored on the hard disk. The synchronization between all pulsed devices (lasers, pulsed valve) was managed by Stanford Research DG535 delay generator. In fluorescence depletion experiments the delay between pump and probe pulses was set to 100-200 ns. Typical jitter between laser pulses was <4ns and was determined by the characteristics of the pumping lasers. The dye laser step motors were controlled via the home made i8255 based step motor controller.

### *2.2. Theoretical methods.*

*Ab initio* calculations were carried out using Gaussian 98 [10] set of programs, using density functional theory (DFT), Hartree-Fock (HF), for ground state calculations, and configuration interaction singles (CIS), for first excited state calculations, in combination with 6-31G(d,p) basis sets. The geometries of some clusters were optimized using 3-21G basis sets. All geometry optimization calculations were followed by calculations of the normal modes, in order to determine the number of the imaginary frequencies. Molecular dynamic (MD) calculations were done using GROMOS96 [11] set of programs with standard GROMOS force field for vacuum. For statistical analysis of MD trajectories my own programs were written.

**References and notes**


1. C. Parmenter, *Farad. Discuss. Chem. Soc.* **75** (1983) 7.
2. A. Amirav, U. Even, J. Jortner, *Chem. Phys. Lett.* **71** (1980) 12.
3. A. Kantovitz, J. Grey, *Rev. Sci. Inst.* **22** (1951) 328.
4. G. Kistiakowski, W. Slitcher, *Rev. Sci. Inst.* **22** (1951) 333.
5. R. Smalley, B. Ramakrishna, D. H. Levy, J. Wharton, *Chem. Phys.* **61** (1974) 4363.
6. K. Bier and B. Schmidt, *Z. Angew. Phys.* **13** (1961) 493.
7. E. L. Knuth, *J. Phys. Chem.* **66** (1977) 3315.
8. EXCITON information bulletin, 1992.
9. U. Brackmann, *Lambrachrome Laser Dyes*, 2nd edition, Lambda Physik GmbH, D-37079 Gottingen, Germany.
10. Gaussian 98, Revision A.7, M. J. Frisch, G. W. Trucks, H. B. Schlegel, G. E. Scuseria, M. A. Robb, J. R. Cheeseman, V. G. Zakrzewski, J. A. Montgomery, Jr., R. E. Stratmann, J. C. Burant, S. Dapprich, J. M. Millam, A. D. Daniels, K. N. Kudin, M. C. Strain, O. Farkas, J. Tomasi, V. Barone, M. Cossi, R. Cammi, B. Mennucci, C. Pomelli, C. Adamo, S. Clifford, J. Ochterski, G. A. Petersson, P. Y. Ayala, Q. Cui, K. Morokuma, D. K. Malick, A. D. Rabuck, K. Raghavachari, J. B. Foresman, J. Cioslowski, J. V. Ortiz, A. G. Baboul, B. B. Stefanov, G. Liu, A. Liashenko, P. Piskorz, I. Komaromi, R. Gomperts, R. L. Martin, D. J. Fox, T. Keith, M. A. Al-Laham, C. Y. Peng, A. Nanayakkara, C. Gonzalez, M. Challacombe, P. M. W. Gill, B. Johnson, W. Chen, M. W. Wong, J. L. Andres, C. Gonzalez, M. Head-Gordon, E. S. Replogle, and J. A. Pople, *Gaussian, Inc.*, Pittsburgh PA, 1998.
11. W. F. van Gunsteren and H. J. C. Berendsen, BIOMOS b. v., Biomolecular software, Laboratory of Physical Chemistry, ETH-Zürich, 1996.

## CHAPTER 3. Experimental results and discussion.

### *3.1. Electronic spectra of anthracene derivatives.*

Figure 3.1 shows a portion (-50 ÷ 500 $cm^{-1}$) of the fluorescence excitation spectra of anthracene derivatives seeded in supersonic free jet in comparison to the spectrum of "bare" anthracene.

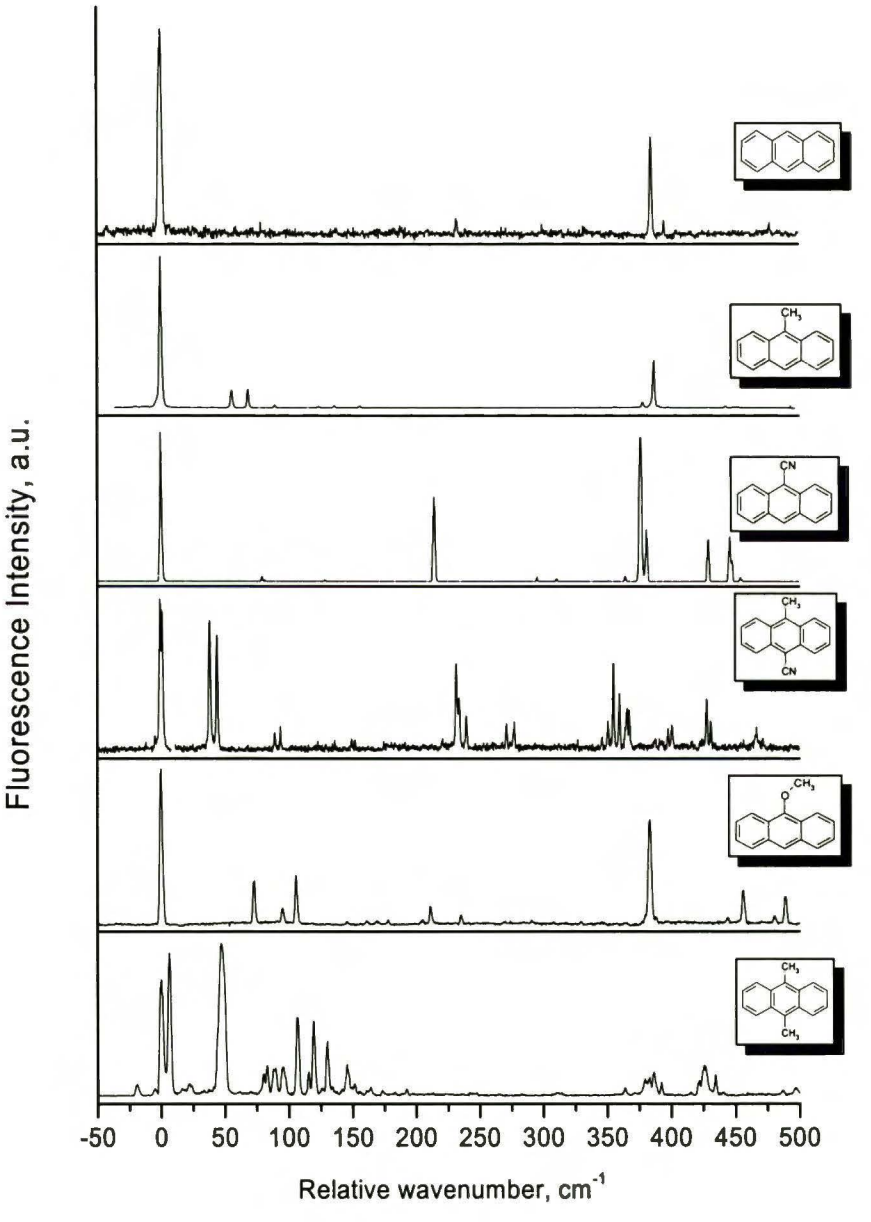


**Figure 3.1.** Portion of the LIF excitation spectra of the anthracene derivatives (-50 ÷ 500 $cm^{-1}$) seeded in helium supersonic free jet. $P_{He}$=3 atm.

The values of the electronic origins of the anthracenes are given in Table 3.1.

| | |
|---|---|
| Anthracene | 27695 $cm^{-1}$ |
| 9-methylanthracene (MA) | 26943 $cm^{-1}$ |
| 9-cyanoanthracene (CNA) | 26171 $cm^{-1}$ |
| 9-cyano-10-methylanthracen (CMA) | 25680 $cm^{-1}$ |
| 9-methoxyanthracene (MeOA) | 26781 $cm^{-1}$ |

**Table 3.1.** Electronic origins of the anthracenes.

The vibronic structure of the majority of anthracene derivatives is identical in the low frequency region. All LIF spectra obtained are in good agreement with those reported in literature [1, 2, 3, 4, 5, 6]. It is easy to identify the $12a_g$ fundamental mode (385 $cm^{-1}$ for anthracene in our experiments) of anthracene framework in these spectra.

The spectrum of the "bare" MA in the low frequency region contains two modes, which were assigned to low frequency methyl group torsion [5]. The $12a_g$ fundamental mode is slightly blue-shifted (387 $cm^{-1}$).

With substitution of cyano group in the 9th position, the band corresponding to the bending mode of cyano group appeared, in the 0-400 $cm^{-1}$ region. In the case of 9-cyanoanthracene the $12a_g$ is red-shifted (377 $cm^{-1}$).

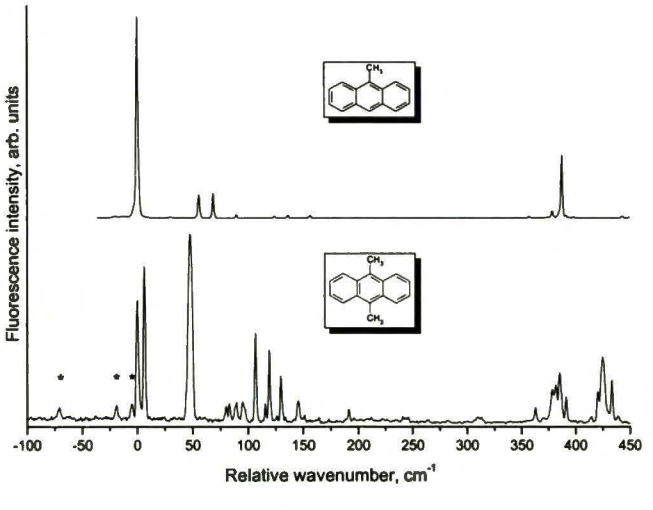


**Figure 3.2.** Comparison of the fluorescence excitation spectra of the DMA (lower) and MA (upper).

By comparing the excitation spectrum of 9-methoxyanthracene and 9-methylanthracene all modes in low frequency region can be easily assigned to the methoxy group rotation and

bending motion.

Due to the presence of the second methyl group, fluorescence excitation spectrum of 9,10-dimethylanthracene (DMA)(Figure 3.2) is much more complicated than the corresponding spectrum of 9-methylanthracene. This effect may be due to the coupling between two hindered methyl rotors. The fluorescence excitation spectrum of DMA is in good agreement to those reported by Tanaka et. al. [6]. In contrary to MA, fluorescence excitation spectrum of DMA exhibits a number of relatively strong vibronic transitions in the 0-180 $cm^{-1}$ range that can be tentatively assigned to low frequency anthracene moiety vibrations coupled with methyl torsion. Tanaka et. al. have noticed that the line around 48 $cm^{-1}$ is broad and its fluorescence lifetime is wavelengths dependent. Indeed, in our experiments the line at 48 $cm^{-1}$ exhibits a large broadening (FWHM=4.2±0.1 $cm^{-1}$). In the case of MA, the 387 $cm^{-1}$ transition is assigned to $12_0^1$ ring "breathing" vibration. For DMA two broad lines with the maxima at 384$cm^{-1}$ and 425 $cm^{-1}$ have been detected. These bands consist of several transitions separated by 4-6 $cm^{-1}$. This effect may be due to appearance of Fermi resonance; anharmonic coupling in anthracene derivatives results in the splitting of 1-10 $cm^{-1}$ [1].

The most striking difference between fluorescence excitation (FE) spectra of DMA and MA is a doublet structure of the electronic origin in the DMA; the spacing of the bands is 6.5 $cm^{-1}$. In order to understand the nature of this phenomenon, fluorescence depletion experiment was carried cut.

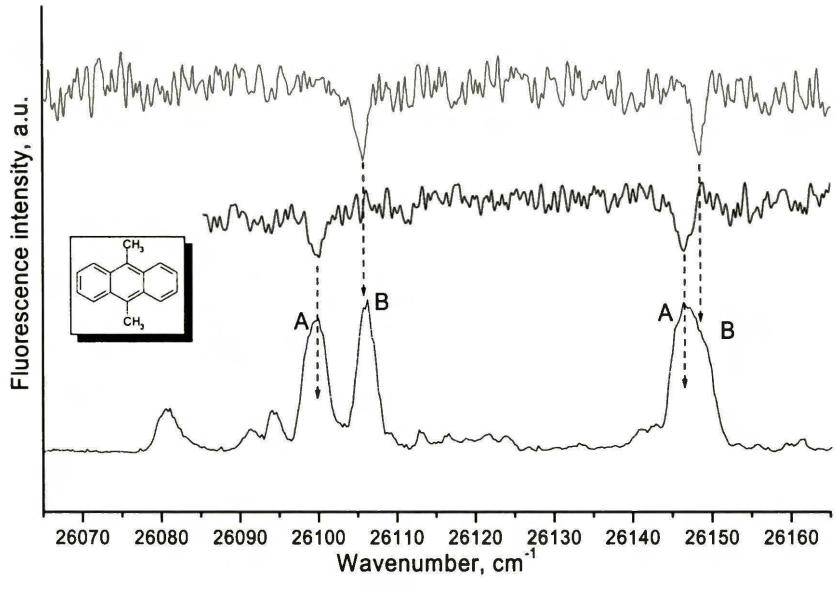


**Figure 3.3.** Fluorescence depletion spectra of the 9,10-dimethylanthracene.

Figure 3.3 shows the hole-burning spectra probed in A (0-0) and B (A+6.5 $cm^{-1}$) bands together with the corresponding part of the fluorescence excitation spectrum. First scan, probed at A band, shows two dips which correspond to the A band itself and transition separated from A by 47.4 $cm^{-1}$. Second scan, probed at B band, also produced two dips: at B band and another one separated by 49.6 $cm^{-1}$. The experiment can be treated as evidence of two different species coexisting under supersonic jet conditions in the electronic ground state. We believe that the resulting fluorescence excitation spectrum is a superposition of two spectra that belong to two isomeric forms of DMA. Due to the large contribution of the scattered light produced by the "pump" laser we were not able to "burn holes" in 60-200 $cm^{-1}$ region.

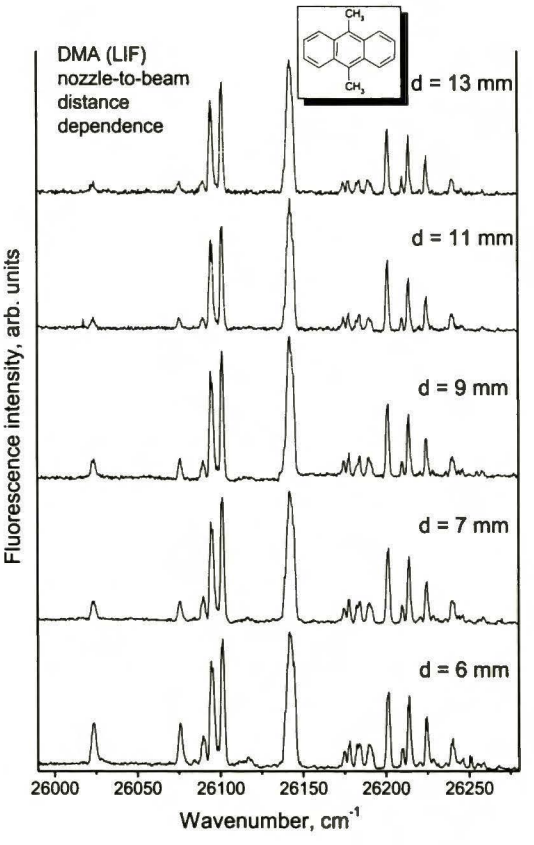


**Figure 3.4.** The distance dependence on the fluorescence intensity. *d* - the distance between the nozzle and the laser beam.

Three bands marked by asterisks in Figure 3.2 at the "red" side of the origin (-5.5, -18, -71 $cm^{-1}$) remain not assigned. Figure 3.4 shows the effect of changing the distance from the nozzle to the laser beam in the LIF excitation spectrum. This experiment has shown that while we improve the "cooling" conditions, the "red" bands disappear. Thus, we can assign these transitions as the hot bands.

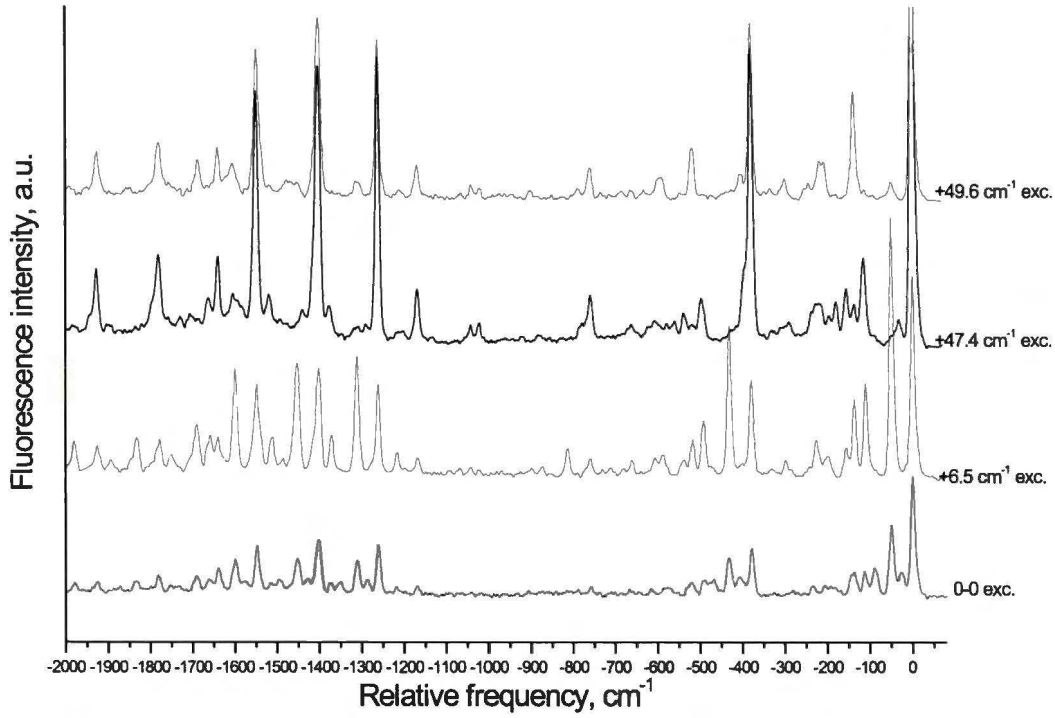


**Figure 3.5.** Dispersed fluorescence spectra of DMA.

Ground state vibrational structure of DMA was studied by SVLF experiments. Figure 3.5 shows the SVLF spectra produced by exciting into the doublet near the origin and the two lowest vibronic transitions of DMA. These spectra have some common high frequency modes (380, 2x380, 1168, 1260, 1403, 1548, 1600, 1640 $cm^{-1}$), which were assigned to vibrations of the anthracene moiety [7]. One can notice the similarity of these spectra in the high frequency region and the large difference in the 0-550 $cm^{-1}$ frequency range. The fluorescence spectrum obtained by excitation to the 0-0 transition exhibits frequency mode of 25 $cm^{-1}$. The mode of this frequency is absent in the fluorescence spectrum observed while exciting to the 0-0+6.5 $cm^{-1}$ feature. This result can be treated as the further confirmation of the presence of two different isomeric forms of DMA under supersonic jet conditions. The *ab initio* calculations with simple basis sets (STO-3G, 3-21G, 6-31G and 6-31G*) predict two stable geometries of the 9,10-dimethylanthracene. On of them has $C_{2v}$ symmetry (*cis*

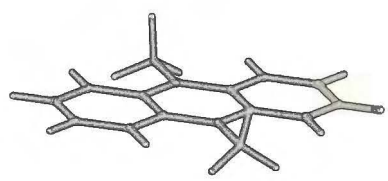

**Figure 3.6.** 9,10-dimethylanthracene geometry predicted by *ab initio* calculations.

conformer). The second belongs to the $C_{2h}$ symmetry group (*trans* conformer). Theoretical calculations with larger basis set (6-31G**) predict only one stable *cis* geometry as shown in Figure 3.6.

### 3.2. Spectroscopy of the anthracene-water clusters.

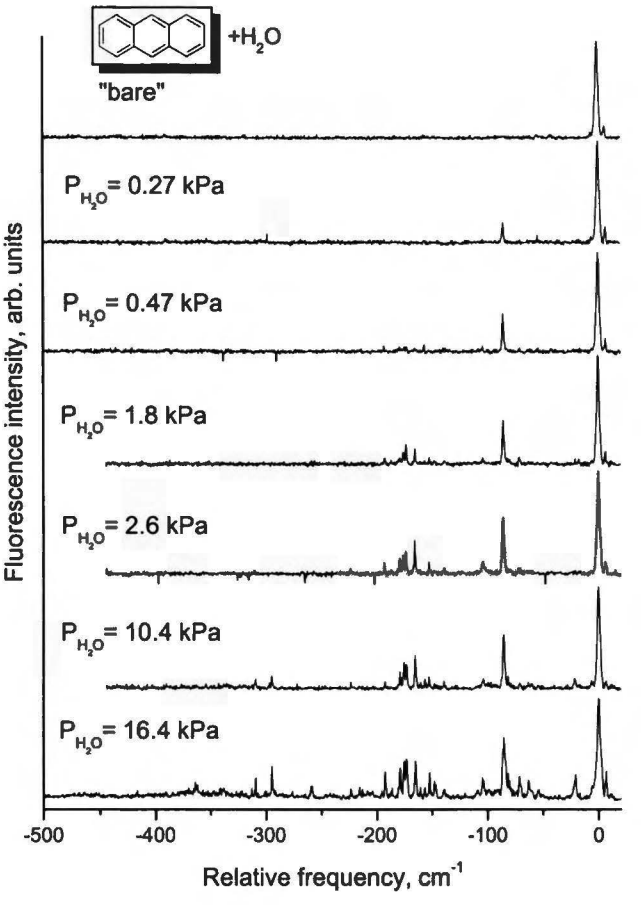


**Figure 3.7.** Fluorescence excitation spectra of anthracene with addition of $H_2O$ vapors.

Figure 3.7 shows the changes in the fluorescence excitation spectrum of anthracene (-500 ÷ 20 $cm^{-1}$) when $H_2O$ vapors are added. Assignments of the coordination number could be made basing on the dependence of the spectra on $H_2O$ vapor pressure. Figure 3.8 shows the assignment of the coordination number of the complex. The assignments are in good agreement with [8], except of small differences in transitions intensities.

For the $n$=1 species the most intense transition is red-shifted by -86 $cm^{-1}$ in respect to the electronic origin of the "bare" anthracene. The narrow, well defined transition, suggests, according to [8], the presence of a single conformer. The authors did not discuss the spectroscopic feature at -105 $cm^{-1}$, which could be due to the presence of the second conformer.

The spectrum of the $n$=2 species exhibits a complex assembly of bands. In contrast to [8], the spectrum consists of five strong transitions (-193, -179, -176, -173, -165 $cm^{-1}$), and only three of them (-193, -176, -165 $cm^{-1}$) were observed in [8] due to lower resolution as compared with our experiments.

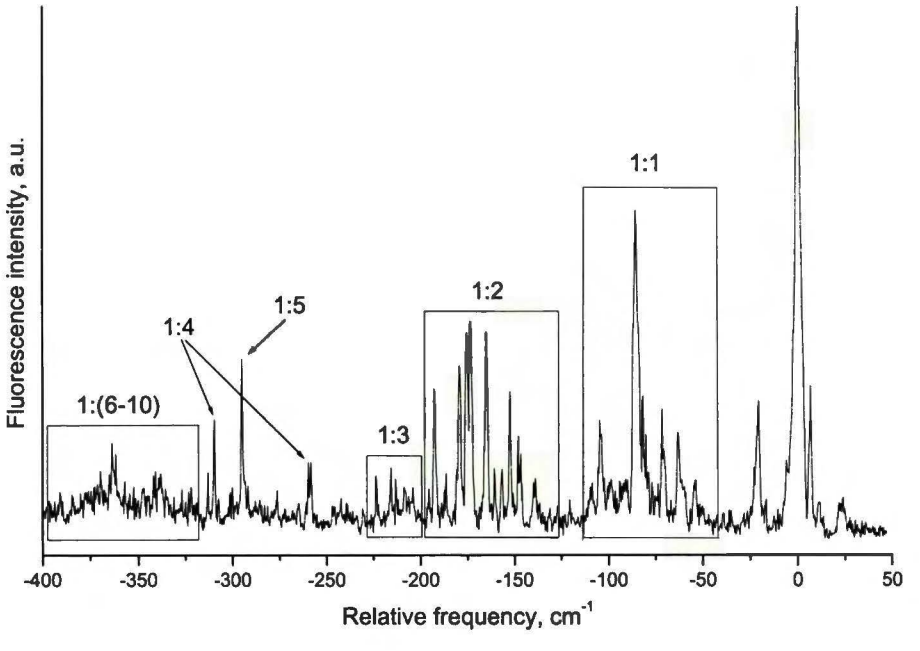


**Figure 3.8.** Fluorescence excitation spectrum of the anthracene taken with $P_{H_2O} = 16.4$ kPa.

The spectral resolution reported in [8] (≤3 $cm^{-1}$), was at least two times worse than it declared. In effect, authors of ref. [8] were unable to resolve two transitions separated by 6 $cm^{-1}$ that were resolved in this work. The splitting of the transition with a center at 176 $cm^{-1}$ could be due to overlapping of the spectra of the multiple $n$=2 conformers.

The spectrum of anthracene with the trimer of water shows very weak signal with 0-0 transition at -223 $cm^{-1}$.

Formation of the tetramer and pentamer leads to further stabilization of the complex. The water tetramer and pentamer spectra exhibit sharp and intense transitions at -310 $cm^{-1}$ and -295 $cm^{-1}$, respectively. It suggests that these complexes correspond to a single conformer. Due to the limitations of the LIF technique it was impossible to resolve vibrational structures for larger

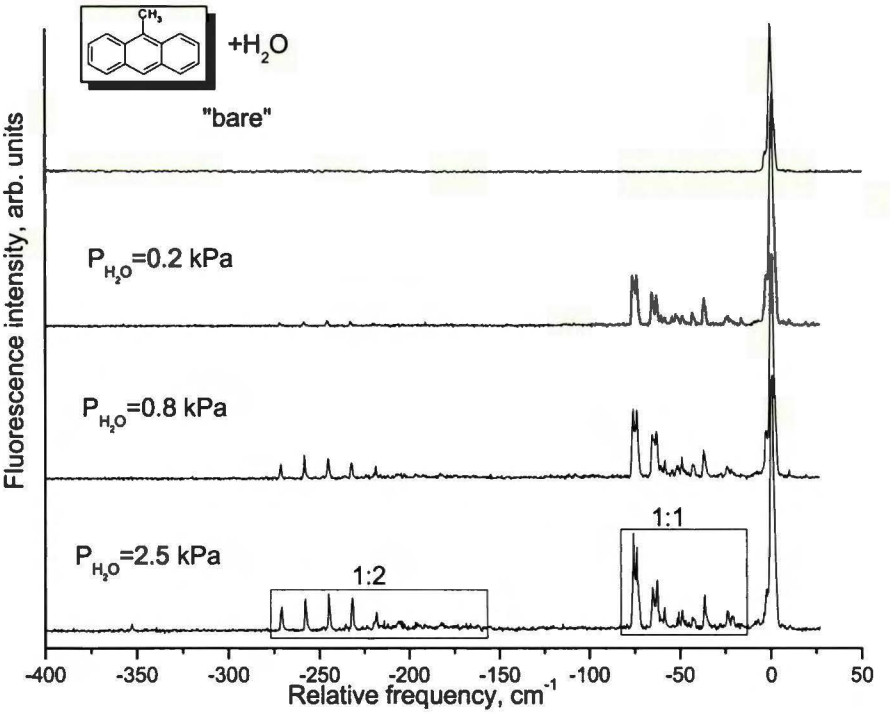


**Figure 3.9.** Fluorescence excitation spectra of 9-methylanthracene-water complex as a function of $P_{H_2O}$

clusters ($n \geq 6$). Identification of these clusters can be made by mass-selective techniques.

In the case of the MA-$(H_2O)_n$ complexes, up to $n$=3 were observed. As shown on Figure 3.9, the MA-water$_1$ complex exhibits two strong red-shifted transitions at -75 cm$^{-1}$ and -64 cm$^{-1}$ and many low frequency van der Waals modes. Both -75 cm$^{-1}$ and -64 cm$^{-1}$ transitions are splitted by 2.5 cm$^{-1}$. The splitting could be due to internal rotation of the methyl group.

The spectrum of the MA-water$_2$ consists of 5 separated by 13 cm$^{-1}$, sharp bands with 0-0 transition at -271 cm$^{-1}$. Starting from -206 cm$^{-1}$ the structured spectrum disappears and a broad, weak fluorescence background is observed. Thus one could expect the dissociation of the complex for 100-150 cm$^{-1}$ of excess of energy and suggests the H-bonded chain geometry of the water$_2$ cluster with one hydrogen connected to the MA aromatic ring. The dissociation energy in case of the water$_2$ cluster is about 0.2 kcal/mol.The spectrum of the MA-water$_3$ cluster exhibits one weak transition with the center at -363 cm$^{-1}$. It suggests the existence only one conformer for such geometry.

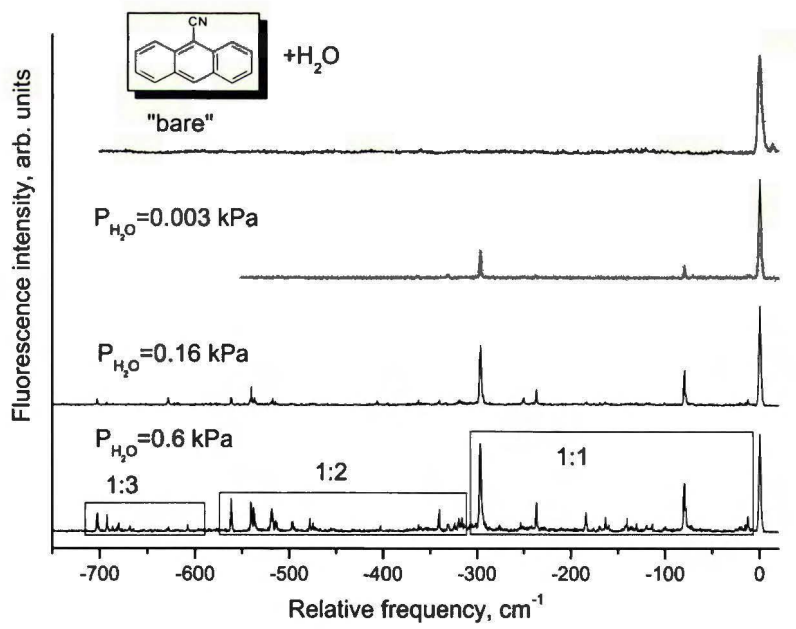


**Figure 3.10.** LIF excitation spectra of the CNA-$H_2O$ mixture.

The LIF spectra of clusters of CNA-water$_n$, $n$=1-3 were observed in the supersonic jet [9]. The structure of the complex 1:1 was well characterized both using experimental and theoretical methods in [10]. The origin of the spectrum of the CNA-water$_1$ complex is observed at -296 cm$^{-1}$. The main progression of the complex is based on 217 cm$^{-1}$ CN-aromatic ring bending vibration of the 9-cyanoanthracene (see Figure 3.10). It suggests that the cyano group is involved in the microsolvation process. There are no low frequency intermolecular vibrations. As suggested, this complex is planar. Water molecule is attached by its hydrogen atom to the cyano group and by oxygen atom to the hydrogen atom in the 1$^{st}$ position of the 9-cyanoanthracene.

The vibronic structure of the 1:2 complex is different. 0-0 transition of this complex at -562 cm$^{-1}$ with respect to the "bare" CNA molecule is followed by two intense low frequency bands (-539 cm$^{-1}$,-519 cm$^{-1}$) exhibiting the splittings of -2 cm$^{-1}$ and -1 cm$^{-1}$, respectively. There is no vibration corresponding to the 217 cm$^{-1}$ bending mode of the "bare" CNA.

Electronic spectrum of the 1:3 complex is very similar to the 1:2. There are three sharp and strong transitions at -702 cm$^{-1}$, -692 cm$^{-1}$ and 680 cm$^{-1}$. This behavior of 1:2 and 1:3 complexes suggests the cluster geometry with water molecules linear or cyclic (the case of 1:3 cluster) structure.

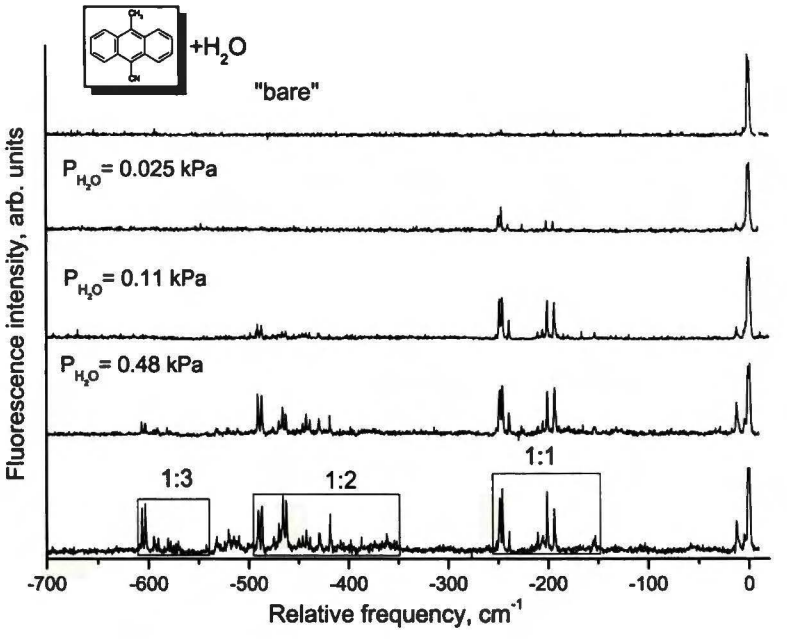


**Figure 3.11.** $P_{H_2O}$ dependence of LIF excitation spectra of the 9-cyano-10-methylanthracene.

Figure 3.11 presents the LIF excitation spectra of the CMA microsolvated by water molecules. It is difficult to assign the bands corresponding to the water complexes with $n$=3 and $n$=4. molecules. The features around -600 $cm^{-1}$ and -440 $cm^{-1}$ are tentatively assigned to the 1:3 and 1:4 clusters, respectively. In order to precisely assign the coordination numbers of these complexes, the mass-selective experiments have to be carried out.

The spectral origin of the 1:1 complex is red-shifted by -245 $cm^{-1}$ with respect to the origin of the "bare" molecule and appears as a doublet, splitted by 2.7 $cm^{-1}$. The splitting was observed for low frequency modes in the spectrum of the "bare" CMA except for the origin in [3]. The splitted 0-0 transition in the 1:1 complex suggests that the barrier for methyl group rotation in the $S_1$ state is lowered upon complex formation. There are two strong low frequency transitions at -201 $cm^{-1}$ and -194 $cm^{-1}$, respectively. The bands exhibit the spacing of about 50 $cm^{-1}$, what is a typical progression for the hindered rotation mode in the $S_1$ state [11]. These transitions could be tentatively assigned to the methyl group rotation within the complex.

The 0-0 transitions of the water dimer and trimer also appeared as doublets. The spacing between two close transitions is about 3.5 $cm^{-1}$ for both $n$=2 and $n$=3 species. This is the evidence of the further barrier lowering for the methyl group rotation. The water trimer exhibits five sharp close laying transitions around -440 $cm^{-1}$.

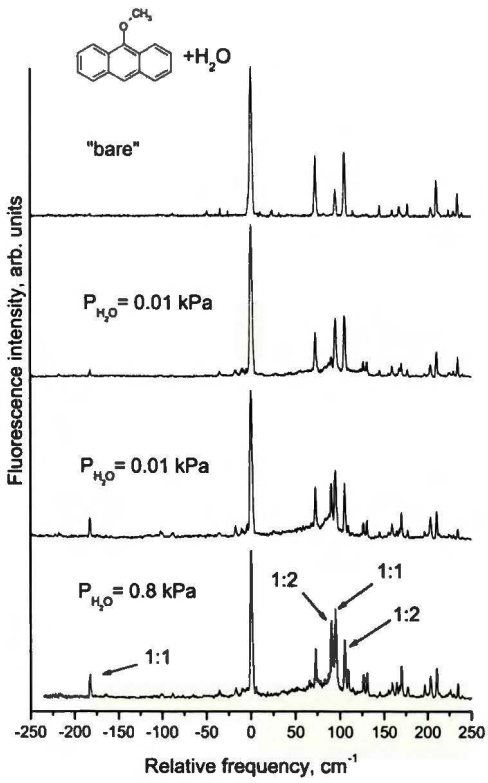


**Figure 3.12.** Fluorescence excitation spectra of the 9-methoxyanthracene-water clusters. $P_{water}$ dependence.

LIF excitation spectra of the MeOA-$H_2O$ clusters in the spectral range from -250 $cm^{-1}$ to 250 $cm^{-1}$ from the 0-0 transition of the MeOA are shown on the Figure 3.12. These spectra are in excellent agreement to those reported in [12] and [13]. Two intense blue-shifted bands by +95 $cm^{-1}$ and +90 $cm^{-1}$ are 0-0 transitions of the 1:1 and 1:2 complexes, respectively.

The band appearing at the red-side from the origin of the MeOA at -182 $cm^{-1}$ could be assigned to the second isomer of the 1:1 cluster, which is attached to the $\pi$-aromatic system of the MeOA. The assumed geometry of the 1:1 complex is: water molecule acts as a proton donor and is attached to the oxygen atom of the methoxy group.

The second water molecule does not change the spectrum significantly. This indicates that the second molecule of water is not attached directly to the aromatic framework but is associated to the first water molecule forming a linear dimer.

### 3.3. Spectroscopy of the anthracenes microsolvated by methanol.

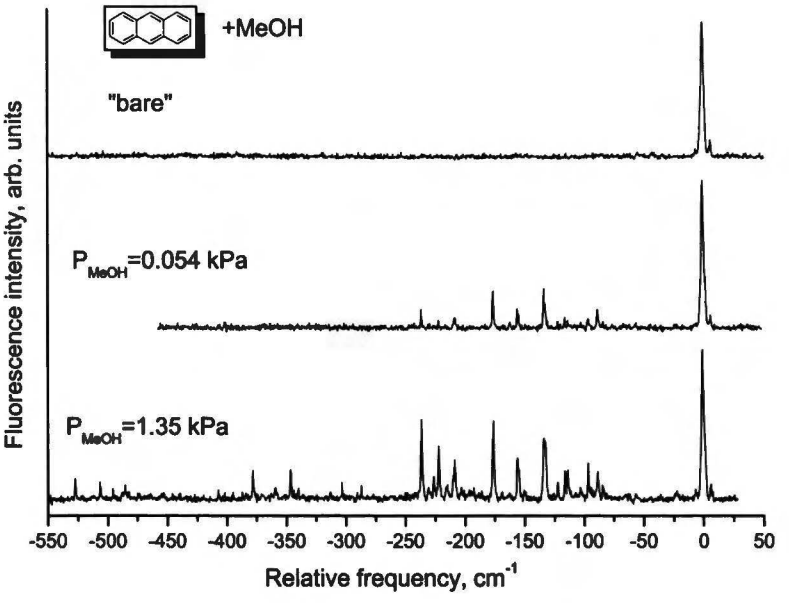


**Figure 3.13.** Fluorescence excitation spectra of anthracene microsolvated by methanol. $P_{CH_3OH}$ dependence.

The spectra displayed on Figure 3.13 show fluorescence excitation of the anthracene-methanol mixture in the range -550 cm$^{-1}$ to 50 cm$^{-1}$ from the anthracene origin. One can notice a complex structure at the red side from the anthracene 0-0 transition. It is hard to assign the cluster stechiometry basing on the methanol pressure dependence only. Figure 3.14 shows the stechiometry of the various clusters taken from the mass-selective experiments [14].

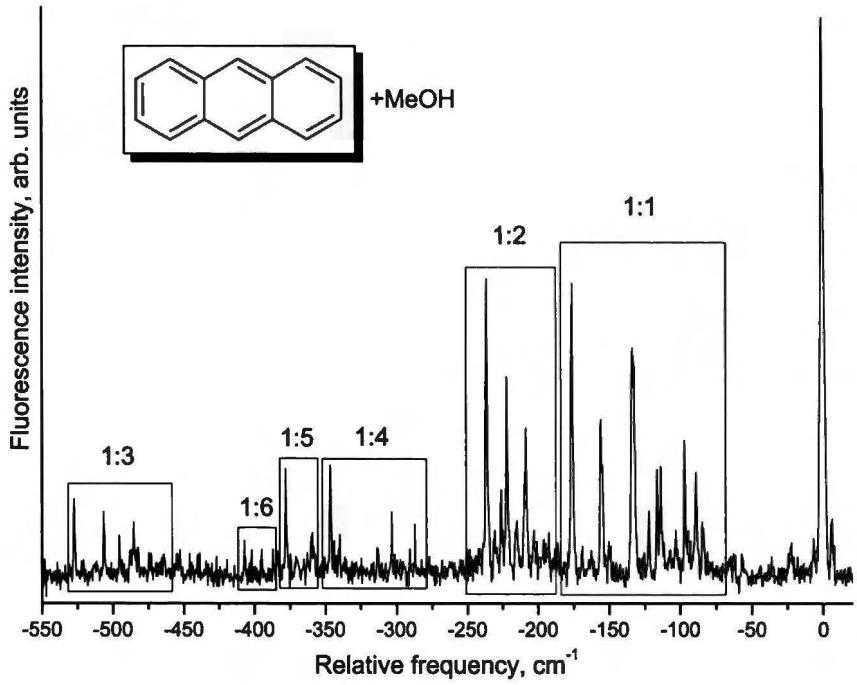


**Figure 3.14.** Fluorescence excitation spectrum of anthracene-methanol clusters. The assignment of the coordination numbers is taken from [14].

The unusual shape of the anthracene-methanol$_1$ spectrum suggests the presence of two electronic origins, and therefore two conformers. To confirm this, the fluorescence depletion experiments have to be done.

In contrast, it appears that the LIF spectrum of the $n$=2 species of anthracene-methanol cluster is built on only one conformer. Analogous result was obtained for perylene-methanol$_2$ [15] and benzene-methanol$_2$ [16] clusters. In these cases methanol molecules were singly hydrogen-bonded from opposite sides of the aromatic molecules.

The $n$=3 species spectrum is significantly red-shifted (-527 cm$^{-1}$). This behaviour also echoes the perylene results [17]. The large red shift is consistent with the cyclic trimer structure having oxygen atom and methyl groups close to planarity.

The single, well defined origin transitions of the $n$=4 and $n$=5 species suggest the presence of one conformer in each case. The structures assigned to these clusters are planar, cyclic tetramers and pentamers, respectively.

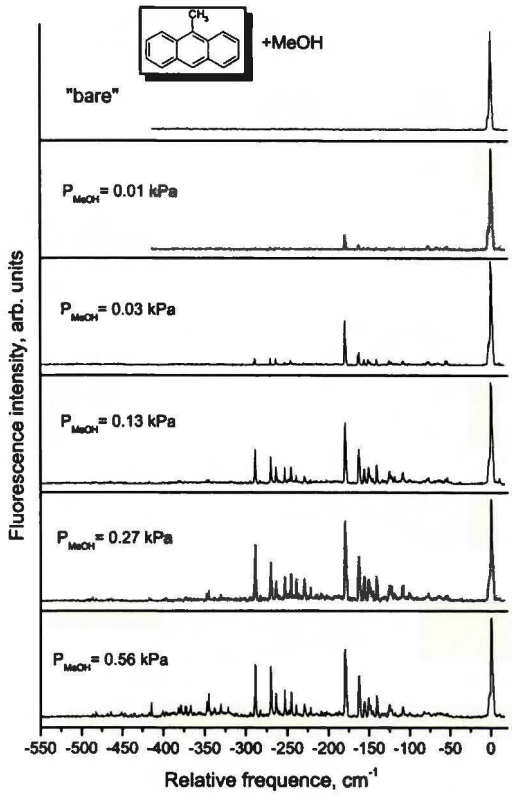


**Figure 3.15.** Fluorescence excitation spectra of the MA-methanol mixture. $P_{MeOH}$ dependence.

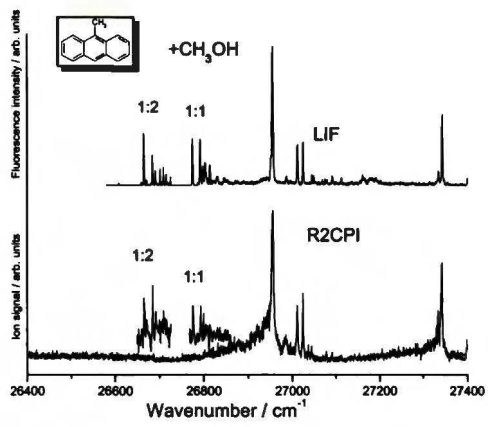


**Figure 3.16.** Comparison between LIF and R2CPI spectra.

The complicated vibronic structure of the n=6 species proves the existence of more than one conformer. Most probably, one of the structures is built by two cyclic trimer rings, hydrogen bonded to opposite sides of the anthracene moiety.

From the spectra of MA-MeOH mixture shown in Figure 3.15 it is easy to determine the transitions belonging to 1:1 and 1:2 clusters (see Figure 3.16). The bands corresponding to higher complexes are also present; therefore the assignment of the coordination numbers will be made in comparison with spectra of the anthracene-methanol.

Vibrational structure of the 1:1 (-180 cm$^{-1}$ origin) and 1:2 (-289 cm$^{-1}$) complexes are similar and are in turn comparable to the vibrational structure of the anthracene-methanol$_2$ cluster. Hence it is possible to conclude that the MA-methanol$_1$ species in contrast to anthracene-methanol$_1$ exists as

one conformer. Most likely it is due to the presence of the methyl group. Similar vibronic structure of the MA-methanol$_{1,2}$ clusters and anthracene-methanol$_2$, suggests the that the second methanol molecule is not attached directly to the aromatic framework but is associated to the first water molecule forming a linear dimer.

It is hard to make assignments for transitions around -500 cm$^{-1}$ ÷ -300 cm$^{-1}$. Tentative assignments were made in comparison to the anthracene-methanol$_{3-6}$ clusters. Features appearing around -425 cm$^{-1}$ ÷ -475 cm$^{-1}$ are assigned to the 1:3 geometry. Transitions at -350 cm$^{-1}$ and -415 cm$^{-1}$ are assigned to the 1:4 and 1:5 clusters, respectively. The spectrum between -360 cm$^{-1}$ ÷ -385 cm$^{-1}$ is assigned to the 1:6 complex.

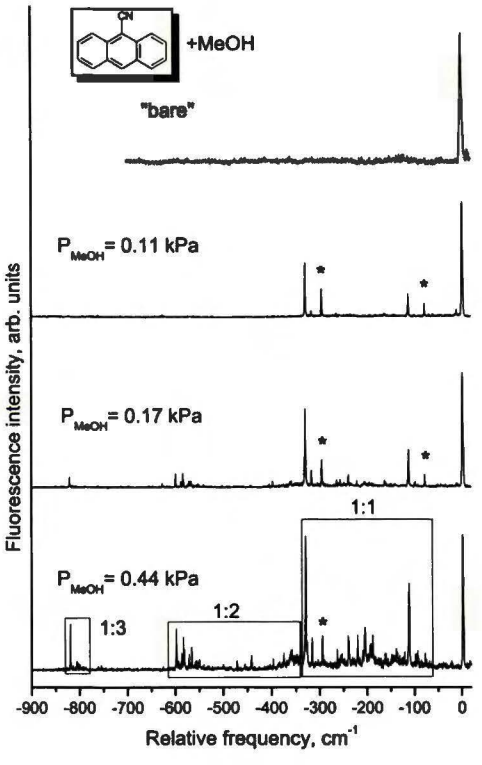


**Figure 3.17.** CNA-methanol fluorescence excitation spectra. $P_{MeOH}$ dependence. Bands marked by asterisk belong to the CNA-water complex.

The vibronic structure of the CNA-methanol$_{1-3}$ clusters is very similar to those observed for anthracene-water$_{1-3}$ clusters. As shown on the Figure 3.17 the 1:1 cluster is characterized by the strong red-shifted origin at -329 cm$^{-1}$. Many low frequency transitions corresponding to the intermolecular van der Waals modes are observed. The next strong band observed at -112 cm$^{-1}$, corresponds to the cyano group bending mode (217 cm$^{-1}$). By analogy to the structure of the CNA-water$_1$ cluster, the most probable geometry is planar with the hydrogen atom of the methanol molecule attached to the cyano group and the oxygen atom hydrogen-bonded to the hydrogen at the 1$^{st}$ position in the anthracene aromatic ring.

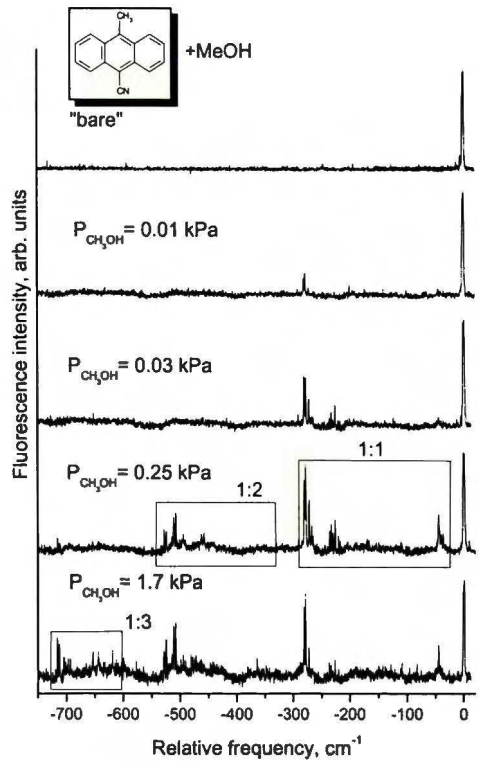


**Figure 3.18.** CMA-methanol fluorescence excitation spectra. $P_{MeOH}$ depencdence.

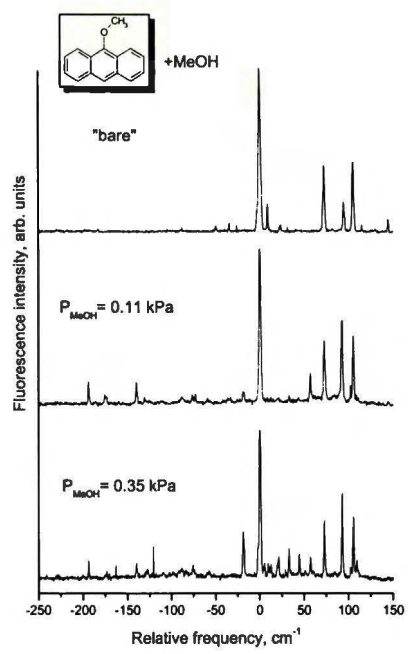


**Figure 3.19.** MeOA-methanol mixture fluorescence excitation spectra. $P_{CH_3OH}$ dependence.

The spectrum of the 1:2 cluster exhibits the intense origin band red-shifted with respect to the origin of the CNA by -598 cm$^{-1}$ and two low frequency intermolecular modes.

As Figure 3.17 shows, the 1:3 species has poor electronic spectrum, the origin band being displaced -819 cm$^{-1}$ from the corresponding CNA feature.

The spectra of CMA-methanol complexes shown in Figure 3.18 are similar to those observed for the CNA-methanol species. Presumably, the vibronic structure is mainly determined by the presence of CN group. The spectrum of the 1:1 complex is characterized by the strong 0-0 transition displaced in respect to the corresponding CMA transition by -280 cm$^{-1}$ and the mode (-44 cm$^{-1}$) corresponding to the cyano group vibration. In the case of the CMA, the low frequency van der Waals modes are weak.

The spectrum of the CMA-methanol$_2$ complex consists of two strong transitions at -510 cm$^{-1}$ and -526 cm$^{-1}$, respectively, due to the presence of two conformers. Many bands corresponding to 1:1 and 1:2 complexes are

splitted by about 1.5 $cm^{-1}$. Similar behaviour can be observed for CMA-water clusters.

The fluorescence excitation spectra of jet-cooled MeOA-methanol mixture are shown on Figure 3.19. New features due to the excitation of complexes are observed in two different spectral regions. Namely, the strongest band is blue-shifted (+94 $cm^{-1}$) with respect to the origin of the MeOA "bare" molecule and is assigned to the 1:1 complexes. A weaker system starting at -197 $cm^{-1}$ is also observed. This structure is assigned to the second conformer of the 1:1 complex. The smaller intensity of this -197 $cm^{-1}$ feature relative to the "blue" one may be due to weaker binding energy of such cluster. The second band is blue-shifted by +54 $cm^{-1}$ and is assigned to the origin of the 1:2 clusters.

### 3.4. Anthracenes microsolvated by chloroform.

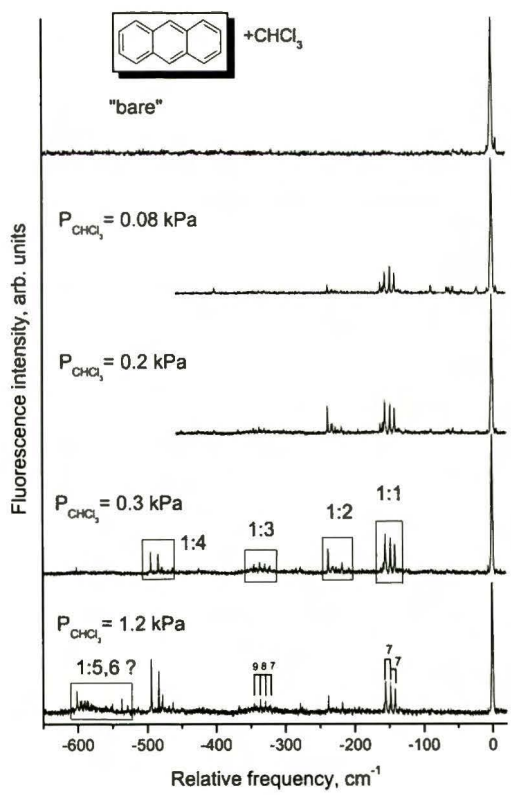


**Figure 3.20.** Flurescence excitation spectra of the anthracene-$CHCl_3$ mixture. $P_{chloroform}$ dependence.

The spectrum of the anthracene-chloroform cluster of 1:1 stechiometry (see Figure 3.20) reveals the red-shifted origin at -156 $cm^{-1}$ followed by two relatively intense bands separated by 6 $cm^{-1}$ (-148 $cm^{-1}$, -142 $cm^{-1}$). Theoretical *ab initio* studies of this cluster at the electronic ground state predict energy minimum for the $C_s$ geometry with the symmetry plane along the short axis of the anthracene molecule. Three *Cl* atoms are attached to the $\pi$-system of the anthracene ring. The

lowest calculated vibrations were 5 $cm^{-1}$, 11 $cm^{-1}$ and 15 $cm^{-1}$.

The spectrum of the 1:2 anthracene-chloroform complex exhibits the relatively strong origin at -238 $cm^{-1}$ followed by three weak intermolecular modes at -231 $cm^{-1}$, -227 $cm^{-1}$ and -218 $cm^{-1}$.

The band of the 1:3 anthracene-chloroform clusters proves the small binding energy of this complex.

In contrast, the spectrum of anthracene-$(chloroform)_4$ have shown a relatively strong fluorescence signal. The spectrum consists of two transitions at -495 $cm^{-1}$ and -484 $cm^{-1}$. Comparable intensity (difference less than 5%) of these bands suggests the presence of two conformers of the cluster of this size.

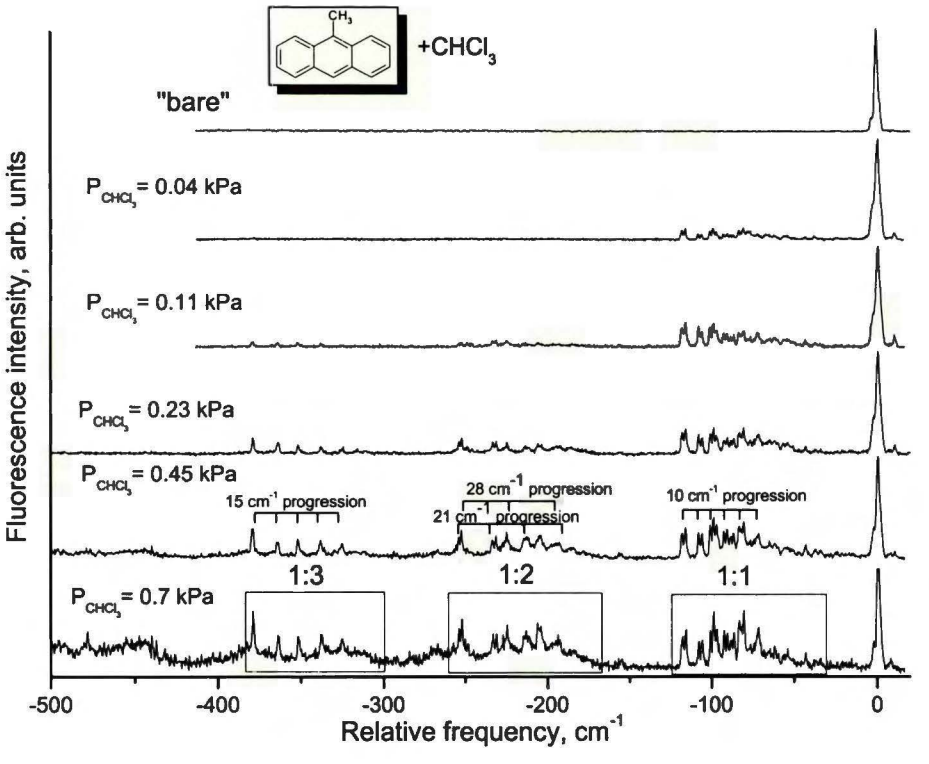


**Figure 3.21.** Fluorescence excitation of the MA-chloroform mixture. $P_{chloroform}$ dependence.

The spectrum of the MA-chloroform 1:1 complexes consists of nine red-shifted intense transitions with the origin at -117 $cm^{-1}$ (see Figure 3.21). Each of these bands exhibits the

doublet structure with the splitting from 2.5 $cm^{-1}$ to 2 $cm^{-1}$. Regular intensity altering, which begins from intense origin, is observed for the fist six transitions. The most probable reason of this effect is the transitions between rotational levels of methyl group splitted by tunnel effect. The barrier for the rotation of methyl group is lowered by complex formation; tunneling splitting increases in comparison to the "bare" molecule. Starting from fourth quanta, a large fluorescence background signal is observed.

The spectrum of the 1:2 MA-chloroform complex consists of the strong red-shifted origin at -252 $cm^{-1}$ and exhibits two low-frequency progressions built on 21 $cm^{-1}$ and 28 $cm^{-1}$.

The LIF spectrum of MA-chloroform 1:3 complexes shows the 15 $cm^{-1}$ progression built on the origin. Further increasing of chloroform vapour pressure leads to the "snow ball" effect. All transitions are coming structureless and appear on a large fluorescence background.Transitions observed around -490 $cm^{-1}$ could be tentatively assigned to 1:4 complexes of MA-chloroform.

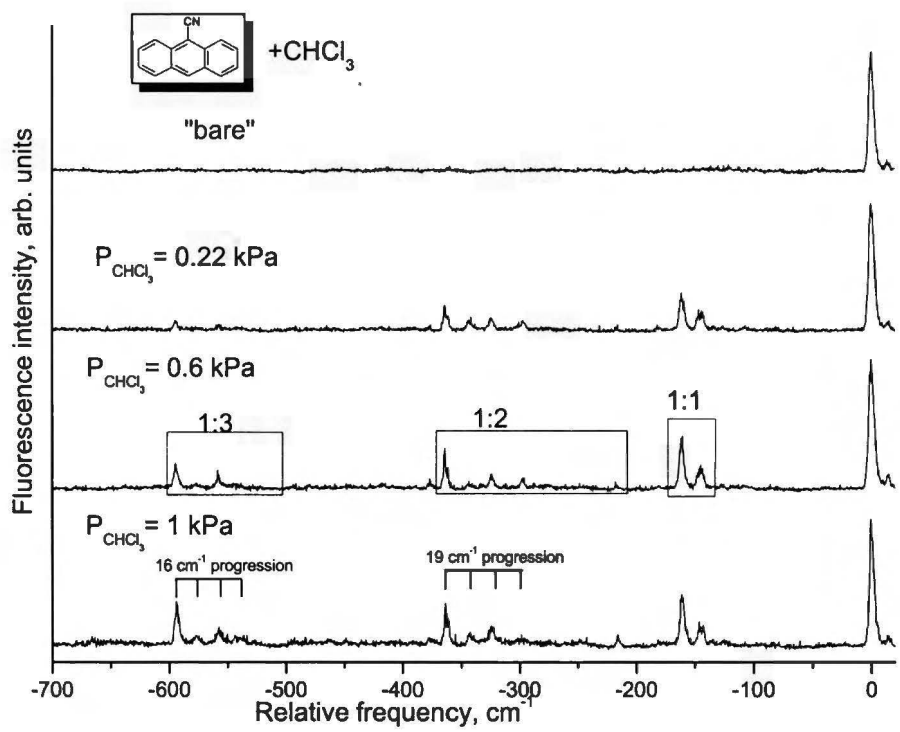


**Figure 3.22.** Fluorescence excitation spectra of the CNA-chloroform mixture. $P_{chloroform}$ dependence.

Figure 3.22 shows the LIF excitation spectrum of CNA-chloroform clusters on the red side of the CNA electronic origin. The strong origin at -161 $cm^{-1}$ and the weak intermolecular band at -145 $cm^{-1}$ correspond to 1:1 CNA-chloroform complexes. The band at -145 $cm^{-1}$ is broad and exhibits an unresolved structure.

The spectrum of 1:2 CNA-chloroform cluster consists of the strong origin band at -365 $cm^{-1}$ and three relatively weak bands at -344 $cm^{-1}$, -323 $cm^{-1}$ and 303 $cm^{-1}$.

The spectrum of the cluster 1:3 exhibits the vibronic structure similar to 1:2 species. The origin is found at -593 $cm^{-1}$ and is followed by the set of bands at -577 $cm^{-1}$, 561 $cm^{-1}$ and the broad transition at -540 $cm^{-1}$. No clusters of the higher coordination number have been observed.

Figure 3.23 shows the LIF excitation spectra of CMA "bare" molecule and its small microclusters with chloroform. An addition of the solvent molecule and further cluster

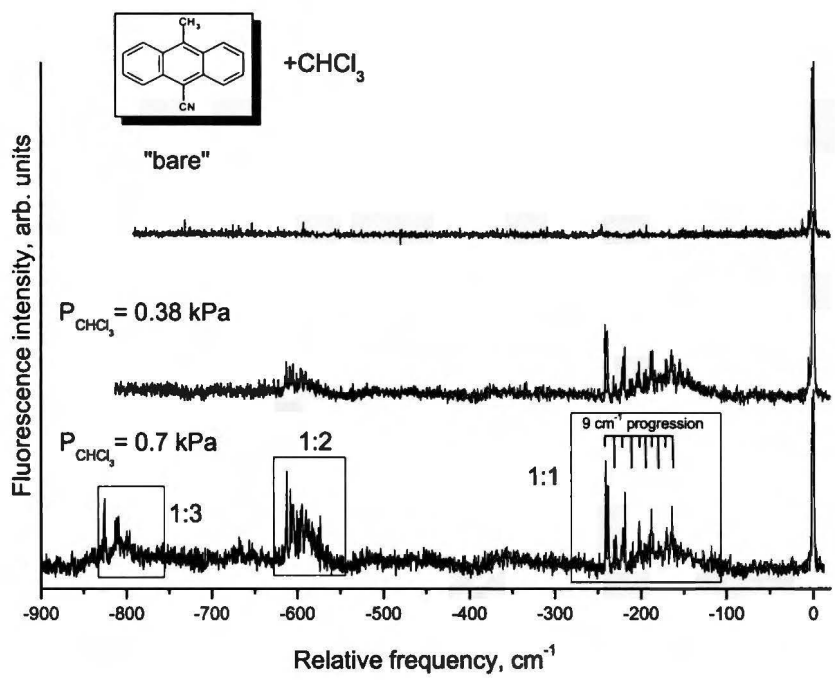


**Figure 3.23.** Fluorescence excitation spectra of the CMA-chloroform mixture. $P_{chloroform}$ dependence.

formation reveals the significant red-shift of the electronic origin in respect to the "bare" molecule. The 0-0 transition of the 1:1 CMA-chloroform cluster is red-shifted by -239 $cm^{-1}$. Most probably, the low frequency progression observed in the excitation spectrum of the 1:1 CMA-chloroform species arises from internal rotor levels of $CH_3$ group of CMA. The origin band as well as transitions at -230 $cm^{-1}$ and 219 $cm^{-1}$ show the doublet structure. Relatively large fluorescence background is observed with the centre at -167 $cm^{-1}$.

The electronic origin of the 1:2 cluster of the CMA-chloroform observed at -613 $cm^{-1}$ is also splitted. The bands at -606 $cm^{-1}$ and -595 $cm^{-1}$ belonging to the 1:2 spectrum of the CMA-chloroform consist of the set of close- laying transitions. Again, the fluorescence background signal with the centre at -590 $cm^{-1}$ is also observed.

By increasing partial pressure of $CHCl_3$ the set of bands corresponding to CNA-chloroform$_3$ complexes has been observed around -820 $cm^{-1}$ with respect to the electronic origin of the "bare" CMA. Two transitions at -813 $cm^{-1}$ and -800 $cm^{-1}$ are situated on the top of the broad background.

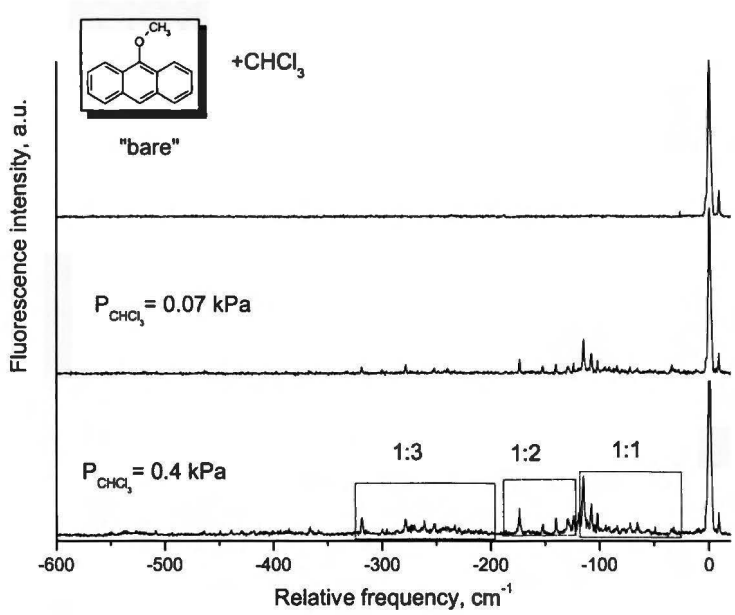


**Figure 3.24.** LIF excitation spectra of the MeOA-chloroform mixture. $P_{chloroform}$ dependence.

Figure 3.24 shows a portion of the fluorescence excitation spectra of the MeOA-chloroform mixture. The $n$=1 species exhibits the strong origin at -115 $cm^{-1}$ followed by two relatively strong bands at -107 $cm^{-1}$ and -102 $cm^{-1}$. These bands probably belong to the rotation of the methyl group strongly modified by clustering. Most probably chloroform molecule is attached to the lone pair electrons on the oxygen atom of the methoxy group. The spectrum of the MeOA-$chloroform_2$ species exhibits the strong signal with red-shifted origin at -174 $cm^{-1}$. The bands corresponding to the rotation of methyl group are not so modified comparing to the 1:1 complex and appear at -152 $cm^{-1}$ and -140 $cm^{-1}$.

Also two low frequency weak bands belonging to the 1:2 MeOA-chloroform cluster spectrum are observed at -129 $cm^{-1}$ and -124 $cm^{-1}$.

The spectrum of the $n$=3 species exhibits the weakest signal comparing to the rest spectra of MeOA-$CHCl_3$ clusters. The electronic origin transition for this cluster was observed at -319 $cm^{-1}$.

### 3.5. Electronic spectroscopy of the anthracenes microsolvated by carbon tetrachloride.

Figure 3.25 shows LIF excitation spectra of anthracene-$CCl_4$ mixture in the region $0 \div -800$ $cm^{-1}$ near the electronic origin of the "bare" anthracene. The origin of the anthracene-$CCl_4$ 1:1 cluster spectrum is observed at -269 $cm^{-1}$. The spectrum is dominated by a relatively strong active modes involved in the progressions with the frequencies of 5.5, 19, 23 $cm^{-1}$. The most prominent progression is clearly built on the 0-0 band extending to about 22 quanta with the intensity maximum at 8$^{th}$ quanta. Figure 3.26 shows the detailed fluorescence excitation spectrum of anthracene-$CCl_4$ 1:1 cluster.

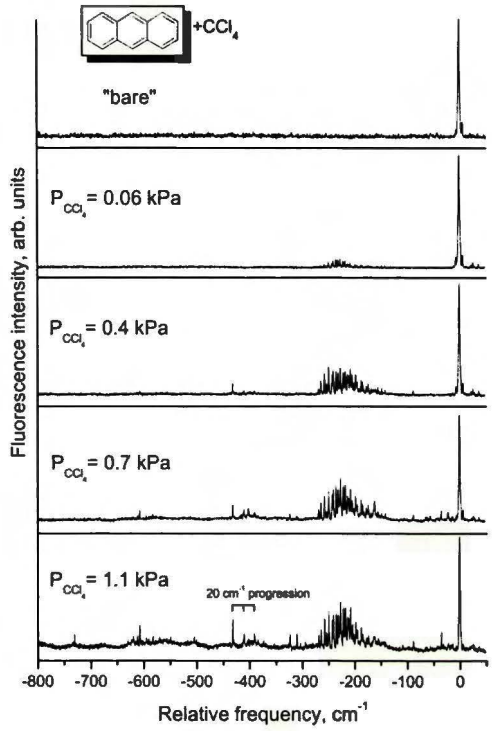


**Figure 3.25.** Fluorescence excitation spectra of the anthracen-$CCl_4$ mixture as function of. $P_{CCl_4}$ partial pressure dependence.

For 1:2 anthracene-$CCl_4$ cluster the dense vibrational structure of vdW complex disappears. The $n$=2 species exhibits a strong and sharp electronic origin red-shifted by -432 $cm^{-1}$ in respect to the 0-0 transition of the "bare" anthracene. Two weak bands at -411 $cm^{-1}$ and -391 $cm^{-1}$ corresponding to the intermolecular van der Waals modes are also observed in the spectrum of the 1:2 anthracene-$CCl_4$ complex.

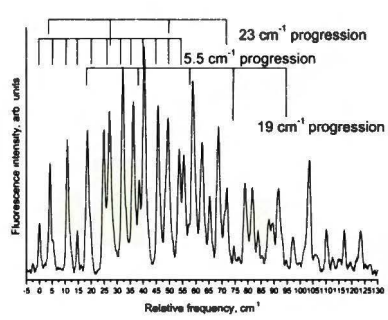


**Figure 3.26.** Fluorescence excitation spectrum of the 1:1 anthracene-$CCl_4$.

The electronic origin of the $n$=3 anthracene-$CCl_4$ cluster observed at -607 $cm^{-1}$ is followed by a weak broad

fluorescence background with two bands of frequency 20 $cm^{-1}$ situated on it.

The band at -731 $cm^{-1}$ we tentatively assign to the electronic origin of the $n$=4 species.

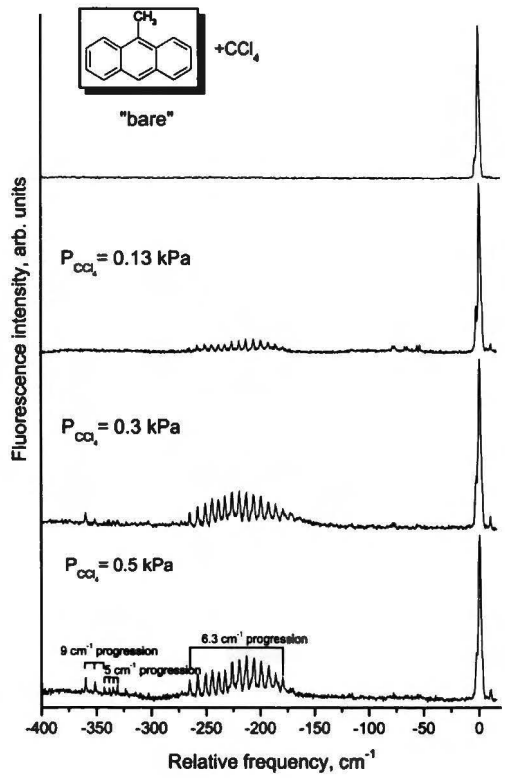


**Figure 3.28.** LIF excitation spectrum of the MA-$CCl_4$ mixture. $P_{CCl_4}$ dependence.

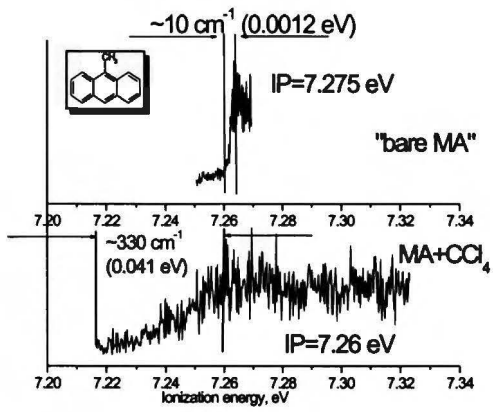


**Figure 3.27.** Ionizatoin threshold spectra of the "bare" MA molecule (upper) and MA-$(CCl_4)_1$ complex (lower).

The LIF excitation spectrum of the MA-$CCl_4$ mixture is presented in Figure 3.28. The electronic origin of the 1:1 complex is observed at -265 $cm^{-1}$ with respect to the corresponding transition of the "bare" MA molecule. The structure of the spectrum resembles the complex of the anthracene-$CCl_4$. The long progression of 12 quanta is built on 0-0 transition. The maximum intensity is observed at $7^{th}$ quanta. One could expect a more complicated structure of the spectrum of MA-$CCl_4$ clusters. In contrary, the vibrational structure of MA-$CCl_4$ 1:1 clusters consists of a set of bands separated by 6.3 $cm^{-1}$. This vibration dominates the spectrum of vdW cluster.

In earlier works [9] it was suggested that the vibronic structure observed for the 1:1 complex of the MA-$CCl_4$ is due to the methyl group rotation involved in the intermolecular vibration of the cluster.

Anthracene-$CCl_4$ that does not have any methyl group also exhibits the similar

vibronic structure. It is not in agreement with the assignment of ref. [9]. Thus, vdW modes observed for 1:1 MA-$CCl_4$ clusters do not involve methyl group vibrations.

The spectrum of the $n$=2 species exhibits a number of weak low frequency modes. The electronic origin is the strongest transition in the spectrum and is observed at -360 $cm^{-1}$ and is followed by low frequency modes observed at -351 $cm^{-1}$, -343 $cm^{-1}$, -338 $cm^{-1}$, -334 $cm^{-1}$, -329 $cm^{-1}$, -324 $cm^{-1}$. The comparison between ionization threshold scans of the "bare" MA molecule and MA-$CCl_4$ 1:1 complex is shown in Figure 3.27. The ionization energy trace of the "bare" MA exhibits a sharp and "fast" rising ion signal with a good signal to noise ratio. The corresponding trace of the 1:1 cluster in contrast to MA has shown broad noisy signal. The ionization threshold energy "window" in which ion signal starts to occur and become saturated in the case of "bare" MA, is 0.001 eV (~10 $cm^{-1}$) wide. In the case of 1:1, the cluster corresponding value is 0.041 eV (~330 $cm^{-1}$).

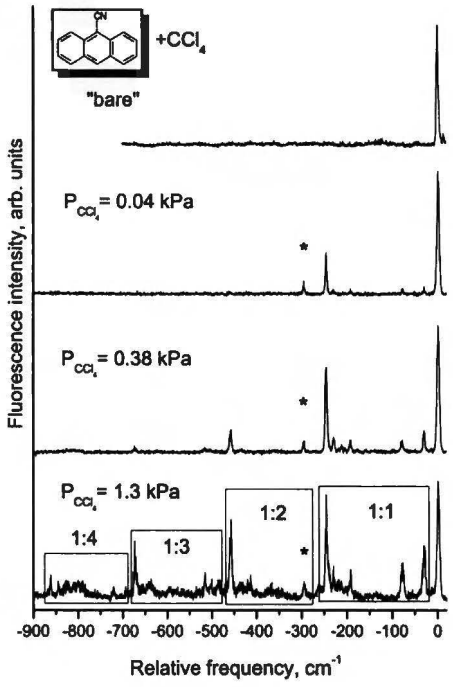


**Figure 3.29.** LIF excitation spectrum of the CNA-$CCl_4$ mixture. $P_{CCl_4}$ dependence. Features marked by asterisk belong to the 0-0 transition of the CNA-$(water)_1$ complex.

Figure 3.29 shows fluorescence excitation spectra of the CNA-$CCl_4$ clusters taken down to -1100 $cm^{-1}$ in respect to the electronic origin of CNA "bare" molecule. The spectrum of $n$=1 species of CNA-$CCl_4$ clusters exhibits completely different vibronic structure than this for 1:1 complexes of anthracene-$CCl_4$ and 1:1 MA-$CCl_4$. The spectrum of the CNA-$(CCl_4)_1$ cluster consists of the strong origin transition at -245 $cm^{-1}$ followed by a set of low frequency bands. One of these bands at -30 $cm^{-1}$ corresponds to the bending mode

($\nu$=215 $cm^{-1}$) of the cyano group in the 1:1 cluster. This frequency has to be compared with 216 $cm^{-1}$ for "bare" CNA molecule.

Electronic origin of the $n$=2 species of the CNA-$CCl_4$ is observed at -457 $cm^{-1}$ and appears on the fluorescence background. Very weak low frequency transitions at -435 $cm^{-1}$, -385 $cm^{-1}$, -363 $cm^{-1}$ and -343 $cm^{-1}$ have also been found.

The spectrum of the $n$=3 species of the CNA-$CCl_4$ consists of one strong electronic origin band observed at -670 $cm^{-1}$.

Very weak signal of the 1:4 complex of CNA-$CCl_4$ appears around -820 $cm^{-1}$. Electronic origin of this species is observed at -861 $cm^{-1}$. Formation of higher clusters (up to 4) required partial pressure of $CCl_4$ as high as 1.3 kPa.

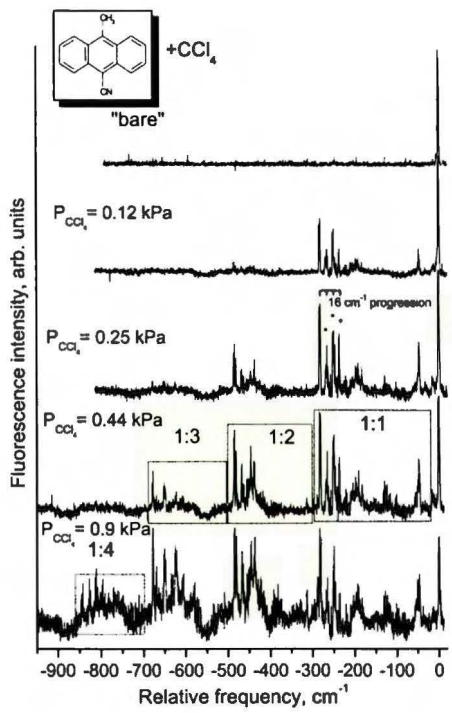


**Figure 3.30.** Fluorescence excitation spectra of the CMA-$CCl_4$ mixture. $P_{CCl_4}$ dependence.

The spectra corresponding to the CMA-$CCl_4$ complexes shown in Figure 3.30 exhibit complex vibrational structure. The origin transitions of clusters of all sizes observed have a multiplet structure. The similar effect has been found for CMA clusters with other solvent molecules. The spectrum of the $n$=1 species exhibits the strong origin at -282 $cm^{-1}$. All bands corresponding to the 1:1 complex show the splitting of 2 $cm^{-1}$. The number (3) of low frequency bands signed in Figure 3.30 by asterisks are observed at the blue side of the origin of the 1:1 cluster. The bands at -265 $cm^{-1}$ and -249 $cm^{-1}$ exhibit a broad fluorescence signal. Both bands exhibit a fine structure. The band at -233 $cm^{-1}$ shows the

doublet structure. The structure of all bands around -197 $cm^{-1}$ is very similar to those appearing in the spectra of the 1:1 cluster of the anthracene-$CCl_4$ and MA-$CCl_4$.

The electronic origin of the 1:2 cluster of the CMA-$CCl_4$ is observed at -484 $cm^{-1}$. The spectrum shows three narrow bands separated by 1.5 $cm^{-1}$. This could be an evidence of the multiple conformations of this cluster. At the blue side of the origin of $n$=2 species a numerous low frequency bands are observed at -468, -462, -456, -446, -438 $cm^{-1}$ (6 $cm^{-1}$ progression)

The origin of the $n$=3 species is observed at -679 $cm^{-1}$ to the red from "bare" CMA molecule. The 0-0 transition of the spectrum of this size shows again a doublet structure with the splitting of 2 $cm^{-1}$. All bands at the red side from the electronic origin of 1:3 cluster (-670 $cm^{-1}$, -649 $cm^{-1}$, -633 $cm^{-1}$) consist of several narrow transitions. This produces some band broadening.

The spectrum of the $n$=4 species of the CMA-$CCl_4$ clusters shows the weakest signal on the fluorescence background with electronic origin at -842 $cm^{-1}$. The low frequency bands at -810 $cm^{-1}$ and -798 $cm^{-1}$ are broad and some narrow features are on the top of it.

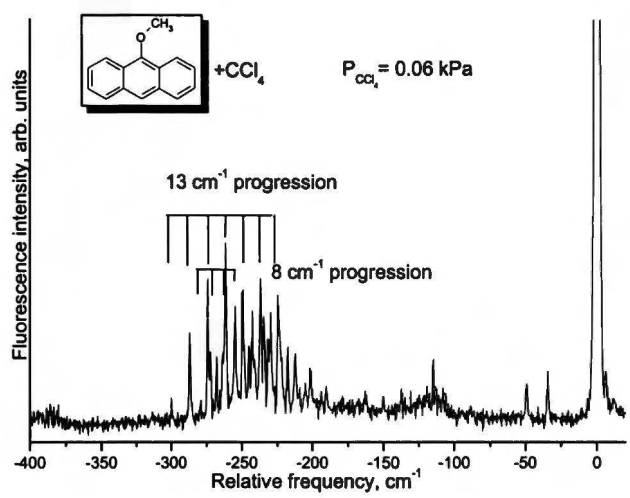


**Figure 3.31.** Fluorescence excitation spectra of the MeOA-$CCl_4$ mixture. $P_{CCl_4}$ dependence.

The LIF excitation spectrum of 1:1 complex of MeOA-$CCl_4$ is shown in Figure 3.31. In the case of MeOA clusters with $CCl_4$ only the complex with coordination number $n$=1 exhibits a measurable fluorescence signal. The vibronic structure of this cluster is similar to those of 1:1 clusters of the anthracene-$CCl_4$ and MA-$CCl_4$. This could be treated as the evidence of the minor role of the methoxy group in a formation of clusters of 9-methoxyanthracene with carbon tetrachloride. The origin of the 1:1 cluster is red-shifted and is observed at -300 $cm^{-1}$. The low frequency progression is built on the 0-0 band with frequencies 8 $cm^{-1}$, 13 $cm^{-1}$. The MeOA fluorescence signal is very weak. By increasing of partial pressure of the $CCl_4$ vapors the total fluorescence intensity dramatically decreases.

The LIF excitation spectra of the jet cooled anthracene mixed with benzene vapours are shown in Figure 3.32. As one can see, the LIF spectrum corresponding to the anthracene-benzene$_1$ is easily recognized. The spectrum of the $n$=1 species of the anthracene-benzene clusters shows the sharp and strong electronic origin transition at -434 cm$^{-1}$. It suggests the existence of only one conformer for this cluster. Three van der Waals intermolecular modes are observed at -404 cm$^{-1}$, -377.5 cm$^{-1}$ and -350 cm$^{-1}$. The transition at -377.5 cm$^{-1}$ exhibits the doublet structure. The splitting is: 3 cm$^{-1}$. Further increasing of the benzene vapours pressure produce a complex vibronic structure. The increase of benzene vapours pressure leads to new intense bands both on the blue and red region of the electronic origin of 1:1 complex.

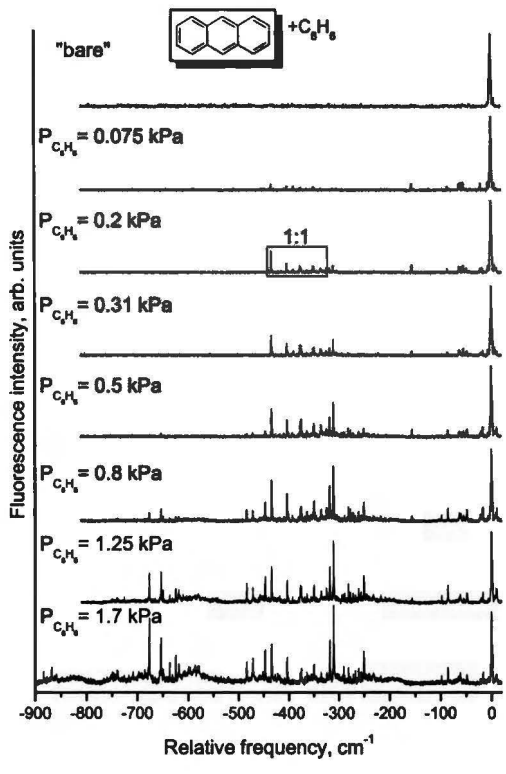


**Figure 3.32.** LIF excitation spectra of the anthracene-benzene mixture. $P_{C_6H_6}$ dependence.

In order to assign coordination numbers corresponding to spectral features observed, the resonance enhanced two colour ionization (R2CPI) experiments were carried out. Figure 3.33 shows R2CPI spectra of $n$=1-5 anthracene-benzene$_n$ clusters taken on the corresponding ion mass channels.

The electronic origin of the 1:2 complex consists of two close-laying strong transitions. These bands are observed at -319 $cm^{-1}$ and -311 $cm^{-1}$. The 0-0 transition is blue-shifted (+150 $cm^{-1}$) with respect to the origin of 1:1 species of the anthracene-benzene clusters.

The mass-resolved excitation spectrum of the $n$=3 species exhibits very weak signal. Three strong transitions at -484 $cm^{-1}$, -471 $cm^{-1}$ and -447 $cm^{-1}$ are observed in the corresponding fluorescence excitation spectrum and have matched peaks in the mass-resolved spectrum. We believe that few different structures of 1:3 complexes are stabilized in the supersonic jet beam.

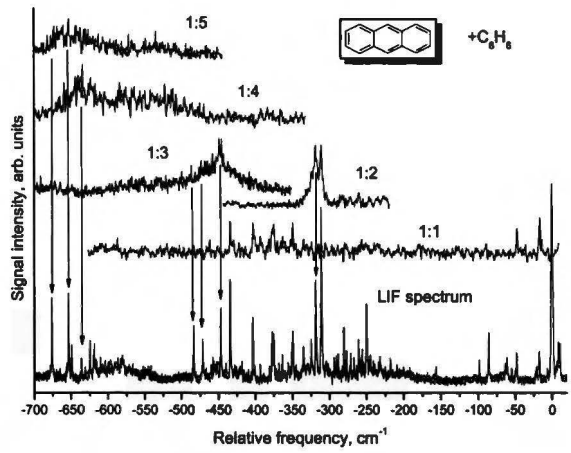


**Figure 3.33.** Sequence of mass-resolved R2CPI excitation spectra of the anthracene-benzene$_n$, ($n$=1-5) clusters. The lowest curve shows corresponding LIF excitation spectrum.

The spectrum taken on the anthracene-benzene$_4$ mass channel exhibits several weak bands on the top of broad and structureless background signal. Comparing the LIF excitation spectrum of the anthracene-benzene mixture with mass-resolved spectrum on the mass corresponding to the anthracene-benzene$_4$ cluster, one could find matching bands.

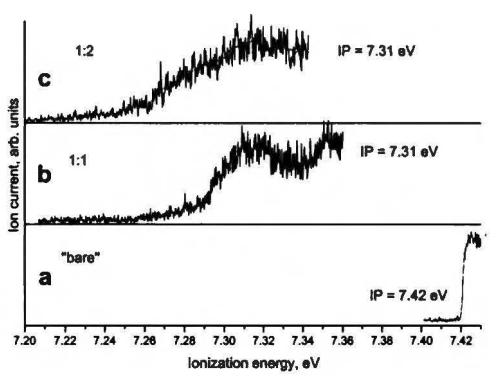


**Figure 3.34.** Ionization energy scans. Trace **a** – "bare" anthracene, trace **b** – 1:1 complex with benzene, trace **c** – 1:2 complex with benzene. All traces were obtained by fixing the wavelength of the first photon in resonance with corresponding electronic origin transition. The wavelength of the second photon was scanned.

The bands observed in the fluorescence excitation spectrum at -636 $cm^{-1}$, -625 $cm^{-1}$ and -619 $cm^{-1}$ are tentatively assigned to three different conformers of the 1:4

complex. The strong bands at -653 $cm^{-1}$ and -676 $cm^{-1}$ with comparable intensities have been observed in the LIF excitation spectrum. According to mass resolved spectrum we assign them to the transitions of 1:5 complex.

Ionization energy threshold scans of the anthracene and its clusters with benzene$_n$, $n$=1,2 are shown in Figure 3.34. The ionization energy trace of the "bare" anthracene exhibits a sharp and "fast" rising ion signal with a good signal to noise ratio. The corresponding traces of the 1:1 and 1:2 clusters in contrast to anthracene have shown broad noisy signals. The ionization threshold energy "window" in which ion signal starts to occur and become saturated in the case of "bare" anthracene, was 0.0045 eV (~36 $cm^{-1}$) wide. In the case of 1:1 and 1:2, the clusters, corresponding values were 0.047 eV (~379 $cm^{-1}$) and 0.09 eV (723 $cm^{-1}$), respectively. The ionization energy of both, the monomer and dimer structures is ~0.11 eV (~887 $cm^{-1}$) lower than this of anthracene.

Figure 3.35 represents fluorescence excitation spectra of the MA-benzene mixture. Further

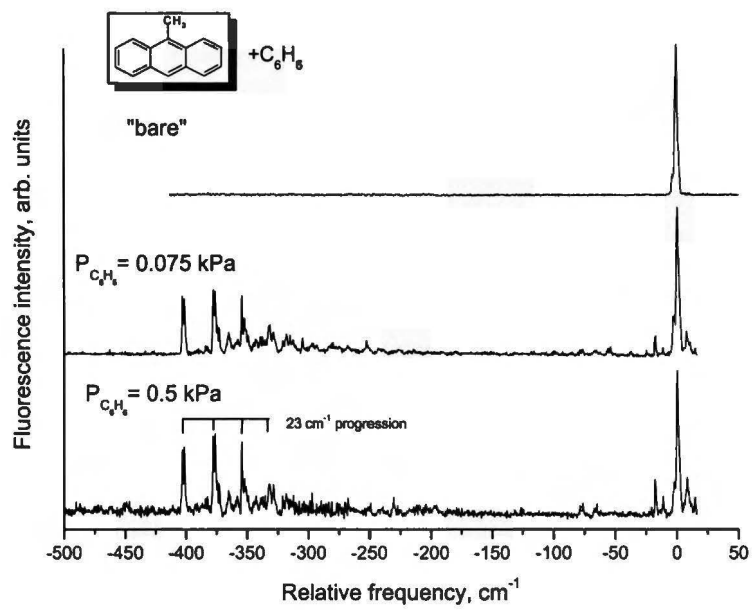


**Figure 3.35.** LIF excitation spectra of the MA-benzene mixture taken with different pressures of benzene vapours.

increase of the benzene vapours pressure results in deterioration of the signal to noise ratio and then the fluorescence signal disappears. Thus, it was not possible to detect the cluster of higher size.

The electronic origin of the spectrum of the 1:1 MA-benzene complex at -401 $cm^{-1}$ is a member of a complex set of bands with comparable intensities. These bands are observed at -377 $cm^{-1}$ and -353 $cm^{-1}$. Such behaviour suggests the presence of the multiple geometries of the 1:1 MA-benzene clusters. Each member of this progression exhibits a doublet structure. The splitting is 2 $cm^{-1}$. The group of weaker bands is also observed on a large fluorescence background signal with maximum signal around -332 $cm^{-1}$.

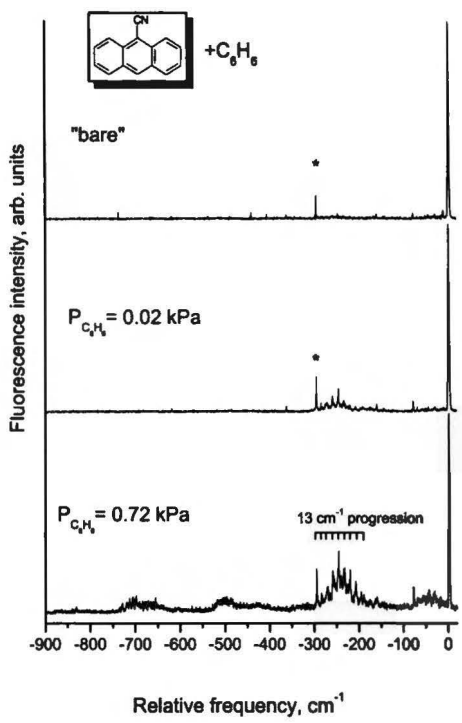


**Figure 3.36.** Fluorescence excitation spectra of the CNA-$C_6H_6$ mixture taken with different pressure of the benzene vapours. The band marked by asterisk at -296 $cm^{-1}$ belongs to the CNA-water 1:1 cluster.

Figure 3.36 shows the fluorescence excitation spectra of the CNA-benzene mixture. Features observed at the red side of the CNA origin around -250 $cm^{-1}$ are assigned to the spectrum of the 1:1 cluster of the CNA-benzene. The electronic origin band of these species is red-shifted by -284 $cm^{-1}$. The low frequency structure consisted of 9 transitions and was built on the origin with maximum at the fourth quanta. The spacing between these transitions is 13 $cm^{-1}$. Similar progression built on the -67 $cm^{-1}$ band occurs near the origin of the "bare" CNA. The transition at -67 $cm^{-1}$ ($\nu$=217 $cm^{-1}$) corresponds to the bending mode of the cyano group. The corresponding bending mode for CNA "bare" molecule is 216 $cm^{-1}$.

Weak and broad fluorescence signal with narrow bands on the top of it appearing around -700 $cm^{-1}$ is assigned to the 1:2 and 1:3 CNA-benzene clusters.

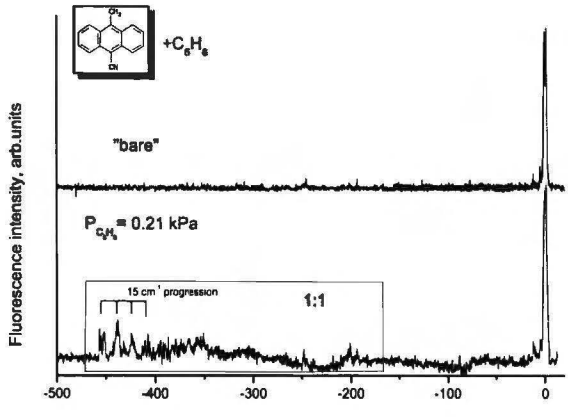


**Figure 3.37.** LIF excitation spectra of the CMA-benzene mixture. $P_{C_6H_6}$ dependence.

Figure 3.37 shows the fluorescence excitation spectra of the CMA-benzene mixture. Three weak bands at -454 $cm^{-1}$, 438 $cm^{-1}$ and -423 $cm^{-1}$ with respect to the electronic origin transition of "bare" CMA molecule are followed by fluorescence background signal. Further increase of the benzene vapours leads to dramatic decrease of the fluorescence signal. Broad and structureless fluorescence signal dominates.

### 3.7. Discussion – the structure of microclusters of anthracenes with selected solvent molecules.

In this section I will discuss the electronic-vibrational spectra obtained for the series of anthracenes microsolvated by different solvents. Only clusters up to three solvent molecules will be discussed. Extraction of the geometries of higher clusters is complex. However, in some cases, when the signal to noise ratio allows the determination of the coordination number of the complex, also larger clusters will be taken into account.

### *3.7.1. The structure of microclusters: anthracenes with $H_2O$ and $CH_3OH$.*

The spectrum of the antracene-water complex 1:1 consists of one strong transition, as shown in Figure 3.8. No low frequency modes that correspond to the vdW vibrations are observed in the LIF spectrum. The lack of the vdW modes could be the proof of rigid structure of the cluster and strong interaction between water hydrogens with anthracene framework. Thus, the rigid structure could be considered as 1:1 anthracene-water complex, where water molecule is doubly H-bonded to the anthracene aromatic ring. In contrast, the spectrum of the 1:2 species has shown multiple intense bands appearing at -180 $cm^{-1}$, -174 $cm^{-1}$, -165 $cm^{-1}$ to the red in respect to the 0-0 transition of the "bare" anthracene. These transitions are due to various geometries of water dimer. Negligible spectral differences in the transitions energies of these species suggest small variations in these structures. Indeed, MD calculations predict 3 stabile structures for anthracene-$(H_2O)_2$. First: two water molecules are H-bonded to each other and, in addition, both form H-bonds to the $\pi$-anthracene framework. Next: each of the water molecules are H-bonded to the anthracene $\pi$-system, but not forming the O-H···O hydrogen bond. Third: "open-chain" structure, where one of water molecules is H-bonded to the anthracene, while the second water is only H-bonded to the first water molecule. Transition observed at -174 $cm^{-1}$ exhibits the doublet structure. The hydrogen atoms of the water molecule can be interconverted through internal rotation, e.g., around the $C_2$ symmetry axis. The quantum tunneling motion produces splitting of each vibronic states of this species. Such interconversion was observed for benzonitrile-water by FTMW spectroscopy [18]. The splitting observed in our experiments is assigned to such tunnelling motions of water hydrogens. The geometry of the water dimer with "open-chain" structure is the most probable geometry with the possibility of proton exchange.

The spectrum of the 1:3 anthracene-water clusters exhibits the weak origin at -223 $cm^{-1}$ followed by several low frequency vdW modes (-216 $cm^{-1}$, -213 $cm^{-1}$, -208 $cm^{-1}$, -204 $cm^{-1}$). In the work [8] authors were unable to resolve vibronic structure of this complex due to low

resolution of the laser. A weak fluorescence signal together with the relative small stabilization of the energy suggests the lack of cyclic, planar geometry of water [8]. We believe that the cyclic structures corresponding to water trimer are not present in the anthracene-water clusters.

The vibrational structure of the spectrum of the 1:1 MA-water clusters (see Figure 3.9) is completely different from this shown for anthracene-(water)$_1$ complexes. The LIF spectrum of MA-$(H_2O)_1$ exhibits the regular progression built on the 11 $cm^{-1}$ mode. Each member of the progression shows the doublet structure. As was mentioned in previous section, this phenomenon may be due to the lowering of the barrier for the methyl group rotation induced by microcluster formation. The splitting of the each member of the low frequency progression could be treated as an indication that the methyl group is involved in the intermolecular vdW vibrations. The water complex with MA is much more flexible than this of anthracene. Presumably, one has to consider the position $10^{th}$ in MA as an attractive site for $H_2O$ attachment.

The spectrum of the 1:2 MA-water complexes exhibits regular structure built on the 13 $cm^{-1}$ mode. This progression consists of 8 quanta with maximum at the third mode. This observation is a strong evidence of large geometry changes between $S_0$ and $S_1$ electronic states. In contrast to the anthracene-$(water)_2$ species, for which multiple structures were observed, the spectrum of the MA-$(water)_2$ proves the existence of the single conformer. As one could notice, small changes in electron density on the anthracene moiety introduced by the effect of hyper conjugation with $CH_3$ group, lead to large changes in spectral behaviour of MA-$(H_2O)_2$ clusters. This could suggests that the binding place to the aromatic rings of the water dimer in the case of MA is completely different from this proposed for anthracene-$(H_2O)_2$ clusters. Most probably, water dimer is bounded rather to the MA $10^{th}$ position than to the $\pi$-electron cloud.

No fluorescence which could be assigned to the MA-$(H_2O)_3$ was observed.

In the case of anthracene-$(CH_3OH)_1$ clusters two relatively strong transitions at -176 $cm^{-1}$ and -133 $cm^{-1}$, with respect to the 0-0 transition of the "bare" anthracene, have been found. Palmer and Topp [17] have assigned them to different isomeric structures of methanol monomer. The LIF spectrum of first conformer is dominated by 20 $cm^{-1}$ progression (see Figure 3.14). The overlap of 20 $cm^{-1}$ overtone and the origin of second conformer produce the broadening of the band at -133 $cm^{-1}$. Earlier work on perylene-ethanol clusters [19] have shown that the clusters exist in two conformations. The structure of both conformers has been identified by rotational coherence spectroscopy [19]. Similar structures to those of perylene-ethanol 1:1 clusters one could propose for the anthracene-$(CH_3OH)_1$ complex (Figure 3.38).

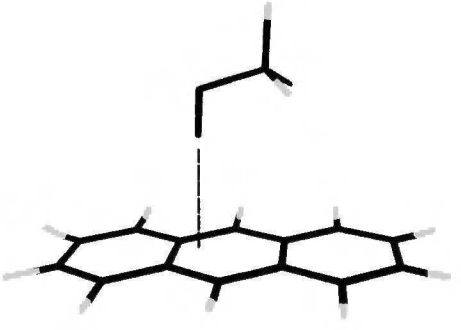

**Figure 3.38.** Antracene-methanol cluster structure.

The similar behaviour is observed in the spectra of the 1:2 anthracene-$CH_3OH$ clusters. Here, the spectrum of the anthracene-$(CH_3OH)_1$ species is dominated by the intermolecular mode of the frequency of 20 $cm^{-1}$. Adding of the second $CH_3OH$ molecule produces further energy stabilization of the cluster in the excited state by 60 $cm^{-1}$. One could notice that for anthracene-$(CH_3OH)_2$ the excited state energy stabilization is less than this for 1:1 species. The LIF excitation spectrum of the anthracene-$(CH_3OH)_2$ is dominated by the 15 $cm^{-1}$ mode, which corresponds to the 20 $cm^{-1}$ mode in the spectrum of anthracene-$CH_3OH$ complex. Again, we believe that the structure of methanol dimer is not very much modified by the presence of anthracene or MA. The proposed structure of $(CH_3OH)_2$ complex with anthracene predicted by our MD calculations is shown in Figure 3.39.

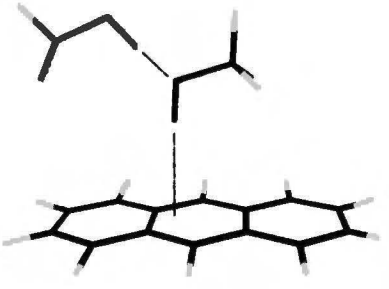

**Figure 3.39.** Anthracene-methanol$_2$ cluster structure.

In the spectrum of the 1:1 MA-$CH_3OH$ complex (see Figure 3.15) two fundamental modes with frequencies 19 $cm^{-1}$ and 29 $cm^{-1}$ can be easily recognized. After adding of the second

methanol molecule the excited state energy of the MA-$(CH_3OH)_2$ exhibits stabilization in the excited state by 289 $cm^{-1}$ with respect to the "bare" MA. Moreover, vibrational structure of the LIF spectrum remains similar to this for the 1:1 complex. In the spectrum of 1:2 MA-$CH_3OH$ cluster the transitions with frequencies 17 $cm^{-1}$ and 25 $cm^{-1}$ are observed. These modes correspond to the 19 $cm^{-1}$ and 29 $cm^{-1}$ vibrations in the MA-$(CH_3OH)_1$ complex, respectively. Small changes in the vibrational structure suggest that the second methanol molecule is attached via its hydrogen to the oxygen of the first methanol.

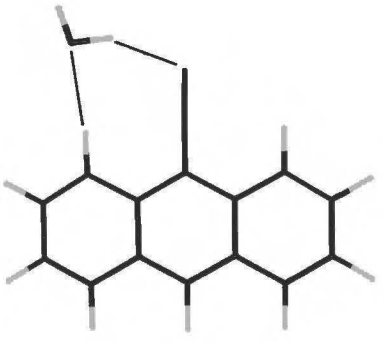

**Figure 3.40.** Cyclic "side-type" structure of the CNA-water cluster [10].

LIF spectra of the 1:3 complexes of anthracene and MA with methanol exhibit different stabilization in the excited state. In the case of anthracene, 0-0 transition of the 1:3 species is red-shifted in respect to the anthracene origin -550 $cm^{-1}$ even more than this for 1:4 and 1:5 complexes. For 1:3 cluster of MA the origin of the complex was observed at only -348 $cm^{-1}$, with respect to the corresponding feature of the "bare" anthracene. Actually, the origin of MA-$(CH_3OH)_3$ is situated between 1:2 and 1:4 complexes. The previous studies [17] of the anthracene-methanol clusters have shown that the anthracene-$(CH_3OH)_3$ complexes are unusually stable in the excited state. The theoretical works on pure methanol clusters [20] predicts that the cyclic structure of the methanol trimer has high binding energy. Therefore, one can conclude that for anthracene cluster the methanol trimer exists predominantly as a planar cyclic structure. For 1:3 methanol complex with MA the lack of the cyclic structure could be explained by the presence of the methyl group. Presumably, the structural changes due to rotation of methyl group prevent the formation of the cyclic trimer structures in the $S_1$ state.

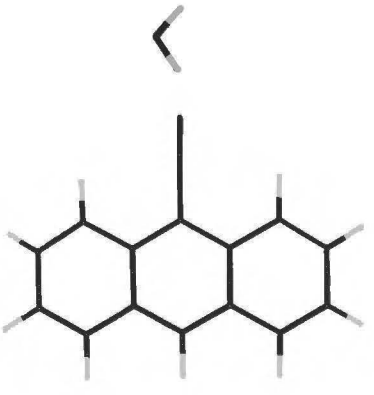

**Figure 3.41.** "Linear-type" structure of the CNA-water cluster [10].

In the CNA-$(H_2O)_1$ excitation spectra (see Figure 3.10), two electronic origins were observed. The first transition is observed at -296 $cm^{-1}$, while the second one at -236 $cm^{-1}$, with respect to the "bare" CNA molecule. In the work [10] rotational coherence experiments recorded on the band at -296 $cm^{-1}$ were carried out in combination with theoretical calculations. The results obtained allow the authors to assign the planar cyclic "side-type" geometry for 1:1 cluster structure, where water molecule is H-bonded to the nitrogen and linked by oxygen to hydrogen in 1st position of the anthracene framework (see Figure 3.40). In agreement with the structure proposed, the spectrum of CNA-$(H_2O)_1$ cluster does not exhibit low frequency vdW modes. Astonishing fact is that the cyclic geometry should appreciably modify the bending mode of the cyano group. However the difference between the frequencies of this mode in the "bare" CNA and CNA-$H_2O$ cluster is only 2 $cm^{-1}$ (214 $cm^{-1}$ and 216 $cm^{-1}$ for CNA and CNA-water complex, respectively). The second origin -236 $cm^{-1}$ with respect to the 0-0 transition of the "bare" CNA exhibits a group of weak features around -200 $cm^{-1}$. These modes correspond to the intermolecular vdW vibrations of the complex. Simultaneously, the CN bending mode is reduced down to 197 $cm^{-1}$. Many low frequency bands observed in this spectrum suggest a "linear-type" (see Figure 3.41) non-rigid geometry with water molecule H-bonded to the cyano group. Both geometries were predicted by means of DFT B3LYP calculations [10].

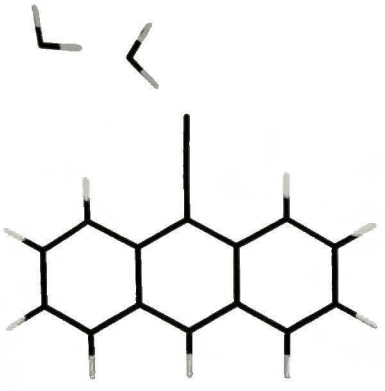

**Figure 3.42.** "Chain" structure of the CNA-$water_2$ cluster.

**Figure 3.43.** Double "side-type" structure of the CNA-$water_2$ cluster.

In the case of CNA-$(H_2O)_2$ at least 3 conformers coexist in the LIF excitation spectrum of the clusters (see Figure 3.10). Two stable geometries of 1:2 water complexes are predicted by means of MD calculations. The first, is "chain-type" form (see Figure 3.42), where a water dimer, which has a chain structure, is H-bonded to the CN group of

cyanoanthracene. The second one is the double "side-type" (see Figure 3.43), where two water molecules are symmetrically attached to both sides of the cyano group. Figure 3.44 shows the spatial probability density distributions of CNA-$(H_2O)_2$ obtained by MD calculations. This is in a good agreement with structures of benzonitrile-$(H_2O)_2$ reported in [21]. Electronic origins of two of structures observed for 1:2 CNA-water spectra exhibit a doublet structure. The most probable reason of this phenomenon is the tunnel splitting effect due to $C_2$ symmetry axis in the water molecule. In accord with this effect the excitation spectra of CNA-$(CH_3OH)_2$ exhibit similar vibrational structure, but all bands appear as single transitions.

The electronic spectrum of the 1:3 CNA-water clusters exhibits two strong transitions. Here, again we can apply the analogy with benzonitrile-$(H_2O)_3$ complex. Quantum mechanical calculations carried out for benzonitrile-water clusters [21] found two stable structures of 1:3 cluster. One is "ring-type" structure, in which $(H_2O)_3$ chain is H-bonded to the CN group and bounded to the ortho hydrogen of benzonitrile. The other structure is a double "side-type", where water dimer and water molecules are located on both sides of CN group. The calculated binding energy difference between these two types of benzonitrile-$(H_2O)_3$ clusters is 3.8 kcal/mol. Nevertheless, the analysis of LIF spectra of CNA-$(H_2O)_3$ allows me to conclude that both "ring-type" and double "side-type" cluster structures are cooled down in the supersonic jet.

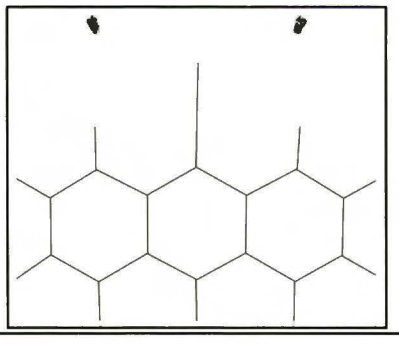

**Figure 3.44.** Spatial probability density distributions of CNA-$(H_2O)_2$

As one can judge from the electronic spectra obtained for CNA-$CH_3OH$ mixture (see Figure 3.17), methanol clusters resemble the behaviour of the water clusters with CNA. From the comparison between electronic spectra of the CNA-water clusters and CNA-methanol I conclude that 1:1 clusters of CNA-methanol have two conformers. One of them we assign as "side-type" geometry, where hydrogen is bounded to the CN group and the methanol oxygen "sits" on the hydrogen in the first position in the anthracene framework. The second conformer exhibits in its electronic

spectrum numerous of intermolecular, low frequency modes. Presumably, the structure of this complex is more flexible.

CNA-$(CH_3OH)_2$ clusters seem to co-exist in the three conformeric forms. The electronic origins for CNA-methanol (1:2) complexes have been found at -598 $cm^{-1}$, -582 $cm^{-1}$ and -566 $cm^{-1}$. As mentioned before, for CNA-$(CH_3OH)_2$ clusters no splitting of the bands have been found. Methanol does not contain $C_2$ axis of symmetry. Thus, in contrast to $H_2O$ it could not exhibit tunnelling effects due to molecule interconversion.

The LIF spectrum of the 1:3 CNA-methanol clusters consists of one intense band. It suggests that only one isomer exists under supersonic jet expansion. The binding energies calculated for benzonitrile-$(water)_3$ clusters [21] show that "ring-type" structure is most favourable in this case. We believe that the structure of this type is most probable for CNA-$(CH_3OH)_3$ cluster. The dominating role plays the interaction with the CN group. Electronic origins of all CMA clusters up to 3 water molecules exhibit doublet structure. The nature of this phenomenon is probably the same as in the case of MA-$H_2O$ 1:1 cluster. The splitting is due to lowering of the barrier for methyl group rotation. Also, the spectra of all clusters CMA-$(H_2O)_n$ ($n$=1-3) exhibit two low frequency bands that could be assigned to methyl group rotation within the cluster. The additive spectral shift of the spectrum of the 1:2 CMA-$H_2O$ complexes suggests that the second water molecule is bounded to the equivalent position of the CMA molecule. The first water molecule forms the planar cyclic dimer structure ("side-type") with the CMA. The second water molecule forms identical cyclic structure on the other side of the cyano group. Relatively small spectral shift of the CMA-$(H_2O)_3$ spectrum and its strong modification of the frequencies corresponding to the methyl group rotation suggests that the binding place of the third water molecule is quite different, as compared to 1:1 and 1:2 species. Most probably, the third water molecule forms the complex, where the hydrogen atom is H-bonded to the $\pi$-system of the anthracene central aromatic ring.

The spectra of the 1:1, 1:2 and 1:3 clusters of the CMA-$CH_3OH$ possess the vibronic level features, which are very similar to their aqueous counterparts. Addition of the second $CH_3OH$ molecule and formation of 1:2 complexes produce the additive spectral shift. Again, the small spectral shift of the electronic origin of the 1:3 clusters is observed. From this I can conclude that the structures of CMA clusters with methanol are comparable with those of water.

### *3.7.2. The structure of microclusters: anthracenes with $CHCl_3$.*

The electronic spectra of the clusters of anthracene, MA, CMA with $CHCl_3$ are dominated by progressions with frequencies of 7 $cm^{-1}$, 10 $cm^{-1}$ and 9 $cm^{-1}$, respectively (see Figure 3.20, Figure 3.21, Figure 3.23) In addition, electronic origins of CMA and MA with chloroform spectra exhibit the doublet structure. This effect is due to lowering of the barrier for methyl group rotation. Additive shift of the 1:*n* (*n*=1-3) clusters of MA-$CHCl_3$ was observed and the vibronic structure corresponding to these clusters does not change much. This suggests that the higher chloroform clusters form a side structure in stepwise manner on opposite sides of the chromophore molecule. *Ab initio* theoretical calculations for benzene-chloroform 1:1 clusters [22] predicted only one stable "umbrella-like" geometry. Unfortunately, for our systems it is very hard or even impossible to perform calculations by *ab initio* electron correlated methods. Molecular dynamic calculations carried out for the chloroform clusters with anthracenes predict two stable geometries for $CHCl_3$. The most stable, as mentioned above, has "umbrella-like" structure, where chloroform is $\pi$-H-bonded to the central aromatic ring. The second geometry structure involves 3 chlorine atoms "sitting" above the anthracene $\pi$-system.

In contrast, spectrum of the CNA-chloroform 1:1 cluster exhibits two broad transitions, which could be assigned to the two different conformeric forms of the cluster.

Our MD calculation for CNA-chloroform 1:1 clusters predicts also 2 stable geometries shown in Figure 3.45. On the other hand, theoretical MP2 electron correlated *ab initio* calculations for fluorobenzene-$CHCl_3$ cluster [22] have found three stable structures. "Umbrella-like" structure calculated by *ab initio* methods has found correspondence to this obtained in our MD calculations. Further addition of chloroform molecules produces additive spectral shift. It suggests that the second chloroform molecule is bounded to the equivalent site in the CNA. The most probable geometry for CNA-$(CHCl_3)_2$ is "opposite-side" structure, when two chloroforms are bounded to the cyano group.

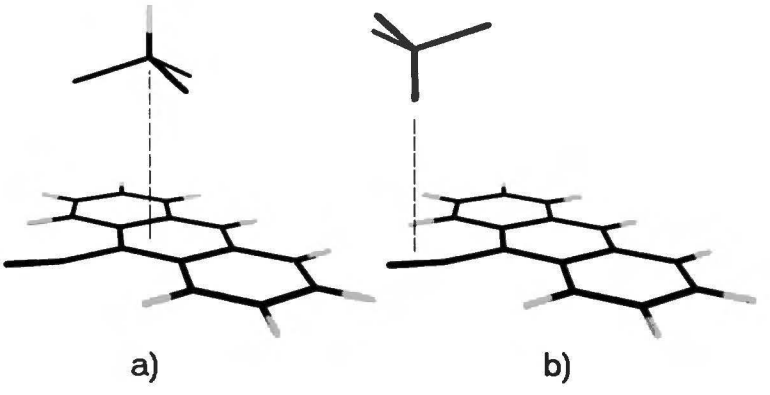


**Figure 3.45.** Two cluster structures of the CNA-$CHCl_3$ predicted by MD calculations. a) "arrow-lake", b) "umbrella-like".

The vibronic structure of the LIF excitation spectra of complexes of the MA with $(CHCl_3)_n$ ($n$=1-3) are very similar. The splitting of vibronic bands of the spectra of 1:1 and 1:2 species of MA-chloroform is 2 $cm^{-1}$. Additive spectral shift of the 1:1 and 1:2 clusters of MA-chloroform suggests that chloroform molecules are bounded to equivalent sites in the MA molecule. No splitting of the vibrational transitions of MA-$(CHCl_3)_3$ has been found.

The spectrum of the CMA-chloroform$_1$ exhibits a long low frequency progression built on frequency of 10 $cm^{-1}$. The vibrational structure is very similar to this for MA. Thus, one could expect that the structures of the complexes CMA-(chloroform)$_1$ and MA-(chloroform)$_1$ are similar and the binding site of the chloroform is the same. MD calculations for CMA predict three binding places of the chloroform molecule, e.g. CN group, central aromatic ring and the outer aromatic ring. But only structure, where chloroform is attached to the central aromatic

ring correlates with this calculated for MA- (chloroform)$_1$ clusters.

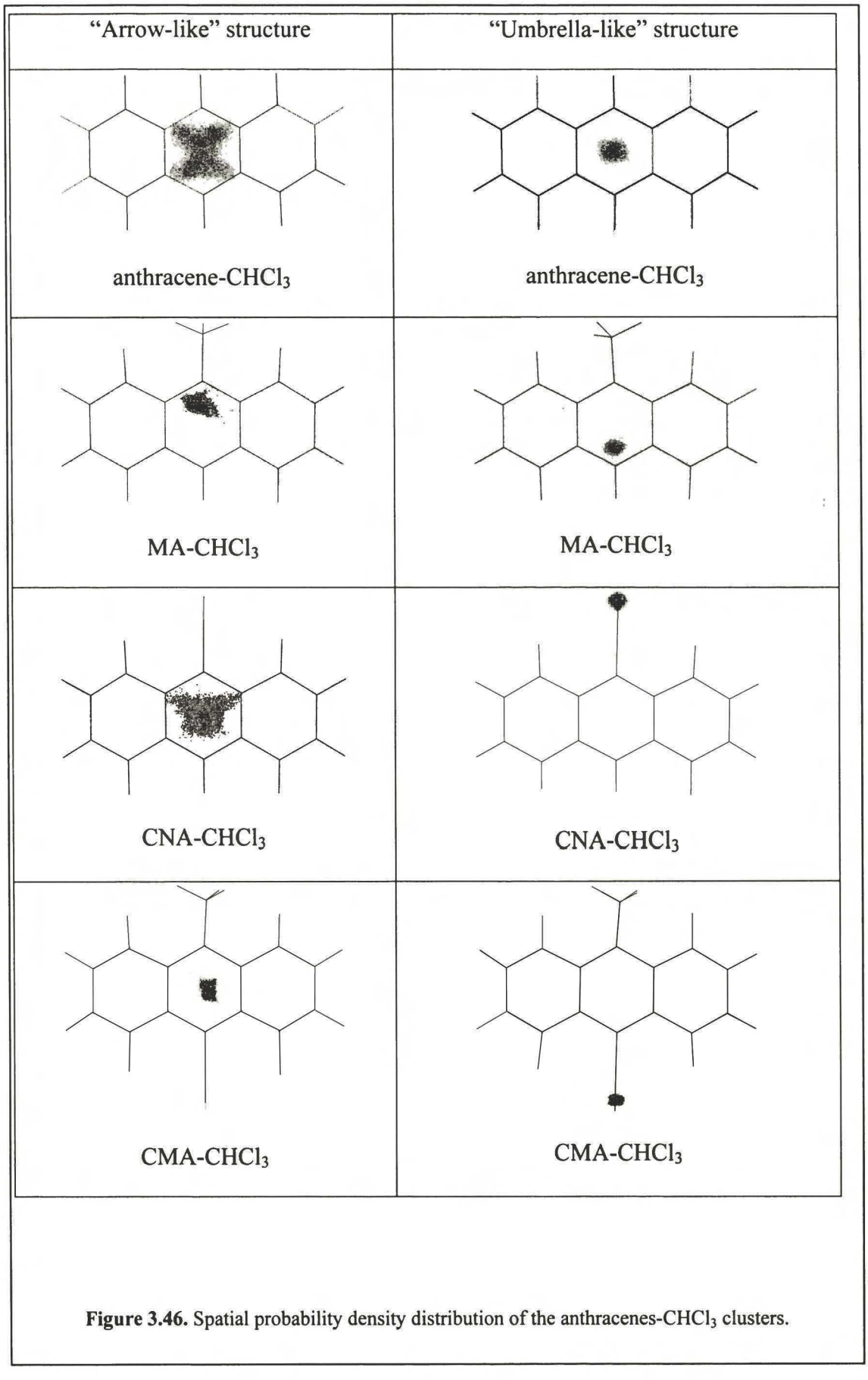


**Figure 3.46.** Spatial probability density distribution of the anthracenes-$CHCl_3$ clusters.

Figure 3.46 shows spatial probability density distribution of the anthracenes-$CHCl_3$ clusters obtained by MD calculations. This figure exhibits the most probable binding sites of the chloroform molecule to the anthracenes.

This spatial distribution was calculated for both types of the anthracenes-chloroform clusters: "umbrella-like" and "arrow-like". From above results I could conclude that the 1:1 species of CMA and MA with chloroform have similar geometry, and the chloroform is π-H-bonded to the anthracene aromatic ring.

The spectrum of the CMA-$(chloroform)_2$ exhibits an enormous red shift of -612 $cm^{-1}$ with respect to the electronic origin of the "bare" CMA molecule. Presumably, an interaction of the second chloroform must involve CN group to form the 1:2 cluster. The spectral shift of the 1:3 CMA-chloroform species is -211 $cm^{-1}$ with respect to the origin of the 1:2 CMA-chloroform species. This value of the stabilization energy is comparable to this for 1:1 CMA-chloroform species. It suggests that the third molecule of chloroform is also π-H-bonded to the anthracene aromatic ring.

### *3.7.3.The structure of microclusters: anthracenes with $CCl_4$.*

All spectra of the complexes of anthracene derivatives with carbon tetrachloride 1:1 species are segregated into two classes. The first type involves anthracene-like clusters. The spectra of this type of clusters exhibit a complex low frequency periodic structure with a weak origin. The second type concerns the cyanoanthracene clusters. This type of complexes is characterized by the strong electronic origin band, together with some weak low frequency vdW modes and a modified frequency of the bending mode of the cyano group.

LIF excitation spectra obtained for the anthracene and MA with $CCl_4$ (1:1) clusters (see Figure 3.25 and Figure 3.28) suggest the large geometry changes in the excited state. A. J.

Gotch et al. [23] have shown that 1:1 complex of the benzene-$CCl_4$ complex has $C_s$ symmetry. DFT B3LYP calculations of the anthracene-$CCl_4$ cluster with simple 3-21g basis set have found minimum energy for the structure of $C_s$ symmetry with the symmetry plane orthogonal to the anthracene plane. Calculation of vibrational frequencies carried out in the ground electronic state for optimized geometry found the lowest frequencies of 5 $cm^{-1}$, 10 $cm^{-1}$, 15 $cm^{-1}$.

Figure 3.47 shows the spatial probability density distributions of anthracenes-$CCl_4$ obtained by MD calculations at temperature of 5K. Coordinates of carbon atom of the $CCl_4$ molecule were monitored to obtain these distributions. As one can see the most probable binding place of the carbon tetrachloride molecule was over the central aromatic ring of the anthracene. The average distance between the carbon atom of the $CCl_4$ and anthracene ring was found to be 4.2 Å.

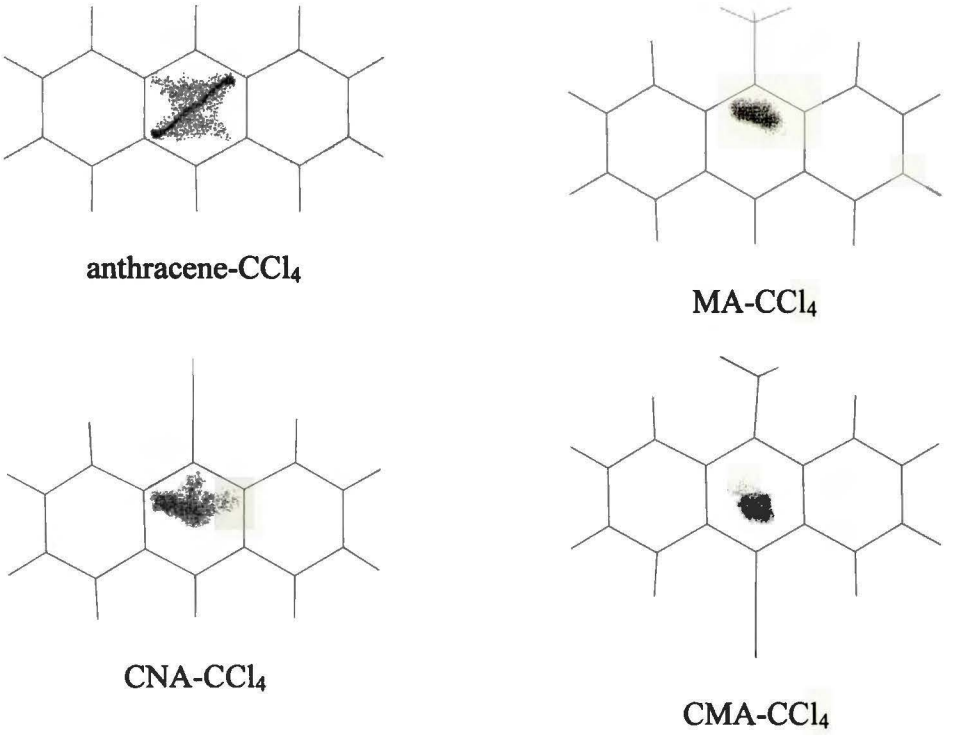


**Figure 3.47.** Spatial probability density distribution of the anthracenes-$CCl_4$ clusters.

One could notice that the spectrum of CNA-$(CCl_4)_1$ exhibits the transition that corresponds to the CN bending mode; this frequency is not modified at all. The same behaviour was

observed in the case of CMA-$(CCl_4)_1$. In both cases the proposed geometry is represented by $CCl_4$ molecule are placed above central aromatic ring of anthracene.

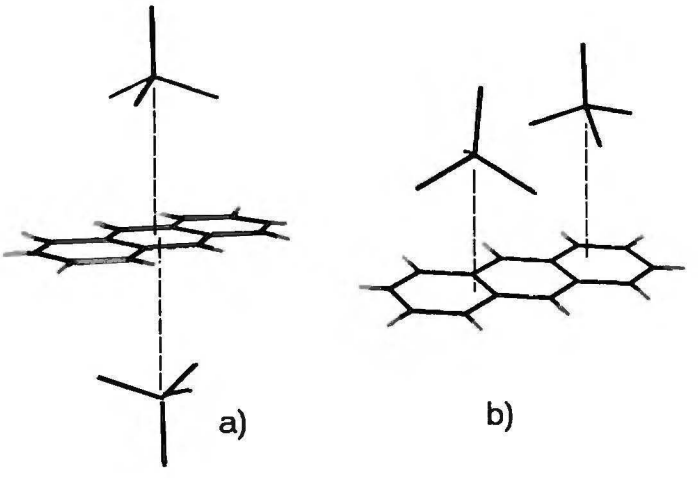


**Figure 3.48.** Structures of the anthracene-$(CCl_4)_2$ clusters predicted by MD calculations.

Two geometries of the 1:2 anthracene-$CCl_4$ clusters (see Figure 3.48) predicted by MD calculation at temperature of 5K was found at nearly the same binding energy (-12.09 kcal/mol "opposite-side" structure (a) and -11.89 kcal/mol "one-side" structure (b)). On the other hand, the binding energy change due to addition of each $CCl_4$ molecule to anthracene was lower in the case of opposite-side structure (-5.99 kcal/mol) than for one-side clusters (-4.98 kcal/mol). In contrast, spectral measurements have found that vibronic structure of the anthracene-$(CCl_4)_2$ clusters is completely different from this observed for anthracene-$CCl_4$ 1:1 clusters. This suggests that the most probable geometry of anthracene-$CCl_4$ 1:2 clusters is rather "one-side" structure.

*3.7.4.The structure of microclusters: anthracenes with benzene.*

Unfortunately, MD calculations could not be conducted for clusters of anthracenes with benzene molecule due to the absence of the parameterization of benzene in the GROMOS96 force field.

The spectrum of the anthracene-benzene clusters exhibits an enormous difference in stabilization energy of the 1:1 species between the ground and first electronic excited state. The spectral shift is -434 $cm^{-1}$, with respect to the electronic origin of the "bare" anthracene; this is the largest shift of those observed before for 1:1 solvent clusters with anthracenes. The similar spectral shifts of the 1:1 benzene clusters for other anthracenes (MA, CNA, CMA) are also observed. Therefore, one could expect that the binding site for benzene molecule is the same for all anthracenes. In the case of CNA-$(benzene)_1$ species electronic spectrum consist of low frequency progression of 13 $cm^{-1}$ built on the origin band. One could easily find in this spectrum the feature corresponding to the bending motion of the CN group (216 $cm^{-1}$ with respect to the origin of the CNA-$(benzene)_1$ clusters). Such a behaviour suggests that CN group plays critical role in the formation of the clusters of CNA with benzene molecules. Astonishing fact is that the spectral behaviour of the benzene 1:1 clusters with CMA, the molecule which contains the CN group too, is completely different.

The electronic origin of the anthracene-$(benzene)_2$ clusters was found blue-shifted by +115 $cm^{-1}$ with respect to the corresponding feature of the anthracene-$benzene_1$ species. The origin consists of two strong bands separated by 8 $cm^{-1}$. Computational analysis of possible structures of the benzene dimer of P. Hobza and Z. Havlas [22] has shown that the benzene dimer exists as T-shaped structure. Earlier, the same structure was reported for phenylalanine [24]. Is seems that T-shaped arrangement of aromatic rings is rather common in a biological environment. Comparing to the calculated structures of the benzene dimer we could suggest that anthracene-$benzene_2$ clusters have geometry, with T-shaped benzene dimer attached to the aromatic ring of

the anthracene. Moreover, mass-selective studies of K. Fung et. al. [25] have shown the splitting of the vibrational bands due to vibrational degeneracy. This effect was observed for the anthracene-$(benzene)_2$ clusters only.

I was unable to found any fluorescence signal which could correspond to the MA-$(benzene)_2$ or CMA-$(benzene)_2$ complexes.

In contrast to the anthracene-$(benzene)_2$ clusters, the corresponding spectrum of CNA-$(benzene)_2$ clusters was found red-shifted by -730 $cm^{-1}$ with respect to the origin of the "bare" CNA molecule. It suggests that T-shaped structure of the benzene dimer rather does not exist in the CNA-$(benzene)_2$ clusters. Most probably, the benzene molecules are attached to the CN group and form a "sandwich" structure.

---

**References and notes**


1. A. Amirav, U. Even and J. Jortner, *Chem. Phys.* **51** (1980) 31.
2. A. Amirav, *Chem Phys* **124** (1988) 163.
3. A. Mordziński, A. Leś, D. H. Levy, Y. Stepanenko, L. Adamowicz, J. Rycombel, to be published.
4. S. Hirayama, F. Tanaka, K. Shobatake, *Chem. Phys. Lett.* **153** (1988) 112.
5. J. A. Syage, P. M. Felker, D. H. Semmens, F. Al Adel and A. H. Zewail, *J. Chem. Phys.* **82** (1985) 2896.
6. F. Tanaka, S. Hirayama, K. Shobatake, *Chem. Phys. Lett.* **195** (1992) 243.
7. S. Zilberg, U. Samuni, R. Fraenkel, Y.Haas, *Chem. Phys.* **186** (1994) 303.
8. P. M. Palmer, M. R. Topp, *Chem. Phys.* **239** (1998) 65.
9. Y. Stepanenko, A. Vdovin, J. Jasny, J. Sepioł, A. Mordziński, *J. Mol. Struct.* **480-481** (1999) 595.
10. K. Egashira, Y. Ohshima, O. Kajimoto, *Chem. Phys. Lett.* **334** (2001) 285.
11. Z. Zhao, C. P. Parmenter, D. Moss, A. J. Bredley, A. E. W. Knight, *J. Chem. Phys.* **96** (1992) 6362.
12. F. Lahmani, E. Bréhéret and J. Sepioł, *J. Photochem. Photobiol. A: Chem* **62** (1991) 33.
13. F. Lahmani and J. Sepioł, *Chem. Phys. Lett.* **189** (1992) 479.
14. P. M. Palmer, M. R. Topp, *Chem. Phys. Lett.* **292** (1998) 307.
15. P. M. Andrews, B. A. Pryor, M. B. Berger, P. M. Palmer, M. R. Topp, *J. Phys. Chem. A* **101** (1997) 224.
16. R. N. Pribble, F. C. Hagemeister, T. S. Zwier, *J. Chem. Phys.* **106** (1997) 2145.
17. P. M. Palmer, M. R. Topp, *Chem. Phys. Lett.* **286** (1998) 113.

18. S. Melandri, D. Consalve, W. Caminati, P. G. Favero, *J. Chem. Phys.* **111** (1999) 3874.
19. P. M. Andrews, B. A. Pryor, M. B. Berger, P. M. Palmer, M. R. Topp, *J. Phys. Chem. A* **101** (1997) 6222.
20. U. Buck, J. G. Siebers, R. J. Wheatkey, *J. Chem. Phys.* **99** (1993) 9428.
21. S. Ishikawa, T. Ebata, N. Mikami, *J. Chem. Phys.* **110** (1999) 9504.
22. P. Hobza, Z. Havlas, *Chem. Rev.* **100** (2000) 4253.
23. A. J. Gotch, A. W. Garret, T. S. Zwier, *J. Phys. Chem.* **95** (1991) 9699.
24. C. A. Hunter, J. Singh, J. M. Thornton, *J. Mol. Biol.* **218** (1991) 837.
25. F. H. Fung, H. L. Selzle and E. W. Schlag, *J. Phys. Chem.* **87** (1983) 5113.

## CHAPTER 4. Conclusions.

This work continues spectroscopical investigations of the structures of the clusters of the aromatic molecules and solvents. Many studies of the molecular clusters of aromatic molecules (benzene and its derivatives, naphthalene, perylene, anthracene) with water and methanol were carried out in the recent years. Much less is known for the complexes of carbon tetrachloride and benzene. In the presented work, the complexes of anthracene derivatives with $H_2O$, $CH_3OH$, $CHCl_3$, $CCl_4$, $C_6H_6$ were investigated by means of optically and mass resolved spectroscopy in the supersonic jets.

For the majority of investigated clusters we were able to measure the excitation spectra and strictly determine the stechiometry of the cluster observed. The structures of complexes were proposed basing on their excitation spectra, together with molecular dynamics studies and *ab initio* calculations.

These studies give us some insight into the early stages of microsolvation of aromatic systems in the gas phase.

Special attention was devoted to the mass resolved spectra, which enabled the determination of the vibronic structures of the anthracene-(benzene)$_n$, $n$=1-5 clusters. The ionization thresholds of these clusters were also obtained in this work.

This thesis leaves also some open questions, which could not have been answered by the present work covered by this thesis and which might be a subject of a future research. In particular, I was not able to distinguish between some conformeric forms of solvent clusters. More sensitive, two resonance depletion experiments have to be done for these cases. On the other hand, this topic seems to be a challenge for new spectroscopic methods such as IR depletion spectroscopy, rotational coherence spectroscopy or spectroscopy in the terahertz spectral region. Also more advanced calculations for molecular clusters, which would be possible in forthcoming years, have to be carried out.

* * *

Niniejsza praca stanowi kontynuacje badań struktury klasterów molekul aromatycznych z małymi cząsteczkami, jak woda, metanol i inne - oddziaływujace specyficznie lub dyspersyjnie. W ostatnich latach pojawiła się duża ilość prać dotyczących badań struktury molekularnych klasterów cząsteczek aromatycznych (benzen i jego pochodne, naftalen, perylen, antracen) z cząsteczkami wody oraz metanolu. Najmniej wiadomo o kompleksach z czterochlorkiem węgla oraz benzenem. Badania moje włączają się w nurt publikowanych ostatnio prac i skupiają się na pochodnych antracenu i ich oddziaływaniu z woda, metanolem, chloroformem, czterochlorkiem węgla i benzenem.

Główny instrument badawczy to laserowa spektroskopia fluorescencyjna i masowo rozdzielcza, w naddźwiękowych wiązkach molekularnych.

- Zmierzono widma wzbudzenia fluorescencji i dokładnie wyznaczono stechiometrie wiekszości badanych klasterów.
- W oparciu o widma wzbudzenia fluorescencji i obliczenia teoretyczne metodami *ab initio* i dynamiki molekularnej zaproponowano struktury tych kompleksów
- Zmierzono masowo rozdzielcze widma klasterów antracen-benzen$_n$, $n$=1-5, oraz 9-metyloantracen-$(CCl_4)_l$, poznanie tych widm pozwoliło na zinterpretowanie struktury wibronowej odpowiednich kompleksów i na wyznaczenie potencjałów jonizacji.

Badania te dają wgląd w pierwsze stadia procesu mikrosolwatacji.

Wyniki powyższe pozostawiają otwartymi szereg problemów, które staną się przedmiotem przyszłych prac.

Nie zostały rozdzielone widma poszczególnych konformerów niektórych klasterów cząsteczek tworzących kompleksy z aromatami; wymagana tu jest większa niż dostępna obecnie czułość techniki "widmowego wypalania dziur".

Praca niniejsza stanowi otwarte pole dla zastosowania nowych technik eksperymentalnych, takich jak "IR depletion spektroscopy", "Rotational coherence spectroscopy", oraz spektroskopii w teraherzowym zakresie widmowym.